Stony Brook University

Biocompatibility and Bioactivity of One- and Two-Dimensional Nanoparticle Reinforced Polymeric Scaffolds for Bone Tissue Engineering Applications

A Dissertation Presented

by

Jason Thomas Rashkow

to

The Graduate School

in Partial Fulfillment of the

Requirements

for the Degree of

Doctor of Philosophy

in

Biomedical Engineering

Stony Brook University

August 2016

Stony Brook University

The Graduate School

Jason Thomas Rashkow

We, the dissertation committee for the above candidate for the

Doctor of Philosophy degree, hereby recommend

acceptance of this dissertation.

Balaji Sitharaman, Ph.D. – Dissertation Advisor
Associate Professor, Department of Biomedical Engineering

Stefan Judex, Ph.D. - Chairperson of Defense
Professor, Department of Biomedical Engineering

Yi-Xian Qin, Ph.D. – Internal Committee Member of Defense
Professor, Department of Biomedical Engineering

Yizhi Meng, Ph.D. – External Committee Member of Defense
Assistant Professor, Department of Materials Science and Engineering

This dissertation is accepted by the Graduate School

Nancy Goroff

Interim Dean of the Graduate School

Abstract of the Dissertation

Biocompatibility and Bioactivity of One- and Two-Dimensional Nanoparticle Reinforced Polymeric Scaffolds for Bone Tissue Engineering Applications

by

Jason Thomas Rashkow

Doctor of Philosophy

in

Biomedical Engineering

Stony Brook University

2016

Limitations associated with current bone grafting techniques utilizing autologous or allogeneic bone have led to an increase in bone tissue engineering strategies. The ideal scheme of repairing a bone defect is to employ a material that can act as a scaffold and assist regeneration of native tissue in the area. Although biodegradable polymers fulfill many of the requirements for synthetic bone grafts, a major limitation is poor integrity under load bearing conditions prompting investigation of nanoparticle-reinforced biodegradable polymer nanocomposites. Recently, incorporation of 0.2 wt% of two-dimensional organic nanostructures (graphene nanoribbons (GONRs) and graphene nanoplatelets (GONPs)) and one- and two-dimensional inorganic nanostructures (molybdenum disulfide nanoplatelets (MSNPs) and tungsten disulfide nanotubes (WSNTs) led to significant enhancement in the compressive modulus, compressive yield strength, flexural modulus, and flexural yield strength of poly(propylene fumarate) (PPF) nanocomposites with when compared to PPF alone or PPF reinforced with single- or multi-walled carbon nanotubes (SWCNTs or MWCNTs). In this work we investigate the cytocompatibility of inorganic nanoparticles to mesenchymal stem cells. We present the *in vitro* bioactivity of these nanocomposite scaffolds through submersion in simulated body fluid (SBF). From this and previous studies, we select two candidate scaffolds to investigate the *in vivo* biocompatibility after implantation in the soft and hard tissue of a rat model. Our results indicate little cytotoxicity of the inorganic nanoparticles at concentrations relevant to these scaffolds. We also observed nanoparticle morphology and composition related influence on bioactivity of these nanocomposite scaffolds allowing us to select GONP and MSNP reinforced scaffolds for *in vivo* investigation. Finally, we observed no deleterious effects from implanting these nanocomposite scaffolds in soft or hard tissue of a rat. The results suggest potential for these nanocomposite scaffolds to serve as bioactive bone tissue engineering scaffolds.

Dedication

For my family –

For always being there with smiles and open arms.

Table of Contents

List of Figures

arrows) and blood vessels (orange arrows) also appear in the images. Fibrous capsule (FC) is visible in some images and appears as pink fibrous connective tissue.

Figure 4.7. Results of histological scoring of (A, B) hard tissue response, (C, D) soft tissue capsule thickness, and (E, F) soft tissue capsule interstitium quality after 2 or 6 weeks implantation. Data are presented as median of n=5. Statistical significance was determined by Kruskal-Wallace test with Dunn's *post hoc* and $p<0.05$ considered significant.

List of Tables

List of Abbreviations

PLGA	Poly(lactic-co-glycolic acid)
MWCNT	Multiwalled carbon nanotubes
MWGONR	Multiwalled graphene oxide nanoribbons
GONP	Graphene oxide nanoplatelets
WSNT	Tungsten disulfide nanotubes
MSNP	Molybdenum disulfide nanoplatelets
MSC	Mesenchymal stem cell
LDH	Lactate dehydrogenase
ALP	Alkaline phosphatase
DSPE-PEG	1,2-Distearoyl-sn-Glycero-3-Phosphoethanolamine conjugated with polyethylene glycol
SBF	Simulated body fluid

Acknowledgments

I would like to first acknowledge Dr. Balaji Sitharaman, my advisor. I appreciate all of your encouragement and kindness during my time here. Thank you for believing in me and agreeing to take me on beyond my Master's work and for having that conversation with me early on. You were an excellent mentor and I feel privileged to know you.

Thank you to Dr. Stefan Judex, Dr. Yi-Xian Qin, and Dr. Yizhi Meng for being a part of my dissertation committee. I appreciate you giving me access to instruments and all of your insight into my thesis.

This work wouldn't have been possible without the support of my fellow lab members, past and present. Dr. Gaurav Lalwani, Dr. Sayan Mullick Chowdhury, Dr. Shruti Kanakia, Dr. Behzad Farshid, Yahfi Talukdar, Sunny Patel, Shawn Xie, Cassandra Surhland and Stephen Lee, thank you all for your help and commiserating during the good times and the bad. Gaurav and Sayan, thanks for the fun times and dance parties. Stephen, from our times at the gym to the backyard barbeques you have been a great friend. Yahfi and Sunny, we started together in the lab and by attending a class we didn't belong in. You two have been fantastic friends and I'm going to greatly miss being able to do fun things with you guys on a whim. Yahfi, I have to give you special recognition, you have been a friend, gym partner, and constant resource for me to learn from. I was truly lucky to get to work on projects with you from the very beginning. You are a gifted teacher and your mentorship never ceases.

I have the best family in the world. My parents, Terri Thomas and Steven Rashkow, and my brother, Brian Rashkow, are just the best people. They've always encouraged me to achieve whatever I wanted in life and pushed just enough to get the point across. They are also hilarious; I'm always laughing when we are together and you can never tell when we might burst into song. I've never seen a closer family and I appreciate all the love and support.

I would also like to extend my sincerest gratitude to my Great Aunt and Uncle, Ellen and Arnold Wald, who continue to be a source of inspiration and the ultimate role models and have always given me endless support.

To my other half, Lisa Covert, you have been the closest person in my life during these five years. Every day I look forward to coming home to your smiling face. You are an incredible person and partner, and so supportive. I don't know if I could have made it through some of the toughest times without you. You always listen, no matter how complex or convoluted, to my task of the day and do your best to make sense of it all. I'm so lucky to have you in my life. I love you.

Thank you to Tatiana Zaliznyak, of NARMIL, for your help and patience with collecting confocal Raman spectra from my challenging samples.

I would like to acknowledge Central Microscopy at Stony Brook University, specifically Susan Van Horn, for her assistance with TEM sample preparation and training.

I appreciate the assistance of Dr. Kenneth Shroyer, MD (Professor and Chair of the Department of Pathology at Stony Brook Medicine) for his assistance with the descriptive light microscopy evaluation of my soft and hard tissue samples.

I would like to thank the Department of Biomedical Engineering at Stony Brook University. This is a special department full of collaborative and supportive people and that made all the difference. Special thanks to all the friends I've made during my five years who have supplied me with lots of good times and memories.

This work was supported by the National Institutes of Health (grants No. 1DP2OD007394-01).

Research carried out at the Center for Functional Nanomaterials, Brookhaven National Laboratory, New York is supported by the U.S. Department of Energy, Office of Basic Energy Sciences, under Contract No. DE-AC02-98CH10886.

Confocal Raman data were acquired in SoMAS' NAno-Raman Molecular Imaging Laboratory (NARMIL), a community facility dedicated to environmental sciences' applications and founded with NSF-MRI grant OCE-1336724.

List of Publications

Peer-Reviewed Journal Articles

Jason T. Rashkow, Gaurav Lalwani and Balaji Sitharaman. "*In Vitro* Bioactivity of One- and Two-Dimensional Nanoparticle Reinforced Bone Tissue Engineering Scaffolds." *In Preparation*

Jason T. Rashkow, Yahfi Talukdar and Balaji Sitharaman. "Soft and Hard Tissue Biocompatibility of One- and Two-Dimensional Nanoparticle Reinforced Bone Tissue Engineering Scaffolds." *In Preparation*

Jason T. Rashkow and Balaji Sitharaman. "A Review of Three-Dimensional Scaffolds for Bone Tissue Engineering." *In Preparation*

Jason T. Rashkow, Yahfi Talukdar, Gaurav Lalwani, Balaji Sitharaman. “Interactions of One and Two Dimensional Layered Inorganic Nanoparticles with Fibroblasts and Human Mesenchymal Stem Cells.” *Future Medicine: Nanomedicine* 10 (11), 1693-1706 (2015).

Jason T. Rashkow, Yahfi Talukdar, Gaurav Lalwani, Balaji Sitharaman. “The effects of graphene nanostructures on mesenchymal stem cells.” *Biomaterials* 35 (18), 4863-4877 (2014).

Jason T. Rashkow, Sunny C. Patel, Ryan Tappero, Balaji Sitharaman. “Quantification of single-cell nanoparticle concentrations and the distribution of these concentrations in cell population.” *Journal of the Royal Society Interface* 11 (94), 20131152 (2014).

Textbook Chapters

Gaurav Lalwani, Yahfi Talukdar, Jason Rashkow and Balaji Sitharaman. “Micro and Nano Technologies to Engineer Bone Regeneration.” Chapter 10, Micro and Nano Technologies in Engineering Stem Cells and Tissues. Wiley-IEEE, 2013, 220-235.

Chapter 1

A Review of Three-Dimensional Biodegradable Scaffolds for Bone Tissue Engineering Applications

Burden of Bone Defects and Current Treatment

Managing bone defects due to trauma, disease or surgical intervention remains a continuous challenge in orthopedic medicine. Some such complications result in a critical sized defect.[1-4] The definition of a critical size varies depending on location and condition of surrounding tissue, however an accepted definition is a defect that cannot heal spontaneously without intervention in the lifetime of the patient.[1,5] More than half a million patients are treated for bone defects in the United States each year, bringing a high burden to medicine with the cost of repair greater than $2.5 billion as of 2012 and expected to grow due to an aging population.[6]

Treatment of bone defects has traditionally been accomplished through the use of autogenous or allogenous bone grafts.[6,7] Autografts, sourced directly from the patient are considered the gold standard graft material. This bone is histo- and biocompatible as it contains all the patient's own genetic material and therefore needs no processing. It also contains all the components to enhance osteoinduction, for instance bone morphogenic proteins (BMPs), Indian Hedgehog, vascular endothelial growth factor, as well as other growth factors. However, as this bone is generally harvested from the patient's iliac crest, there is limited availability and requires an additional surgery along with all costs and potential complications, including pain, scarring, and infection.[7,8] Allografts, sourced from a donor are also likely histocompatible as the major histocompatibility complex profile of the tissue should be similar within the same species. Allografts can also be processed into many forms including whole bone, cortical or trabecular grafts, bone chips, and demineralized bone matrix. Nevertheless, this type of graft is associated with increased likelihood of immunogenicity or disease transfer, and donor bone loses much osteoinductive potential during processing.[9] Additionally, allograft bone faces the limitation of

inadequate donor supply to patient demand.[4,6] These problems with traditional grafts have encouraged research toward synthetic grafting materials and bone tissue engineering strategies.

Bone Tissue Engineering

The ideal scheme of repairing a bone defect is to employ a material that can act as a biomimetic scaffold and assist regeneration of native tissue in the area, known as bone tissue engineering. The goal of this paradigm would be to resolve the issues with current grafting materials, the need for a second surgery site, concern about immunogenicity, disease transfer, and limited supply.[6] A bone tissue engineering scaffold must be able to similarly perform the functions of native bone. To this end, it is critically important to have knowledge of bone biology, formation, repair, structure, and mechanics so that a developed construct leads to fully functional restored bone.

Bone Development and Repair

Bone is composed of about 25% organic matrix, 70% inorganic material, and 5% water of which the organic phase is mainly collagen type 1 while the inorganic phase consists mainly of hydroxyapatite.[10] The structure of bone has multiple levels of organization, illustrated in Figure 1.1, from macro-level cortical and trabecular bone to submicro-level collagen type 1 fiber matrix combined with mineralized carbonated apatite to nano-level hydroxyapatite crystals that reinforce the collagen 1 fibers.[6,11] Bone development occurs in one of two ways. For cranial and mandibular bones, development occurs by the intramembraneous pathway by which mesenchymal progenitor cells differentiate directly into osteoblasts and begin forming calcified

tissue. For long bones and vertebrae, development occurs by the endochondral pathway, which dictates that growth of new bone occurs through mesenchymal progenitors first differentiating to chondrocytes that deposit a cartilaginous template that is calcified over time.[6,10] Both types of development involve important growth factors and proteins including the BMPs, Indian Hedgehog, parathyroid hormone related peptide, and vascular endothelial and fibroblastic growth factors.[12] In addition, regardless of which type of development, remodeling of the structure must occur to maintain healthy bone.[10]

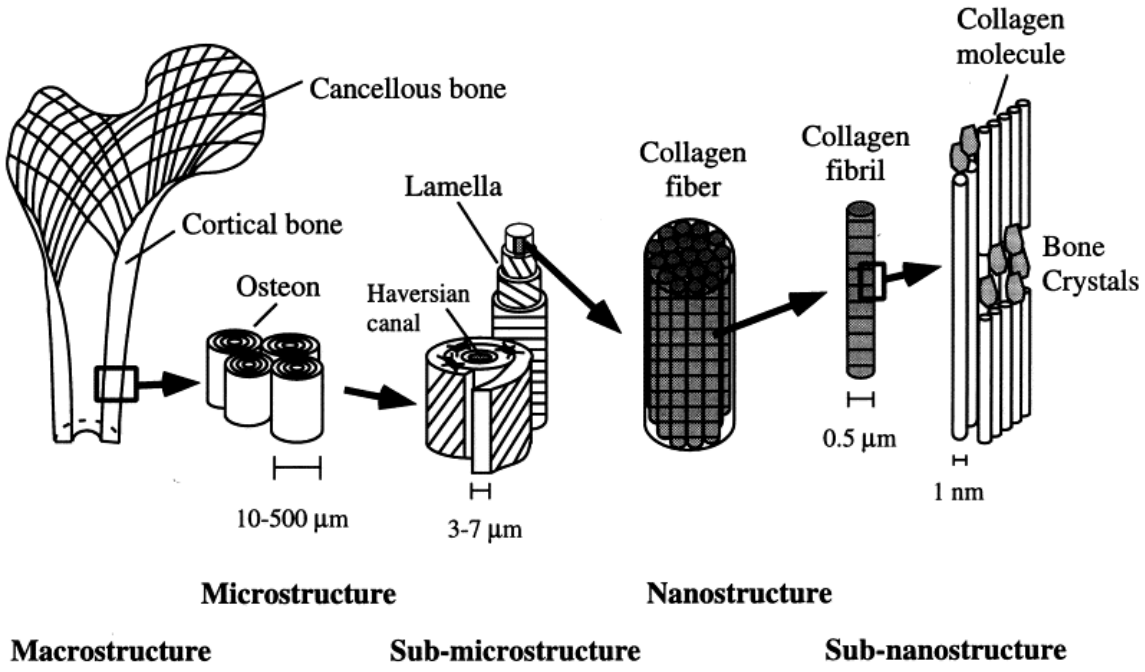

Figure 1.1. The hierarchical structure of bone. Reproduced with permission from Rho J-Y. et al. "Mechanical properties and the hierarchical structure of bone." Medical Engineering & Physics, 1998. Copyright 1998 Elsevier Publishing Group.

After a defect or fracture, repair occurs through four steps, highlighted in Figure 1.2, leading to a remodeled bone without scar tissue. First, the body creates a hematoma and inflammatory response to protect the site and fight any potential infection.[13] Next, a callous is formed through rapid formation of cartilage by chondrocytes to stabilize the area. With new vasculature infiltrating the area and through activity by factors listed above for bone

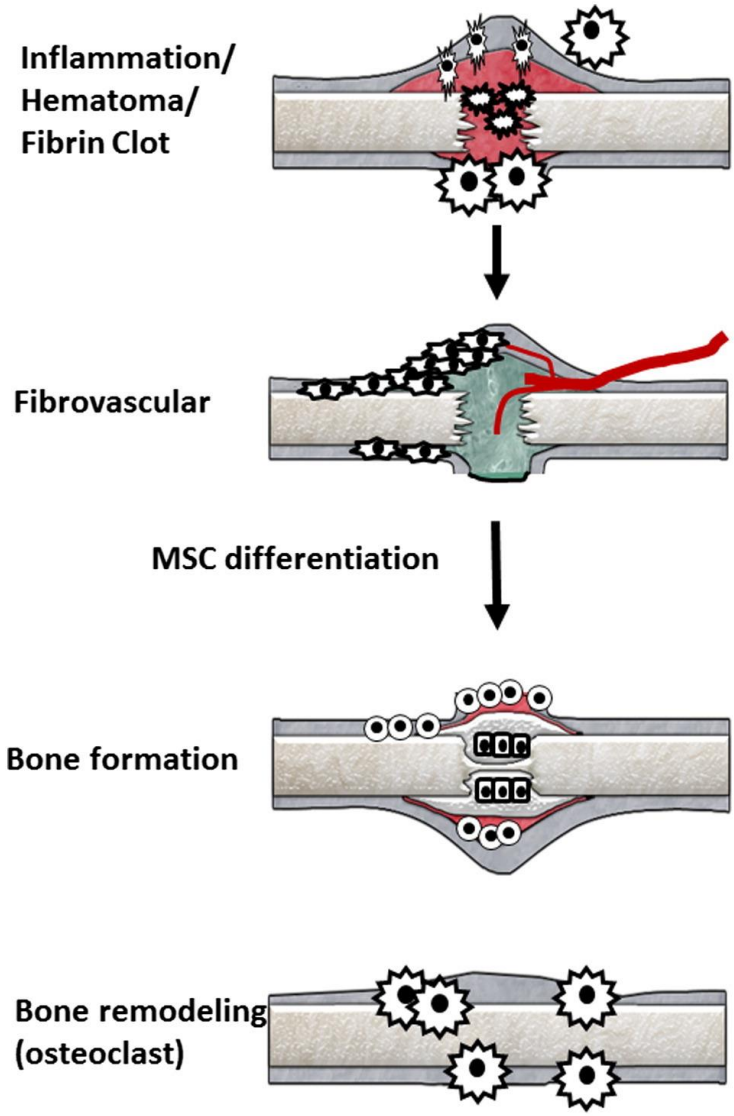

Figure 1.2. The phases of the bone repair process. Adapted with permission from Hankenson, K.D. et al. "Extracellular signaling molecules to promote fracture healing and bone regeneration." Advanced Drug Delivery Reviews, 2015. Copyright 2015 Elsevier Publishing Group.

development, the cartilage is resorbed by chondroclasts and osteoblasts then deposit new bone. Finally, remodeling activity follows, reorganizing any rapidly formed unorganized bone into an organized and continuous cortex.[6,13,14] While bone biology is complex, it is important to learn from nature and to keep the bone development and repair processes in mind while developing scaffolds for bone tissue engineering applications. Since these processes vary depending on site, these will dictate the physical properties of a synthetic graft as well as the appropriate factors or cell types to deliver.

Scaffold Design and Material Selection

The interactions between tissue engineering construct and bone is greatly related to the osteoinductive factors involved in bone formation and repair. Synthetic materials often have intrinsic osteoconductivity, or the ability to act as a scaffold for cellular attachment, but lack in ability to impact bone formation.[15,16] Yet, bone tissue engineering scaffolds may be modified to release cells or other factors after implantation to influence host biology. In this way, a construct may also be bioactive, able to influence bone growth through formation of an apatite layer on the surface to influence attachment and differentiation of osteogenic cells; or osteoinductive, able to influence native mesenchymal stem cells (MSCs) to become osteogenic through release of growth factors or BMPs.[6,15]

From a material perspective, in order to best mimic bone morphology and allow for integration there are four major requirements that an ideal bone tissue engineering scaffold should possess. The first of these requirements is a three-dimensional and highly porous structure to allow for flow of nutrients and ingrowth of native tissue. A minimum pore size of 100 μm is necessary for cellular infiltration and transport of nutrients and waste, however scaffolds with pores of 300 μm show greater vascularization and osteogenesis.[17] Second are mechanical properties similar to that of the surrounding native tissue as dissimilarity in these can have a deleterious effect on healing. Poor mechanical integrity of the implant may lead to reduced stability of the healing bone, especially in weight bearing situations. Conversely, implants with mechanical properties much greater than that of the surrounding tissue may lead to stress shielding, or resorption of the natural bone due to lack of mechanical stresses.[18] However, while this is the view point of many researchers, there are others who believe that an implanted

material should be stronger than the bone it would replace due to the impaired structure or that any implanted material should receive a fixation device to prevent collapse.[19] Regardless of which view, it is important to consider the mechanical stability of implanted materials during the design process so as to withstand handling during surgery and a patient's normal activity.[20] Additionally, the mechanical properties of a scaffold will depend on where and in what type of bone it is implanted. A comparison of elastic modulus and compressive strength of bone to some commonly investigated material classes can be found in Figure 1.3. The third requirement is appropriate surface properties to allow cellular attachment, proliferation, and differentiation. This relates to the information above concerning the hierarchical structure of bone, with nanocrystals of hydroxyapatite within the matrix of collagen type 1 and other proteins.[10] Finally, the ideal construct would be biocompatible and bioresorbable with non-toxic degradation products and a controllable degradation rate to match bone tissue ingrowth.[6,21] This final point also plays an important role in the mechanical properties of a material. Over time, as the scaffold degrades, the mechanical properties will decrease, putting increased stress on the newly formed bone. During the design process, it is important to consider the material degradation rate so that these stresses are appropriately transferred to the newly formed bone.[19,20] To this end, much effort has been applied toward finding the material to fulfill the above criteria.

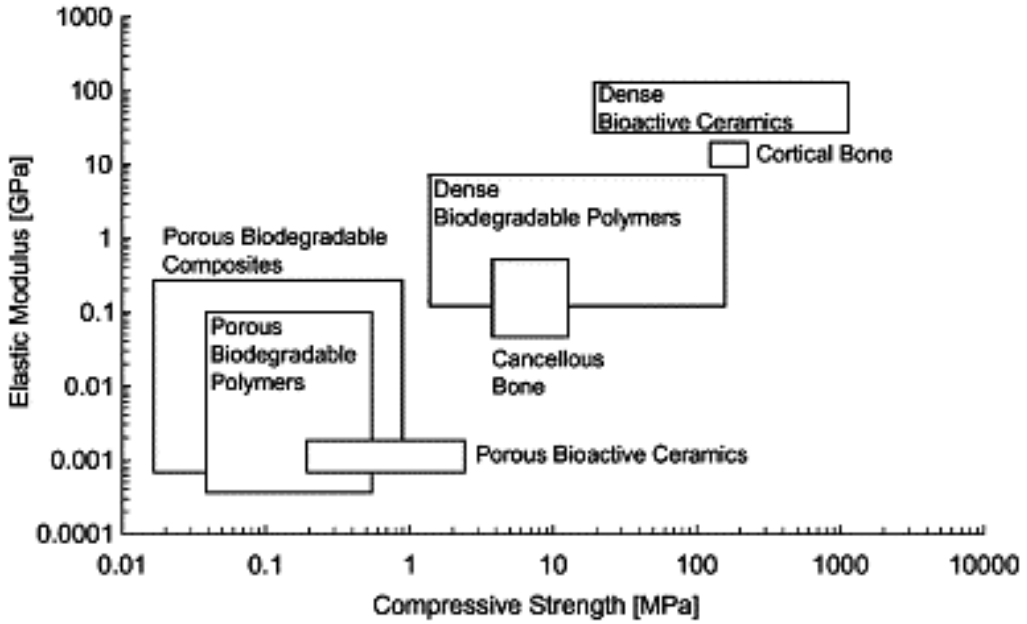

Figure 1.3. Elastic modulus and compressive strength of bone compared to biodegradable polymers, bioactive ceramics and composites. Reproduced with permission from Rezwan, K. et al. "Biodegradable and bioactive porous polymer/inorganic composite scaffolds for bone tissue engineering." Biomaterials, 2006. Copyright 2006 Elsevier Publishing Group.

Ceramics

Due to similarity in chemistry to bone mineral, natural or synthetic hydroxyapatite and calcium phosphate ceramics have been investigated for many years as a bone graft materials. These materials have been made porous by foaming and sintering ceramic or glass particles at high temperatures,[22] sol-gel techniques,[23] and by coating polymer foams with slurry and burning out the polymer template.[24] The key advantages to these materials are excellent biocompatibility and bioactivity, allowing for a chemical integration with the surrounding bone. However, one disadvantage to these materials is slow biodegradation. One clinical study found integration of intact porous hydroxyapatite implants 6 to 7 years post-surgery.[25] Another disadvantage to these

ceramics is that they are very brittle compared to bone and that has limited the ability to easily shape the construct and its use in load-bearing applications.

Bioactive glass and glass ceramics are named as such due to the ability to form a strong chemical bond with bone. These silicate-, phosphate-, or borosilicate-based glasses containing ions of calcium and phosphate form a bond with bone through interaction of a hydroxycarbonate apatite layer that forms on the surface of the glass during the initial stages of dissolution. This layer interacts with the collagen type 1 and hydroxyapatite in the surrounding bone.[26] This ionic dissolution also allows for controllable degradation, helping to remedy one of the disadvantages of hydroxyapatite and calcium phosphate ceramics. However, the disadvantage of poor tensile strength and fracture toughness remains a problem for bioactive glass and glass ceramics.

Polymers

Biodegradable polymers used for bone tissue engineering scaffolds can be broken into two categories: natural and synthetic. Natural polymers include polysaccharides and proteins such as starch, alginate, chitosan, hyaluronic acid, collagen, fibrin, and silk. There are many synthetic polymers that have been studied for these applications; some of the more commonly studied include the saturated aliphatic polyesters poly(lactic acid) (PLA), poly(glycolic acid) (PGA), and copolymer poly(lactic-co-glycolic acid) (PLGA), as well as poly(ε-caprolactone) (PCL); and unsaturated linear polyester poly(propylene fumarate) (PPF).[27] Synthetic polymers have found greater research interest due to easier reproducibility in synthesis with fewer impurities and therefore less concern with immunogenicity or infection.

One advantage of biodegradable polymers is the ability to easily add porosity and form them to any shape. The most common way to create porous polymer scaffolds is by use of the

solvent-casting and particulate leaching technique, where a porogen (typically sodium chloride (NaCl)) is mixed with the polymer solution and molded to the desired shape. After solidification, the scaffold is soaked in water to dissolve the porogen, leaving a porous structure.[27] However, many methods have been tested for fabricating scaffolds, some of which can be found in Figure 1.4, including gas foaming,[28] freeze drying,[29] electrospinning,[30] phase separation,[31] powder-forming,[32] hydrogel[33] and sol-gel techniques.[34] More recently, solid freeform fabrication techniques have been investigated that use computer aided design to model the scaffold to the desired structure[35] followed by fabrication through selective laser sintering,[36,37] laminated object manufacturing,[37] ink-jet or 3D printing,[38,39] or fused deposition modelling.[40]

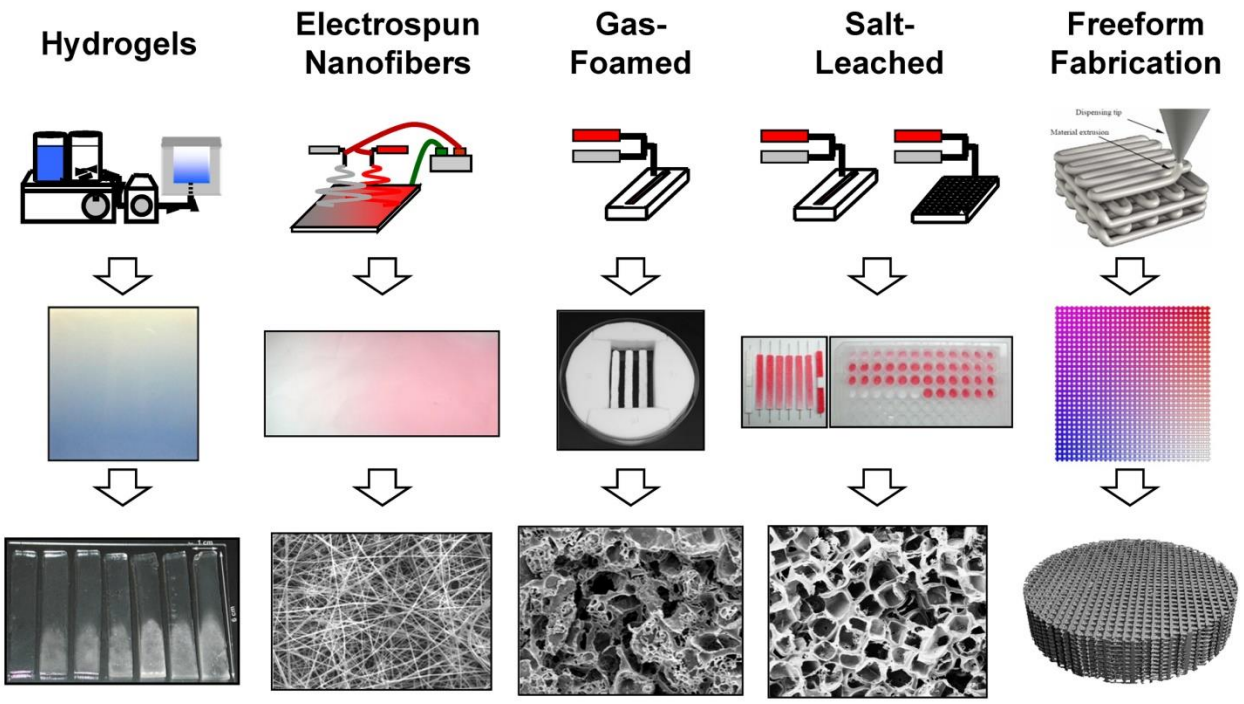

Figure 1.4. Common methods for polymer scaffold synthesis. Adapted with permission from Simon Jr., C.G. "3D Scaffold Libraries." U.S. Department of Commerce, National Institute of Standards and Technology, Material Measurement Laboratory, Biosystems and Biomaterials Division, Biomaterials Group.

Biodegradable polymers are generally highly biocompatible with PLA, PGA, PLGA, PCL, and poly(ethylene oxide) (PEO) approved by the U.S. Food and Drug administration with

degradation products that can be metabolized by the body.[33,41,42] The exception is in areas with low flow where acidic degradation products can lower the local pH and cause an inflammatory response.[42] Degradation of biodegradable polymers occurs through hydrolysis. This occurs through one of two ways depending on the polymer; bulk or surface degradation. Bulk degradation begins by random hydrolytic cleavage of polymer chains followed by weight loss due to diffusion of oligomers. Polymers that undergo surface erosion follow the same process as bulk degradation polymers though only where surface and water contact is made.[16]

Biodegradable polymers show much promise to match the requirements of the ideal scaffold.[6,21] However, little bioactivity and weak mechanical properties of most bioresorbable polymers are a major limitation toward application in bone tissue engineering.[16,43]

Composites

With the goal of increasing the mechanical strength of the biodegradable polymers, discussed above, for weight bearing applications, there has been increased research in incorporating reinforcing agents.[44-46] The advantage of a composite is two-fold; first is mechanical reinforcement, and second is the effect of the reinforcing material toward the interaction with the *in vivo* environment. Most biodegradable polymer scaffolds are osteoconductive, but lack bioactivity. The addition of bioactive fillers can increase the bioactivity of a scaffold. In addition to bioactivity, the concentration of reinforcing agents can also be used to alter the degradation rate of a construct.[16]

Ceramic and bioactive glass fillers have been extensively investigated as reinforcing agents for scaffolds.[24,47-56] The tough but brittle ceramic particles combined with flexible but weak polymers are synergistic, leading to increased compression modulus and yield strength of

composites.[47,50,52,56] Indeed, in a study of poly(D,L-lactide) (PDLLA) and PLGA reinforced with bioactive glass particles, the authors found that incorporation of glass particles significantly increased the rigidity of the composites compared to the neat polymers.[50] In addition to mechanical reinforcement, the addition of hydroxyapatite or bioactive glass has increased the deposition of apatite on scaffolds after incubation in simulated body fluid compared to polymer alone.[51,53,57] These reinforcing agents have also shown good biocompatibility and increased bone formation *in vitro*[48,51] and when implanted *in vivo*.[49]

Nanomaterials as Reinforcing Agents

To allow for further manipulation of the interactions of a bone tissue engineering scaffold with the surrounding native bone, nanomaterials have been utilized as reinforcing agents. Nanoparticles can be defined by dimensionality with zero-dimensional particles having no dimensions greater than 100 nm, one-dimensional particles having a single dimension greater than 100 nm, and two-dimensional particles having two dimensions greater than 100 nm.[58] The addition of nanomaterials to a scaffold harkens back to the hierarchical structure of bone, adding a nano-component for interactions with cells and other factors in the *in vivo* environment. In addition, due to their size and surface area, many nanomaterials can be used as probes for bioimaging or to deliver drugs or growth factors.[59] Hydroxyapatite nanoparticles are the most investigated due to their physical and chemical similarity to natural bone and osteointegrative properties, but metallic and ceramic nanoparticles such as titanium dioxide, alumoxane, and iron have also been incorporated into nanocomposites leading to increased mechanical properties and bioactivity without altering cytocompatibility or biocompatibility of the base material.[60-62] This

observed bioactivity of these nanocomposites may be due in great part to added nanotopography and improved surface hydrophilicity.[63,64]

Carbon-based and inorganic dichalcogenide nanoparticles, with varying nanomorphologies and interesting physicochemical properties have been investigated for applications in fields such as water filtration,[65] electronics,[66] optics,[67] solid lubrication,[68] and biomedicine.[69] Organic nanostructures, zero-dimensional fullerenes and one-dimensional single and multi-walled carbon nanotubes (SWCNT/MWCNT), known as some of the strongest materials in the world,[70] have been thoroughly investigated as reinforcing agents for biodegradable polymer nanocomposites.[45,71,72] These materials reinforce biodegradable polymers;[72-81] and may elicit bioactivity as described by Sitharaman et al. (Figure 1.5), who observed 200% greater bone ingrowth into ultra-short carbon nanotube reinforced PPF compared to PPF alone after 12 weeks implanted in a femoral condyle defect in a rabbit model.[63]

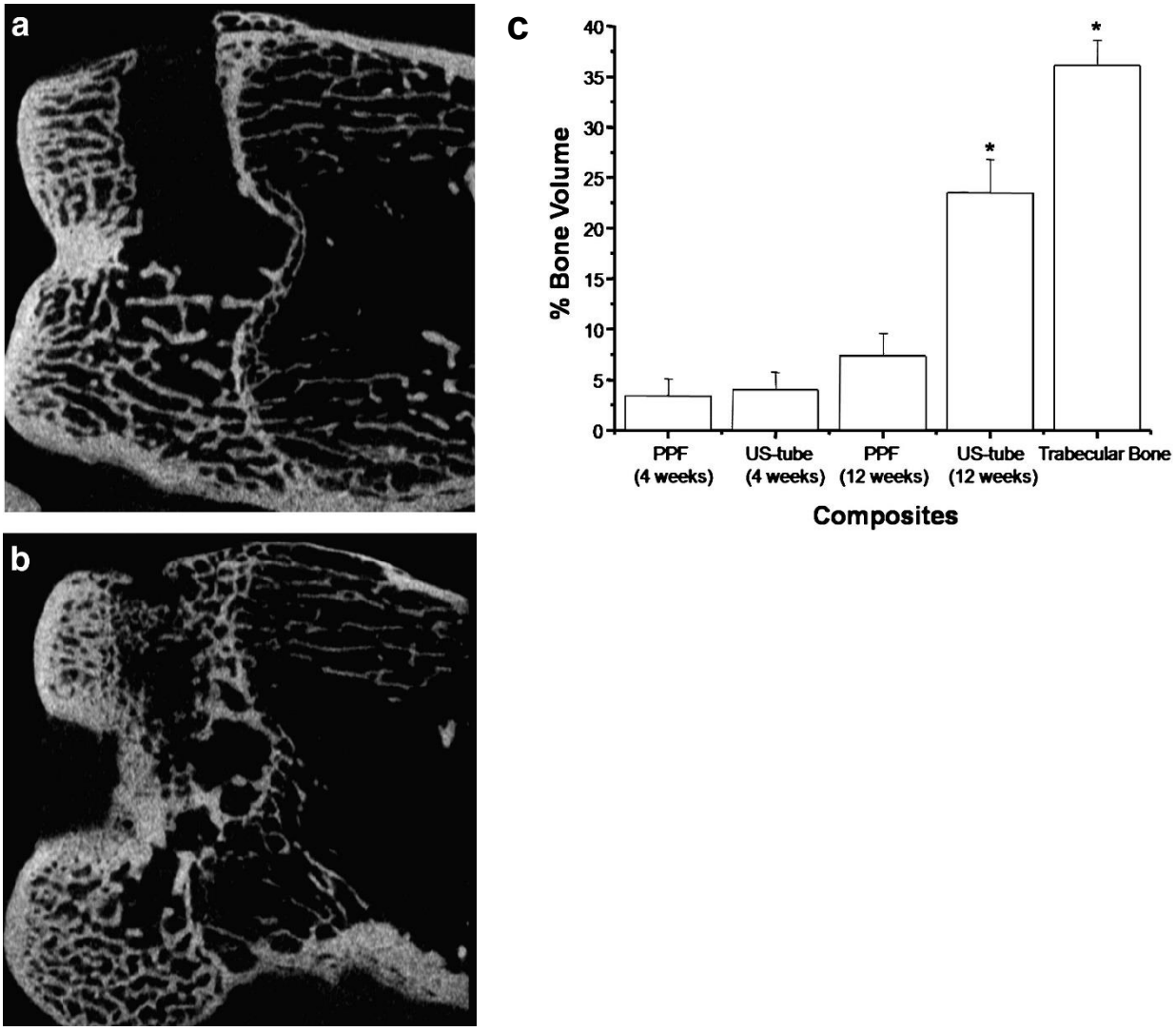

Figure 1.5. Image of bone ingrowth into (a) PPF and (b) ultra-short carbon nanotube reinforced PPF after 12 weeks implanted in a rabbit model. (c) MicroCT results of % bone area after 4 and 12 weeks compared to surrounding healthy trabecular bone. (*) indicates statistical significance compared to the other groups ($p<0.05$). Adapted with permission from Sitharaman, B. et al. "*In vivo* biocompatibility of ultra-short single-walled carbon nanotube/biodegradable polymer nanocomposites for bone tissue engineering." Bone, 2008. Copyright 2008 Elsevier Publishing Group.

In addition to added mechanical reinforcement, bioactivity, and drug delivery, the incorporation of carbon-based or inorganic dichalcogenide nanoparticles to nanocomposites may have further possibilities in bone tissue engineering due to their interesting physicochemical

properties. For instance, the electrical conductivity or optical properties of these particles may be able to be harnessed for electrical or photoacoustic stimulation therapy for bone regeneration.[82,83]

More recently, two-dimensional organic (single and multi-walled graphene oxide nanoribbons (SWGONR / MWGONR), graphene oxide nanoplatelets (GONP)) and one- and two-dimensional inorganic nanomaterials (tungsten disulfide nanotubes (WSNT), molybdenum disulfide nanoplatelets (MSNP)) were investigated for this application. Incorporation of 0.2 wt% of two-dimensional organic and one- or two-dimensional inorganic nanoparticles have led to enhancement of up to 108% in compressive modulus and 53% in flexural modulus of non-porous polypropylene fumarate (PPF) nanocomposites when compared to PPF alone or PPF reinforced with single or multi-walled carbon nanotubes. These increased mechanical properties are still lower than reported values for cortical bone but reach the levels of trabecular bone.[44,46] Moreover, all PPF nanocomposites showed little cytotoxicity to MC-3T3 preosteoblasts (78-100% viability) indicating possible biocompatibility.[84]

As biodegradable scaffolds resorb, incorporated nanoparticles are released into the extracellular matrix (ECM) and interact with surrounding tissue. Therefore, it is of the utmost importance to determine that released nanoparticles will not significantly affect the viability of exposed cells. While the cytocompatibility and biocompatibility of the above ceramic/glass and one-dimensional carbon-based nanoparticle reinforcing agents are well studied, the effects of two-dimensional organic and one- or two-dimensional inorganic dichalcogenide nanoparticles are less known. Only, the *in vitro* interactions of MWGONRs and GONPs with MSCs have previously been reported. This study found that incubating MSCs with concentrations of these particles less than 50 μg/ml for 24 hours did not significantly affect stem cell viability or differentiation capability.[85] However, the effects that a nanoparticle will have on cells and tissues

will vary depending on particle composition, morphology, and even synthesis method. Therefore, it is necessary to investigate the cytocompatibility and biocompatibility of all nanoparticles and their nanocomposites.

Conclusions and Motivation for this Work

Many materials and scaffold fabrication techniques have been used in attempt to create the ideal tissue engineering scaffold in order to overcome the limitations of current treatments. However, limitations of mechanical properties of available biodegradable ceramics and mechanical and bioactive properties of polymers have led to investigation of composite materials. While composites reinforced with ceramic particles have improved the mechanical properties and bioactivity of biodegradable polymers, further improvements could be made. Nanomaterials including zero and one-dimensional carbon-based nanoparticles with interesting physicochemical properties, including excellent mechanical properties, have also been investigated as scaffold reinforcing agents. These nanomaterials show promise in this capacity and may elicit bioactivity of the nanocomposites as well. Further studies of two-dimensional carbon-based and one- or two-dimensional inorganic dichalcogenide nanoparticles have shown even greater mechanical reinforcement but more studies of cytocompatibility and biocompatibility of these nanoparticles and nanocomposites are needed.

With the objective of finding a suitable scaffold for bone tissue engineering applications, it is the goal of this work to determine which nanoparticle chemistry and dimensionality provides the most promising results for application as a bone tissue engineering scaffold reinforcing agent. Toward this objective, we begin by determining potentially safe concentrations of MSNPs and

WSNTs for use as reinforcing agents in biodegradable polymer nanocomposites. We then investigate the bioactivity through evaluation of apatite collection on PLGA nanocomposite scaffolds reinforced with the two-dimensional organic (MWGONR and GONP) and inorganic (MSNP) nanoparticles that led to the greatest enhancement of mechanical properties (compressive and flexural modulus) when incorporated into non-porous PPF. Additionally, to investigate the effect of nanoparticle dimensionality, we include the one-dimensional organic (MWCNT) and inorganic (WSNT) nanoparticles that showed the highest mechanical properties. Finally, utilizing the information gained from these studies and previous work, we select the two most promising candidate nanoparticles, GONPs and MSNPs, and investigate the hard and soft tissue biocompatibility of nanocomposite scaffolds implanted in a non-critical sized tibial defect and subcutaneously on the dorsum of a rat model.

References

1 Nauth, A. *et al.* Managing bone defects. *Journal of Orthopaedic Trauma* **25**, 462-466 (2011).

2 Nishida, J. & Shimamura, T. Methods of reconstruction for bone defect after tumor excision: a review of alternatives. *Medical Science and Technology* **14**, RA107-RA113 (2008).

3 Zimmermann, G. & Moghaddam, A. *Trauma: non-union: new methods* in *European Instructional Lectures*. 15-19 (Springer, 2010).

4 Brydone, A., Meek, D. & Maclaine, S. Bone grafting, orthopaedic biomaterials, and the clinical need for bone engineering. *Proceedings of the Institution of Mechanical Engineers, Part H: Journal of Engineering in Medicine* **224**, 1329-1343 (2010).

5 Spicer, P. P. *et al.* Evaluation of bone regeneration using the rat critical size calvarial defect. *Nature Protocols* **7**, 1918-1929 (2012).

6 Amini, A. R., Laurencin, C. T. & Nukavarapu, S. P. Bone Tissue Engineering: Recent Advances and Challenges. *Critical Reviews in Biomedical Engineering* **40**, 363-408 (2012).

7 Finkemeier, C. G. Bone-grafting and bone-graft substitutes. *Journal of Bone and Joint Surgery. American Volume.* **84-A**, 454-464 (2002).

8 Dodd, C., Fergusson, C., Freedman, L., Houghton, G. & Thomas, D. Allograft versus autograft bone in scoliosis surgery. *Journal of Bone and Joint Surgery. British Volume* **70**, 431-434 (1988).

9 Culpepper, B. K., Morris, D. S., Prevelige, P. E. & Bellis, S. L. Engineering nanocages with polyglutamate domains for coupling to hydroxyapatite biomaterials and allograft bone. *Biomaterials* **34**, 2455-2462 (2013).

10 Kini, U. & Nandeesh, B. N. *Physiology of bone formation, remodeling, and metabolism* in *Radionuclide and Hybrid Bone Imaging*. 29-57, (Springer, 2012).

11 Rho, J.-Y., Kuhn-Spearing, L. & Zioupos, P. Mechanical properties and the hierarchical structure of bone. *Medical Engineering & Physics* **20**, 92-102 (1998).

12 Yang, Y. Skeletal morphogenesis during embryonic development. *Critical Reviews in Eukaryotic Gene Expression* **19**, 197-218 (2009).

13 Fazzalari, N. L. Bone fracture and bone fracture repair. *Osteoporosis International: a journal established as result of cooperation between the European Foundation for Osteoporosis and the National Osteoporosis Foundation of the USA* **22**, 2003-2006 (2011).

14 Hankenson, K. D., Gagne, K. & Shaughnessy, M. Extracellular signaling molecules to promote fracture healing and bone regeneration. *Advanced Drug Delivery Reviews* **94**, 3-12 (2015).

15 Blokhuis, T. & Arts, J. C. Bioactive and osteoinductive bone graft substitutes: definitions, facts and myths. *Injury* **42**, S26-S29 (2011).

16 Rezwan, K., Chen, Q., Blaker, J. & Boccaccini, A. R. Biodegradable and bioactive porous polymer/inorganic composite scaffolds for bone tissue engineering. *Biomaterials* **27**, 3413-3431 (2006).

17 Hutmacher, D. W., Schantz, J. T., Lam, C. X. F., Tan, K. C. & Lim, T. C. State of the art and future directions of scaffold-based bone engineering from a biomaterials perspective. *Journal of Tissue Engineering and Regenerative Medicine* **1**, 245-260 (2007).

18 Kokubo, T., Kim, H.-M. & Kawashita, M. Novel bioactive materials with different mechanical properties. *Biomaterials* **24**, 2161-2175 (2003).

19 Hollister, S. J., Maddox, R. & Taboas, J. M. Optimal design and fabrication of scaffolds to mimic tissue properties and satisfy biological constraints. *Biomaterials* **23**, 4095-4103 (2002).

20 Wagoner Johnson, A. J. & Herschler, B. A. A review of the mechanical behavior of CaP and CaP/polymer composites for applications in bone replacement and repair. *Acta Biomaterialia* **7**, 16-30 (2011).

21 Hutmacher, D. W. Scaffolds in tissue engineering bone and cartilage. *Biomaterials* **21**, 2529-2543, (2000).

22 Yuan, H., de Bruijn, J. D., Zhang, X., van Blitterswijk, C. A. & de Groot, K. Bone induction by porous glass ceramic made from Bioglass® (45S5). *Journal of Biomedical Materials Research* **58**, 270-276 (2001).

23 Jones, J. R. & Hench, L. L. Factors affecting the structure and properties of bioactive foam scaffolds for tissue engineering. *Journal of Biomedical Materials Research Part B: Applied Biomaterials* **68B**, 36-44 (2004).

24 Chen, Q. Z., Thompson, I. D. & Boccaccini, A. R. 45S5 Bioglass®-derived glass–ceramic scaffolds for bone tissue engineering. *Biomaterials* **27**, 2414-2425 (2006).

25 Marcacci, M. *et al.* Stem cells associated with macroporous bioceramics for long bone repair: 6- to 7-year outcome of a pilot clinical study. *Tissue Engineering* **13**, 947-955 (2007).

26 Jones, J. R. Review of bioactive glass: From Hench to hybrids. *Acta Biomaterialia* **9**, 4457-4486 (2013).

27 Liu, X. & Ma, P. X. Polymeric scaffolds for bone tissue engineering. *Annals of Biomedical Engineering* **32**, 477-486 (2004).

28 Nam, Y. S., Yoon, J. J. & Park, T. G. A novel fabrication method of macroporous biodegradable polymer scaffolds using gas foaming salt as a porogen additive. *Journal of Biomedical Material Research* **53**, 1-7 (2000).

29 Wu, X. *et al.* Preparation of aligned porous gelatin scaffolds by unidirectional freeze-drying method. *Acta Biomaterialia* **6**, 1167-1177 (2010).

30 Yoshimoto, H., Shin, Y., Terai, H. & Vacanti, J. A biodegradable nanofiber scaffold by electrospinning and its potential for bone tissue engineering. *Biomaterials* **24**, 2077-2082 (2003).

31 Nam, Y. S. & Park, T. G. Porous biodegradable polymeric scaffolds prepared by thermally induced phase separation. *Journal of Biomedical Material Research* **47**, 8-17 (1999).

32 Chen, Q.-Z. & Thouas, G. A. Fabrication and characterization of sol–gel derived 45S5 Bioglass®–ceramic scaffolds. *Acta biomaterialia* **7**, 3616-3626 (2011).

33 Drury, J. L. & Mooney, D. J. Hydrogels for tissue engineering: scaffold design variables and applications. *Biomaterials* **24**, 4337-4351 (2003).

34 Pereira, M. M., Jones, J. R. & Hench, L. L. Bioactive glass and hybrid scaffolds prepared by sol–gel method for bone tissue engineering. *Advances in Applied Ceramics* **104**, 35-42 (2005).

35 Thavornyutikarn, B., Chantarapanich, N., Sitthiseripratip, K., Thouas, G. A. & Chen, Q. Bone tissue engineering scaffolding: computer-aided scaffolding techniques. *Progress in Biomaterials* **3**, 61-102 (2014).

36 Williams, J. M. *et al.* Bone tissue engineering using polycaprolactone scaffolds fabricated via selective laser sintering. *Biomaterials* **26**, 4817-4827 (2005).

37 Yang, S., Leong, K.-F., Du, Z. & Chua, C.-K. The design of scaffolds for use in tissue engineering. Part II. Rapid prototyping techniques. *Tissue Engineering* **8**, 1-11 (2002).

38 Lam, C. X. F., Mo, X., Teoh, S.-H. & Hutmacher, D. Scaffold development using 3D printing with a starch-based polymer. *Materials Science and Engineering: C* **20**, 49-56 (2002).

39 Patel, S. C., Lalwani, G., Grover, K., Qin, Y.-X. & Sitharaman, B. Fabrication and cytocompatibility of in situ crosslinked carbon nanomaterial films. *Scientific Reports* **5**, doi:10.1038/srep10261 (2015).

40 Zein, I., Hutmacher, D. W., Tan, K. C. & Teoh, S. H. Fused deposition modeling of novel scaffold architectures for tissue engineering applications. *Biomaterials* **23**, 1169-1185 (2002).

41 Sung, H. J., Meredith, C., Johnson, C. & Galis, Z. S. The effect of scaffold degradation rate on three-dimensional cell growth and angiogenesis. *Biomaterials* **25**, 5735-5742 (2004).

42 Liu, H., Slamovich, E. B. & Webster, T. J. Less harmful acidic degradation of poly(lactic-co-glycolic acid) bone tissue engineering scaffolds through titania nanoparticle addition. *International Journal of Nanomedicine* **1**, 541-545 (2006).

43 Rhee, S.-H. & Lee, S. J. Effect of acidic degradation products of poly(lactic-co-glycolic)acid on the apatite-forming ability of poly(lactic-co-glycolic)acid-siloxane nanohybrid material. *Journal of Biomedical Materials Research, Part A* **83A**, 799-805 (2007).

44 Lalwani, G. *et al.* Two-dimensional nanostructure- reinforced biodegradable polymeric nanocomposites for bone tissue engineering. *Biomacromolecules* **14**, 900-909 (2013).

45 Shi, X. *et al.* Fabrication of porous ultra-short single-walled carbon nanotube nanocomposite scaffolds for bone tissue engineering. *Biomaterials* **28**, 4078-4090 (2007).

46 Lalwani, G. *et al.* Tungsten disulfide nanotubes reinforced biodegradable polymers for bone tissue engineering. *Acta Biomaterialia* **9**, 8365-8373 (2013).

47 Kothapalli, C. R., Shaw, M. T. & Wei, M. Biodegradable HA-PLA 3-D porous scaffolds: Effect of nano-sized filler content on scaffold properties. *Acta Biomaterialia* **1**, 653-662 (2005).

48 Ma, P. X., Zhang, R., Xiao, G. & Franceschi, R. Engineering new bone tissue *in vitro* on highly porous poly(alpha-hydroxyl acids)/hydroxyapatite composite scaffolds. *Journal of Biomedical Materials Research* **54**, 284-293 (2001).

49 Higashi, S. *et al.* Polymer-hydroxyapatite composites for biodegradable bone fillers. *Biomaterials* **7**, 183-187 (1986).

50 Maquet, V., Boccaccini, A. R., Pravata, L., Notingher, I. & Jérôme, R. Porous poly(α-hydroxyacid)/Bioglass® composite scaffolds for bone tissue engineering. I: preparation and *in vitro* characterisation. *Biomaterials* **25**, 4185-4194 (2004).

51 Kim, S.-S., Park, M. S., Gwak, S.-J., Choi, C. Y. & Kim, B.-S. Accelerated bonelike apatite growth on porous polymer/ceramic composite scaffolds *in vitro*. *Tissue Engineering* **12**, 2997-3006 (2006).

52 Boccaccini, A. R. & Maquet, V. Bioresorbable and bioactive polymer/Bioglass® composites with tailored pore structure for tissue engineering applications. *Composites Science and Technology* **63**, 2417-2429 (2003).

53 Roether, J. A. *et al.* Development and *in vitro* characterisation of novel bioresorbable and bioactive composite materials based on polylactide foams and Bioglass® for tissue engineering applications. *Biomaterials* **23**, 3871-3878 (2002).

54 Hong, Z., Reis, R. L. & Mano, J. F. Preparation and *in vitro* characterization of scaffolds of poly(l-lactic acid) containing bioactive glass ceramic nanoparticles. *Acta Biomaterialia* **4**, 1297-1306 (2008).

55 Dorj, B. *et al.* Robocasting nanocomposite scaffolds of poly(caprolactone)/hydroxyapatite incorporating modified carbon nanotubes for hard tissue reconstruction. *Journal of Biomedical Materials Research, Part A* **101**, 1670-1681 (2013).

56 Mistry, A. S., Mikos, A. G. & Jansen, J. A. Degradation and biocompatibility of a poly(propylene fumarate)-based/alumoxane nanocomposite for bone tissue engineering. *Journal of Biomedical Materials Research, Part A* **83A**, 940-953 (2007).

57 Zhang, R. & Ma, P. X. Porous poly (L-lactic acid)/apatite composites created by biomimetic process. *Journal of Biomedical Materials Research* **45**, 285-293 (1999).

58 Tiwari, J. N., Tiwari, R. N. & Kim, K. S. Zero-dimensional, one-dimensional, two-dimensional and three-dimensional nanostructured materials for advanced electrochemical energy devices. *Progress in Materials Science* **57**, 724-803 (2012).

59 Wahajuddin, S. A. Superparamagnetic iron oxide nanoparticles: magnetic nanoplatforms as drug carriers. *International Journal of Nanomedicine* **7**, 3445 (2012).

60 Gerhardt, L.-C., Jell, G. & Boccaccini, A. Titanium dioxide (TiO_2) nanoparticles filled poly(D, L lactid acid) (PDLLA) matrix composites for bone tissue engineering. *Journal of Materials Science: Materials in Medicine* **18**, 1287-1298 (2007).

61 Mistry, A. S. *et al. In vivo* bone biocompatibility and degradation of porous fumarate-based polymer/alumoxane nanocomposites for bone tissue engineering. *Journal of Biomedical Materials Research, Part A* **92**, 451-462 (2010).

62 Tran, N. & Webster, T. J. Increased osteoblast functions in the presence of hydroxyapatite-coated iron oxide nanoparticles. *Acta Biomaterialia* **7**, 1298-1306 (2011).

63 Sitharaman, B. *et al. In vivo* biocompatibility of ultra-short single-walled carbon nanotube/biodegradable polymer nanocomposites for bone tissue engineering. *Bone* **43**, 362-370 (2008).

64 Dorj, B. *et al.* Robocasting nanocomposite scaffolds of poly(caprolactone)/hydroxyapatite incorporating modified carbon nanotubes for hard tissue reconstruction. *Journal of Biomedical Materials Research, Part A* **101A**, 1670-1681 (2013).

65 Savage, N. & Diallo, M. S. Nanomaterials and water purification: opportunities and challenges. *Journal of Nanoparticle Research* **7**, 331-342 (2005).

66 Wang, C., Takei, K., Takahashi, T. & Javey, A. Carbon nanotube electronics–moving forward. *Chemical Society Reviews* **42**, 2592-2609 (2013).

67 Lee, H. S. *et al.* MoS_2 nanosheet phototransistors with thickness-modulated optical energy gap. *Nano Letters* **12**, 3695-3700 (2012).

68 Dallavalle, M., Sandig, N. & Zerbetto, F. Stability, dynamics, and lubrication of MoS_2 platelets and nanotubes. *Langmuir* **28**, 7393-7400 (2012).

69 Dubey, N. *et al.* Graphene: a versatile carbon-based material for bone tissue engineering. *Stem Cells International* **2015**, 804213 (2015).

70 Treacy, M. J., Ebbesen, T. & Gibson, J. Exceptionally high Young's modulus observed for individual carbon nanotubes. *Nature* **381**, 678-680 (1996).

71 Shi, X. *et al.* Rheological behaviour and mechanical characterization of injectable poly (propylene fumarate)/single-walled carbon nanotube composites for bone tissue engineering. *Nanotechnology* **16**, S531 (2005).

72 Sitharaman, B. *et al.* Injectable in situ cross-linkable nanocomposites of biodegradable polymers and carbon nanostructures for bone tissue engineering. *Journal of Biomaterials Science, Polymer Edition* **18**, 655-671 (2007).

73 Jell, G. *et al.* Carbon nanotube-enhanced polyurethane scaffolds fabricated by thermally induced phase separation. *Journal of Materials Chemistry* **18**, 1865-1872 (2008).

74 Lau, C., Cooney, M. J. & Atanassov, P. Conductive macroporous composite chitosan− carbon nanotube scaffolds. *Langmuir* **24**, 7004-7010 (2008).

75 Ma, P.-C., Siddiqui, N. A., Marom, G. & Kim, J.-K. Dispersion and functionalization of carbon nanotubes for polymer-based nanocomposites: a review. *Composites Part A: Applied Science and Manufacturing* **41**, 1345-1367 (2010).

76 MacDonald, R. A., Laurenzi, B. F., Viswanathan, G., Ajayan, P. M. & Stegemann, J. P. Collagen–carbon nanotube composite materials as scaffolds in tissue engineering. *Journal of Biomedical Materials Research, Part A* **74**, 489-496 (2005).

77 Sahithi, K., Swetha, M., Ramasamy, K., Srinivasan, N. & Selvamurugan, N. Polymeric composites containing carbon nanotubes for bone tissue engineering. *International Journal of Biological Macromolecules* **46**, 281-283 (2010).

78 Shi, X. *et al.* Injectable nanocomposites of single-walled carbon nanotubes and biodegradable polymers for bone tissue engineering. *Biomacromolecules* **7**, 2237-2242 (2006).

79 Venkatesan, J., Ryu, B., Sudha, P. & Kim, S.-K. Preparation and characterization of chitosan–carbon nanotube scaffolds for bone tissue engineering. *International Journal of Biological Macromolecules* **50**, 393-402 (2012).

80 Gupta, A. *et al.* Biocompatibility of single-walled carbon nanotube composites for bone regeneration. *Bone and Joint Research* **4**, 70-77 (2015).

81 Paiyz, E. M. *et al.* Functionalized carbon nanotube reinforced scaffolds for bone regenerative engineering: fabrication, *in vitro* and *in vivo* evaluation. *Biomedical Materials* **9**, 035001 (2014).

82 Boccaccini, A. R. *et al.* Carbon nanotube coatings on bioglass-based tissue engineering scaffolds. *Advanced Functional Materials* **17**, 2815-2822 (2007).

83 Sitharaman, B., Avti, P. K., Schaefer, K., Talukdar, Y. & Longtin, J. P. A novel nanoparticle-enhanced photoacoustic stimulus for bone tissue engineering. *Tissue Engineering Part A* **17**, 1851-1858 (2011).

84 Farshid, B., Lalwani, G. & Sitharaman, B. *In vitro* cytocompatibility of one-dimensional and two-dimensional nanostructure-reinforced biodegradable polymeric nanocomposites. *Journal of Biomedical Materials Research, Part A* **103**, 2309-2321 (2015).

85 Talukdar, Y., Rashkow, J. T., Lalwani, G., Kanakia, S. & Sitharaman, B. The effects of graphene nanostructures on mesenchymal stem cells. *Biomaterials* **35**, 4863-4877 (2014).

Chapter 2

Interactions of One- and Two-Dimensional Layered Inorganic Nanoparticles with Fibroblasts and Human Mesenchymal Stem Cells

Portions of this chapter have been reproduced from:

Jason T. Rashkow, Yahfi Talukdar, Gaurav Lalwani, Balaji Sitharaman. "Interactions of One and Two Dimensional Layered Inorganic Nanoparticles with Fibroblasts and Human Mesenchymal Stem Cells." *Future Medicine: Nanomedicine* 10 (11), 1693-1706 (2015).

*The authors listed in the above manuscript have contributions towards the data reported in this chapter

Abstract

This study investigates the effects of tungsten disulfide nanotubes (WSNTs) and molybdenum disulfide nanoplatelets (MSNPs) on fibroblasts (NIH-3T3) and mesenchymal stem cells (MSCs) to determine safe dosages for potential biomedical applications. Cytotoxicity of MSNPs and WSNTs (5–300 μg/ml) on NIH-3T3 and MSCs was assessed at 6, 12 or 24 h. MSC differentiation to adipocytes and osteoblasts was assessed following treatment for 24 h. Only NIH-3T3 cells treated with MSNPs showed dose or time dependent increase in cytotoxicity. Differentiation markers of MSCs in treated groups were unaffected compared with untreated controls. MSNPs and WSNTs at concentrations less than 50 μg/ml are potentially safe for treatment of fibroblasts or MSCs for up to 24 h.

Introduction

Layered transition metal dichalcogenides such as the one dimensional (1D) tungsten disulfide nanotubes (WSNTs) and two dimensional (2D) molybdenum disulfide nanoplatelets (MSNPs), analogous to carbon nanotubes and graphene, exhibit interesting physiochemical properties that have been harnessed for tribiological, optical, and electronic applications [1-3]. For instance, these nanomaterials are excellent lubricants even in the absence of moisture or at high temperatures.[4,5] Therefore, when included as lubrication additives to motor oils, the combustion of these oils in motor vehicles and oil waste plants will lead to higher environmental exposure of these nanoparticles. For biomedical applications, MSNPs and WSNTs have been proposed for potential use as additives to lubricants used on catheters and coatings for orthodontic or orthopedic implants and wires.[5-8] Recently, we have investigated these nanomaterials as reinforcing agents in polymer nanocomposites for bone tissue engineering.[9,10] For this application, the mechanical properties of the nanocomposites should ideally be similar to that of native bone tissue.[11] Our results indicate that, compared to carbon nanoparticles such as graphene and carbon nanotubes, these inorganic nanoparticles are more efficacious as reinforcing agents. Additionally, these inorganic nanoparticles due to their large surface area could serve as a versatile scaffold to append drugs, genetic material and imaging agents.

The possible environmental impact and potential biomedical applications of WSNTs and MSNPs necessitates thorough evaluation of their cyto- and biocompatibility. Few studies have reported the toxicity of these inorganic nanoparticles compared to carbon nanoparticles such as carbon nanotubes and graphene.[12-16] These reports investigated *in vitro* the interaction and effects of WSNTs and MSNPs on cells environmental exposure through inhalation or ingestion.[6,17]

Pardo *et al.* investigated the cytotoxicity of WSNTs and MSNPs towards lung fibroblasts, human liver cells and macrophages. Their results indicated no toxicity and minimal immune response from exposure to WSNTs or MSNPs at concentrations ranging from 0 to 100 μg/ml.[17] Additionally, MSNP particles were found to be relatively non-toxic (~100% survivability) to human epidermal fibroblasts, lung adenocarcinoma cells, and leukemic cells at concentrations ranging from 0 to 3.52 mg/L.[6] While these studies provide some insights on the effects of these nanoparticles under environmental exposure conditions, additional investigations are needed to examine their response on biological systems (e.g. cells, tissues) to determine the potentially safe doses relevant for biomedical applications.

An important cell type these nanoparticles will interact with when utilized for biomedical applications is the mesenchymal stem cell (MSC). MSCs are multipotent adult or somatic stem cells that readily differentiate into cells of various tissues such as osteoblasts, adipocytes and chondrocytes, and are critical for the in the regeneration / restoration of these tissue types.[18] Recent studies also show that MSCs assist the expansion of hematopoietic stem cell or embryonic stem cell cultures.[19] These attributes of MSCs are being utilized in the development of therapies to repair, regenerate and restore damaged tissues. The *in vitro* interactions of MSCs with a variety of metallic, carbon, ceramic, and polymeric nanoparticles have also been reported for stem cell applications.[20-23] However, the effects of transition metal dichalcogenides on MSC viability and differentiation are yet to be reported.

In this study, we have assessed the *in vitro* response of NIH-3T3 cells and MSCs to treatment with WSNTs and MSNPs dispersed in 1,2-Distearoyl-sn-Glycero-3-Phosphoethanolamine conjugated with polyethylene glycol (DSPE-PEG). We report the dose- and time-dependent cytotoxicity of these inorganic nanoparticles on NIH-3T3 cells and MSCs,

their effect on MSC differentiation capability, and characterize the intracellular distribution of these nanoparticles to determine potentially safe dosages for biomedical applications.

Materials and Methods

Nanoparticles

Molybdenum trioxide (MoO_3) and sulfur (S) powder was purchased from Sigma-Aldrich. MSNPs were synthesized as mentioned previously.[24] Briefly, we added MoO_3 and sulfur to an alumina crucible and placed it in a horizontal tube furnace. Prior to heating, the tube was evacuated by nitrogen gas (N_2) flow for 30 min. The furnace was then heated to 700 ^oC for 2.5 hours under N_2 atmosphere. After 2.5 hours, the furnace was allowed to cool back to room temperature under N_2 atmosphere. The product was further annealed in the furnace to 1000 ^oC for 1 hour under N_2 atmosphere. Once the furnace cooled back to room temperature, we collected the silvery black MSNPs from the crucible. WSNTs were purchased from APNano (NY, USA).

Nanoparticle Characterization

Transmission electron microscopy (TEM) was done to characterize the morphology and structure of the nanoparticles. Samples for TEM were prepared as follows. Nanoparticles were added to a solution of water and 100% ethanol at a ratio of 1:1, to obtain a concentration of ~ 1 mg/ml. This solution was dispersed by probe sonication (Cole Parmer Ultrasonicator LPX 750) using a 1 sec “on”, 2 sec “off” cycle for one minute. The solution was centrifuged at 10,000 rpm for 5 minutes and the supernatant was collected and drop cast on a lacey carbon grid (300 mesh size, copper support, Ted Pella, CA, USA). TEM was performed on a JOEL 2100F high-resolution analytical transmission electron microscope with an accelerating voltage of 200 kV.

Raman spectroscopy was employed to identify the nanoparticles based on characteristic spectral analysis. The nanoparticles were added to isopropanol at a concentration of about 1

mg/ml. The samples were sonicated for 30 minutes to disperse the particles and were then drop cast onto a silicon wafer (Type P: (Boron), Orientation <100>, Ted Pella). Raman spectra were obtained on a 532 nm Nd-YAG excitation laser equipped WITec alpha300R Micro-Imaging Raman Spectrometer (TN, USA). Spectra were recorded between 50 -3750 cm^{-1} at room temperature.

Cell Culture

Mouse embryo fibroblast cell line (NIH-3T3) and human adipose derived stem cells (MSCs) (Lifeline Cat No. FC-0034) isolated from lipoaspirate were used for this study. Dulbecco's Modified Eagle's Medium (DMEM) media (Invitrogen, Cat No. 12491-015) with 10% fetal bovine serum and 1% penicillin streptomycin was used for cell culture of NIH-3T3 cells, while StemLifeTM MSC medium (Lifeline, Cat No. LL-0034) was used for stem cell cultures. Media was changed every 2-3 days and the cells were incubated at 37 $^{\circ}C$ and 5% CO_2 throughout the experiment. Passages 4-8 of MSCs were used for the studies.

Cytotoxicity Assays

Presto Blue (Invitrogen, Grand Island, NY), and Lactate Dehydrogenase (LDH, Sigma-Aldrich) assays were used to assess cytotoxicity of MSNPs and WSNTs on NIH-3T3 and MSCs. Cells were seeded in 96-well plates at a density of 10,000 cells/well. Nanoparticles were coated with DSPE-PEG to impart water-dispersibility. MSNPs or WSNTs nanoparticle dispersions (10 vol%) were added 24 hours after plating to bring the final concentrations of MSNPs and WSNTs in culture media to 0 μg/ml (DSPE-PEG), 5 μg/ml, 10 μg/ml, 50 μg/ml, 100 μg/ml, and 300 μg/ml. For Presto Blue assay, we used untreated cells and cells treated with ice-cold methanol for 30 minutes as positive and negative controls respectively. Acellular dispersions of MSNPs

and WSNTs were used to determine interference in fluorescence intensity by the presence of nanoparticles. We performed the assays at 6, 12 and 24 hours following treatment (n=6) with the nanoparticle dispersions. For Presto Blue assay at each time point the wells were washed with phosphate buffered saline (PBS) and 90 µl of fresh media followed by 10µl of Presto Blue reagent was added. The plate was incubated for 2 hours at 37 ^{o}C. The fluorescence was measured at 580 nm emission with 530 nm excitation.

We performed LDH assays as described in the protocol provided in the Tox-7 kit (Sigma-Aldrich). Briefly, following incubation with nanoparticle dispersions, the culture plates were centrifuged at 250 g for 5 minutes and aliquots of 100 µl of media from each well was removed and placed on a flat bottom 96-well plate. We prepared LDH assay mixture by mixing equal amounts of assay substrate, enzyme and dye solution and added 50 µl of assay mixture to each well containing 100 µl of culture media. Then we covered the plates with foil to protect them from light. Following 30 minutes of incubation, we added 15 µl of 1 N hydrochloric acid to each well to stop the reaction. We measured absorbance of each well at 490 nm and subtracted background measurements taken at 690 nm. For LDH assay, we used groups treated with lysis buffer and untreated cells as positive and negative controls respectively.

MSC Differentiation

MSCs were plated in 24-well plates at a density of 20,000 cells/well. Cells were treated with DSPE-PEG or nanoparticle solutions of 10 µg/ml or 50 µg/ml concentrations. After 24 hours of treatment, cells were washed and osteogenic or adipogenic differentiation media (hMSC Osteogenic / Adipogenic BulletKit, Lonza, Switzerland) was added. MSCs were maintained with media changes every 2-3 days for 14 days for osteogenic media. Following incubation, media was removed; wells were washed with PBS and filled with 2 ml DI water. Cell lysate, prepared

by sonicating the wells in a bath sonicator for 5 minutes, was used for analyzing cell number, alkaline phosphatase (ALP) activity, and calcium content. Alizarin Red S staining was performed in a separate set of wells for qualitative analysis. For adipogenic differentiation, adipogenic induction media was used for the first three media changes followed by incubation with adipogenic maintenance media for a total of 21 days. Once differentiation media cycles were complete, adipogenic differentiation was analyzed by Oil Red O staining and elution.

Oil Red O

Following incubation with adipogenic differentiation media, cells were washed with 1ml of PBS. 1 ml of 4% paraformaldehyde was added for fixation and incubated for 10 min at room temperature. Paraformaldehyde was removed and fresh 1 ml of 4% paraformaldehyde was added and incubated for 1 hr. Once fixed, paraformaldehyde was removed and cells were washed twice with deionized water and then washed with 60% isopropanol for 5 min at room temperature. Cells were then allowed to dry completely before addition of 0.5 ml Oil Red O working solution, two parts Oil Red O stock solution (0.35% solution in isopropanol) with three parts isopropanol and incubation for 10 min. After incubation, Oil Red O solution was removed and cells were washed with deionized water four times. Images of Oil Red O staining were acquired on BX-51 Olympus microscope (Hamburg, Germany). Oil Red O stain was then eluted by addition of 100% isopropanol and incubation for 10 min with shaking. Absorbance of aspirated isopropanol was measured at 500 nm (Varioskan Flash, Thermo Electron, Finland) with 100% isopropanol serving as blank.

Alizarin Red S

To observe mineralization in MSCs differentiated to osteoblasts, we stained the culture wells with Alizarin Red S. We removed the osteogenic media and washed the wells with PBS before fixing and staining. We fixed the cells with 1 ml of 4% paraformaldehyde at room temperature for 15 min. After incubation, cells were washed with deionized water two times and 40 mM Alizarin Red S dye (adjusted to pH of 4.1 using 0.5 N ammonium hydroxide) was added in each well. Plates were incubated while shaking at room temperature for 20 min. Dye was removed and MSCs were washed with deionized water four times with shaking for 5 min. Cell staining was observed using a BX-51 Olympus microscope (Hamburg, Germany).

Cell Number

DNA in cell lysate was used to determine the number of cells per well with Quantifluor Dye Systems (Progmega, Madison, WI). A standard curve of known number of MSCs was used to determine the number of cells per well. A hundred microliters of 1x TE buffer was added to 100 µl of a QuantiFluor dye working solution. The mixture was then added to 100 µl of cell lysate in a 96 well plate, covered with foil and incubated at room temperature for 10 minutes. Fluorescence was measured at an excitation wavelength of 480 nm and an emission wavelength of 570 nm and data was presented as average number of cells per well.

Alkaline Phosphatase (ALP) Activity

ALP activity was presented as ALP activity in µmol per minute per cell. To measure ALP activity, 100 µl of p-Nitrophenyl Phosphate (pNPP) was added to a 96-well plate containing 100 µl of 4 nitrophenol standard or cell lysate in triplicate and was incubated for 1 hour at 37 °C.

Post incubation, 100 µl of 0.2M NaOH stop solution was added and absorbance was measured at 405 nm (Varioskan Flash, Thermo Electron, Finland). Data for ALP was presented as µmol/ min/ cell.

Extracellular Calcium

To quantify the extracellular calcium in each well, we added 100 µl of 1 M acetic acid to 100 µl of cell lysate and placed the mixture on a shaker overnight. We placed 20 µl of the sample mixture or calcium chloride standard in 96-well plate and added 280 µl of Arsenazo III Calcium Assay reagent. Samples from each well were analyzed in triplicates. We measured absorbance of each well at 650 nm (Varioskan Flash, Thermo Electron, Finland).

Nanoparticle Uptake

MSCs, cultured on ACLAR films (Ted Pella), were treated with 10 volume percent of 50 µg/ml MSNP or WSNT dispersions for 24 hours. Media was then removed and cells were washed with PBS and fixed using 1 ml of 1% gluteraldehyde for 1 hour after which 1% osmium tetroxide in 0.1 M PBS was added. After fixation, cells were dehydrated in graded ethanol washes and embedded in Durcupan resin (Sigma Life Science). The samples were cut in to 80 nm sections using a Reichert-Jung UltracutE ultramicrotome (NY, USA) and were then placed on formvar coated slot copper grids. The sections were counterstained with uranyl acetate and lead citrate. We imaged the samples using a JOEL-JEM-1400 transmission electron microscope (MA, USA) with a Gatan CCD Digital Camera system (CA, USA).

Statistics

All graphs are presented as average ± standard deviation. For viability assays, one-way ANOVA with Tukey post hoc was used to analyze significance. Differences with $p<0.05$ were considered significant. For Differentiation assays, Kruskal-Wallace test with Dunn post hoc was performed to analyze significance of differences between the groups with $p<0.05$ considered statistically significant.

Results

Nanoparticle Characterization

Figure 2.1 shows representative TEM images of MSNPs and WSNTs. MSNPs (Figure 2.1 A) are circular platelet shaped particles with diameters ranging from 60-90 nm and 8 nm thickness [9]. WSNTs (Figure 2.1 B) are smooth nanotube structures with diameters of 50-100 nm and lengths ranging from 1-15 μm. Raman spectra for the two nanomaterials, presented in Figure 2.1 C, shows clear bands at 378 cm^{-1}, 404 cm^{-1}, and 476 cm^{-1} for MSNPs and bands at 344 cm^{-1} and 414 cm^{-1} for WSNTs. The two major bands in the spectra for both nanoparticles signify the $E_{2g}{}^1$ and A_{1g} Raman active modes. The band at 476 cm^{-1} in the MSNP spectrum is due to unreacted MoO_3.

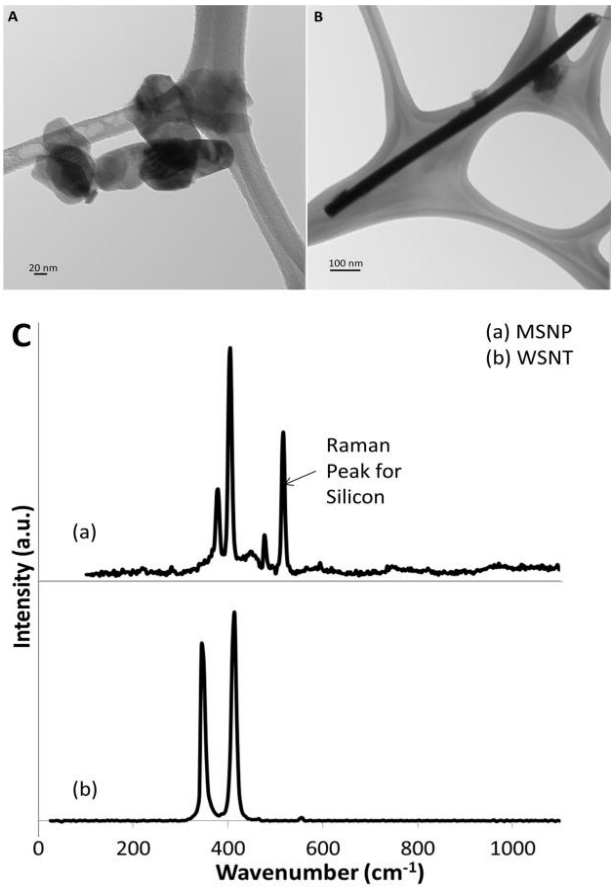

Figure 2.1. Representative TEM images of MSNPs (A) and WSNTs (B). (C) Representative Raman spectra of MSNPs (a) and WSNTs (b).

Cytotoxicity

Presto Blue

Presto Blue is a resazurin based viability assay that works due to reduction of non-fluorescent resazurin to fluorescent resorufin by live cells. Figure 2.2 A and B shows viability of NIH-3T3 and MSCs treated with MSNPs at 5, 10, 50, 100 and 300 µg/ml concentrations for 6, 12 and 24 hours normalized to untreated controls. All dispersions were stable and did not settle to the bottom of the plate during the entire study duration. At concentrations below 10 µg/ml, there were no significant differences compared to untreated controls. At concentrations 50, 100 and 300 µg/ml, there was a dose and time dependent toxicity with groups treated at 300 µg/ml having viability as low as 20% after 24 hours. MSCs treated with MSNPs show no decrease in viability at any concentration or time point. Interestingly, groups treated with low concentrations of 5 µg/ml and 10 µg/ml at 24 hours had significantly higher viability compared to untreated groups. The increase in viability was highest for groups treated with 5 µg/ml; 37% greater than untreated controls.

Figure 2.2 C and D shows viability of NIH-3T3 and MSCs treated with WSNTs at concentrations between 5-300 µg/ml for 6, 12 and 24 hours. MSCs and NIH-3T3 treated with WSNTs showed no time dependent or dose dependent cytotoxicity. NIH-3T3 cells treated with 300 µg/ml WSNTs for 24 hours showed significantly higher viability (about 17%) compared to untreated controls. MSCs showed significantly higher viability compared to untreated groups for all concentrations at the 24 hour time point with viability 45% greater than untreated cells at 300 µg/ml concentration.

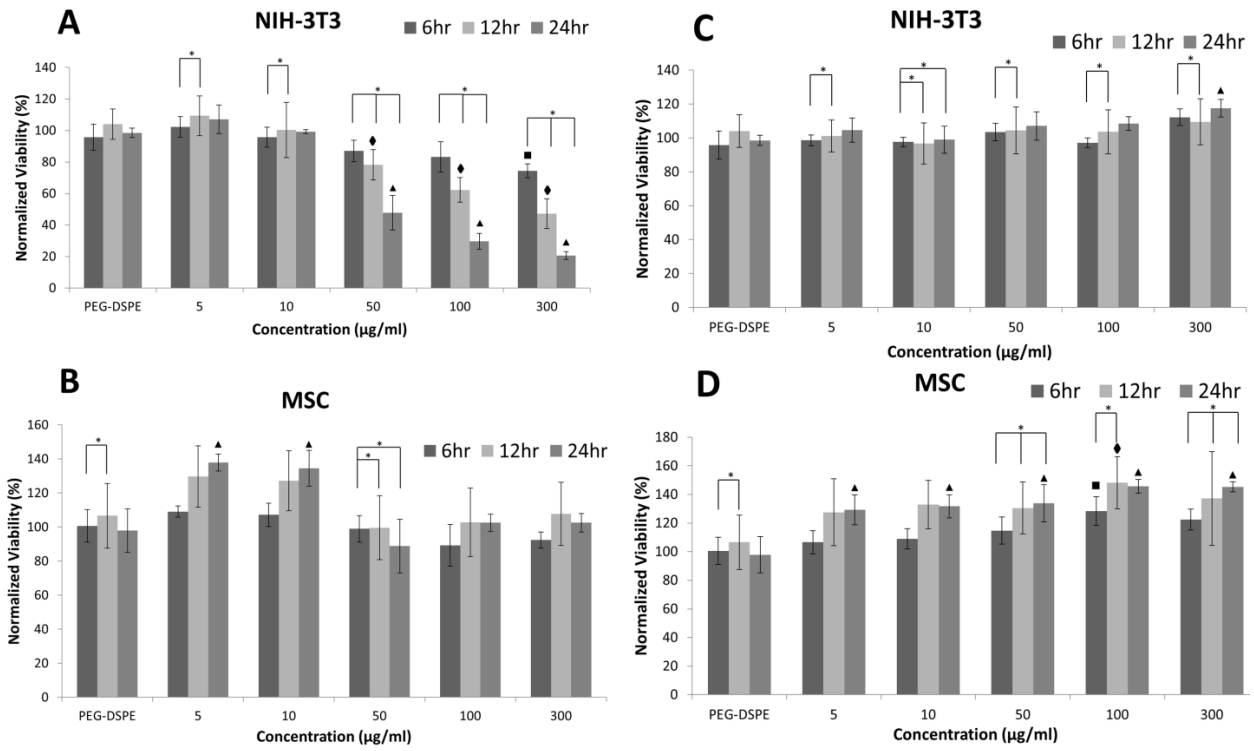

Figure 2.2. Presto Blue assay results at 6, 12, and 24 hours after treatment with MSNPs (A) and WSNTs (B) for NIH-3T3 fibroblasts; after treatment with MSNPs (C) and WSNTs (D) for MSCs. For each nanoparticle, cells were treated with PEG-DSPE, 5 µg/ml, 10 µg/ml, 50 µg/ml, 100 µg/ml, and 300 µg/ml concentrations. Data are presented as mean ± standard deviation of percentage viability compared to untreated cells (n = 4). Statistical significance (p = 0.05) with respect to untreated groups at 6, 12 and 24 hours are denoted by (■), (◊), (▲) respectively. Statistical significance between time points within groups is denoted by (*).

Lactate Dehydrogenase

LDH is a cell membrane integrity assay, measured by the absorbance of lactate dehydrogenase released into the media by lysed cells.[25] Figure 2.3 shows the LDH released by cells treated with MSNPs and WSNTs dispersions at 5, 10, 50, 100 and 300 µg/ml concentrations for 6, 12 and 24 hours. Data for each group is normalized to positive control group treated with lysis buffer in which all the cells were lysed and LDH contained within the cells were released into the culture media. Figure 2.3 A indicates that NIH-3T3 cells treated with MSNPs exhibit a time dependent cytotoxicity with the highest normalized LDH level at 24 hours for all concentrations. Figure 2.3 B indicates that LDH released from MSCs treated with MSNPs

have neither time nor dose dependence. MSCs treated with 5 µg/ml of MSNPs had significantly higher LDH release compared to DSPE-PEG treated groups at the 6 hour time point. The increase in LDH release compared to DSPE-PEG groups was not observed in higher concentrations.

Figure 2.3 C and D shows the LDH release from NIH-3T3 and MSCs treated with WSNTs respectively. The data suggests a time dependent increase in LDH release from NIH-3T3 at 24 hour time points with no significant differences from DSPE-PEG treated groups at any time points. MSCs treated with WSNTs at 5 µg/ml at 300 µg/ml had significantly higher LDH release compared to DSPE-PEG groups.

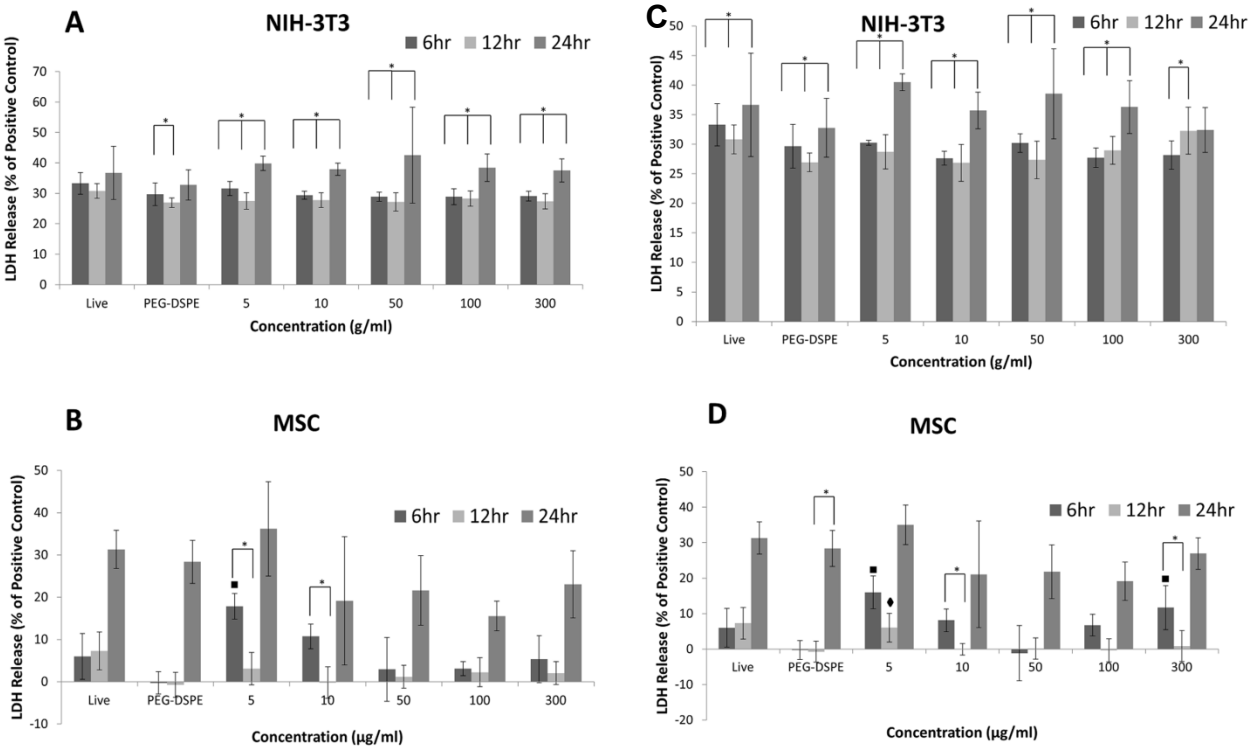

Figure 2.3. LDH assay results at 6, 12, and 24 hours after treatment with MSNPs (A) and WSNTs (B) for NIH-3T3 fibroblasts; after treatment with MSNPs (C) and WSNTs (D) for MSCs. For each nanoparticle, cells were treated with PEG-DSPE, 5 µg/ml, 10 µg/ml, 50 µg/ml, 100 µg/ml, and 300 µg/ml concentrations. Data are presented as mean ± standard deviation of percentage viability compared to untreated cells (n = 4). Statistical significance (p = 0.05) with respect to untreated groups at 6, 12 and 24 hours are denoted by (■), (◊), (▲) respectively. Statistical significance between time points within groups is denoted by (*).

Differentiation

Oil Red O Staining and Elution

Oil Red O is a lipid-soluble dye that stains fat vacuoles in adipocytes and is used to determine the extent of adipogenic differentiation.[22,26] Figure 2.4 A shows representative images of MSCs stained with Oil Red O following 21 days in adipogenic differentiation media after 24 hours treatment with 0, 10, or 50 μg/ml of MSNPs or WSNTs. For all groups fat vacuoles were observed throughout the culture wells. In the groups treated with nanoparticles, aggregates were present around the cells in the images. Elution of the Oil Red O stain (Figure 2.4 B) showed significantly higher staining in groups treated with 10 μg/ml of MSNPs and WSNTs compared to groups treated with 50 μg/ml concentrations and untreated controls. The increase in elution was ~50% for both MSNPs and WSNTs.

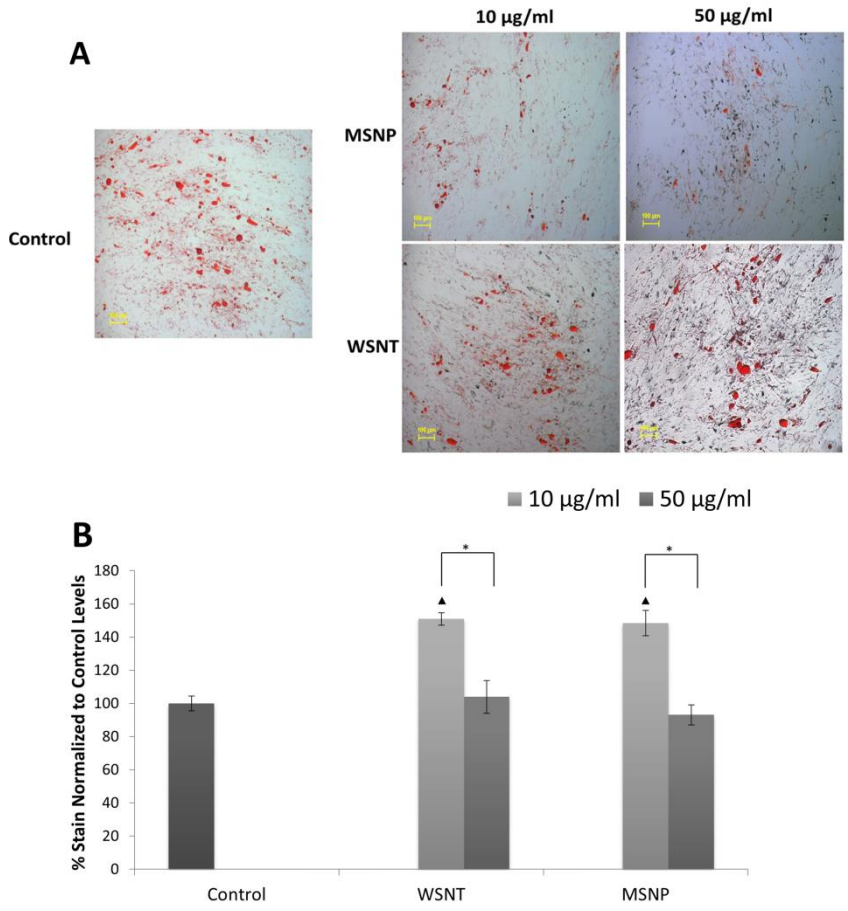

Figure 2.4. Adipogenesis results. (A) Histological specimens of MSCs incubated with MSNPs and WSNTs for 24 h, followed by incubation with adipogenic differentiation media for 21 day, stained by Oil Red O. (B) Elution of Oil Red O stain. Data are normalized to control values and presented as mean ± standard deviation (n = 3). Statistical significance ($p < 0.05$) was determined by the Kruskal-Wallis test with Dunn's post hoc compared to the control (▲) or within groups is denoted by (*).

Alizarin Red S

Alizarin Red S stains extracellular calcium and is used as a marker for osteo-differentiation of stem cells.[22,27] Figure 2.5 shows representative images of MSCs stained with Alizarin Red S for calcium deposits after treatment with 0 (Control), 10, or 50 µg/ml of MSNPs or WSNTs for 24 hours and incubation in osteogenic differentiation media for 14 days. For all groups red staining of calcium was observed. Nanoparticles could be seen around the cells for the treated groups with larger aggregates seen in the groups treated with the higher concentration. In all the groups the cells were seen to be elongated and spread out as expected from healthy pre-osteoblast and osteoblast cultures. There were no observable differences in staining pattern or intensity between any of the groups.

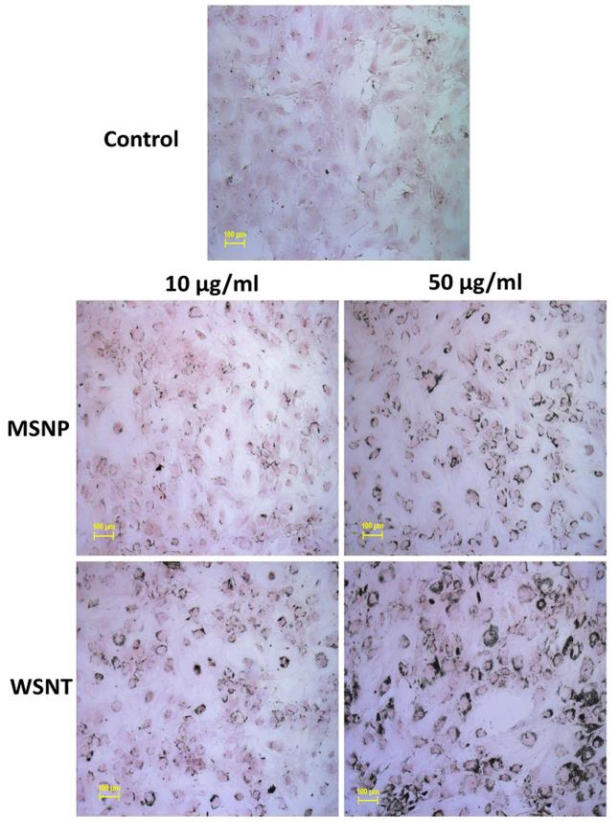

Figure 2.5. Osteogenesis results. MSCs after treatment for 24 h with either 10 or 50 µg/ml of MSNPs or WSNTs respectively, followed by 14 days incubation with osteogenic differentiation media stained with Alizarin Red S.

Cell Number

Number of cells per well was used to determine ALP activity. Figure 2.6 A shows average number of cells per well in groups treated with 10 and 50 µg/ml of MSNPs or WSNTs and untreated controls for 24 hours and incubated for 14 days in osteogenic differentiation media. Groups treated with WSNTs had no significant differences from untreated controls. Groups treated with both low and high concentrations of MSNPs had significantly lower cells per well compared to untreated groups. The decrease in cell number was ~25% for both concentrations of MSNPs compared to untreated controls.

Alkaline Phosphatase (ALP) Activity

Figure 2.6 B shows ALP activity of groups treated with 10 and 50 µg/ml of MSNPs or WSNTs and untreated controls for 24 hours and incubated for 14 days in osteogenic

differentiation media represented as activity/µmol/min/cell. ALP is an early stage marker for osteogenesis.[22] MSCs treated with 10 or 50 µg/ml MSNPs or WSNTs for 24 hours, and then incubated with osteogenic differentiation media for 14 days were examined for this marker. MSCs treated with MSNP dispersion of 10 µg/ml concentration showed significantly higher ALP activity; approximately 50% greater compared to MSCs treated with 50 µg/ml MSNP dispersion. However, the ALP activity of neither of these groups was significantly different from the untreated control group. Groups treated with 10 µg/ml of WSNTs showed 27% higher ALP activity compared to groups treated with 50 µg/ml of WSNTs. However, the ALP activity of both the groups were not significantly different from untreated controls.

Extracellular Calcium

Extracellular calcium is a late stage marker for osteogenesis.[22] Figure 2.6 C shows calcium levels of MSCs treated with 10 or 50 µg/ml MSNPs or WSNTs for 24 hours and incubated for 14 days in osteogenic differentiation media. Extracellular calcium content for MSCs treated with MSNPs at 10 and 50 µg/ml were 69 mmol/L and 65 mmol/L, respectively. Untreated control groups had a calcium concentration of 62 mmol/L. There were no statistical significant differences between the any groups. MSCs treated with WSNTs at 10 and 50 µg/ml had 63 mmol/L and 69 mmol/L calcium concentration, respectively. There were no statistically significant differences between the groups or with untreated controls.

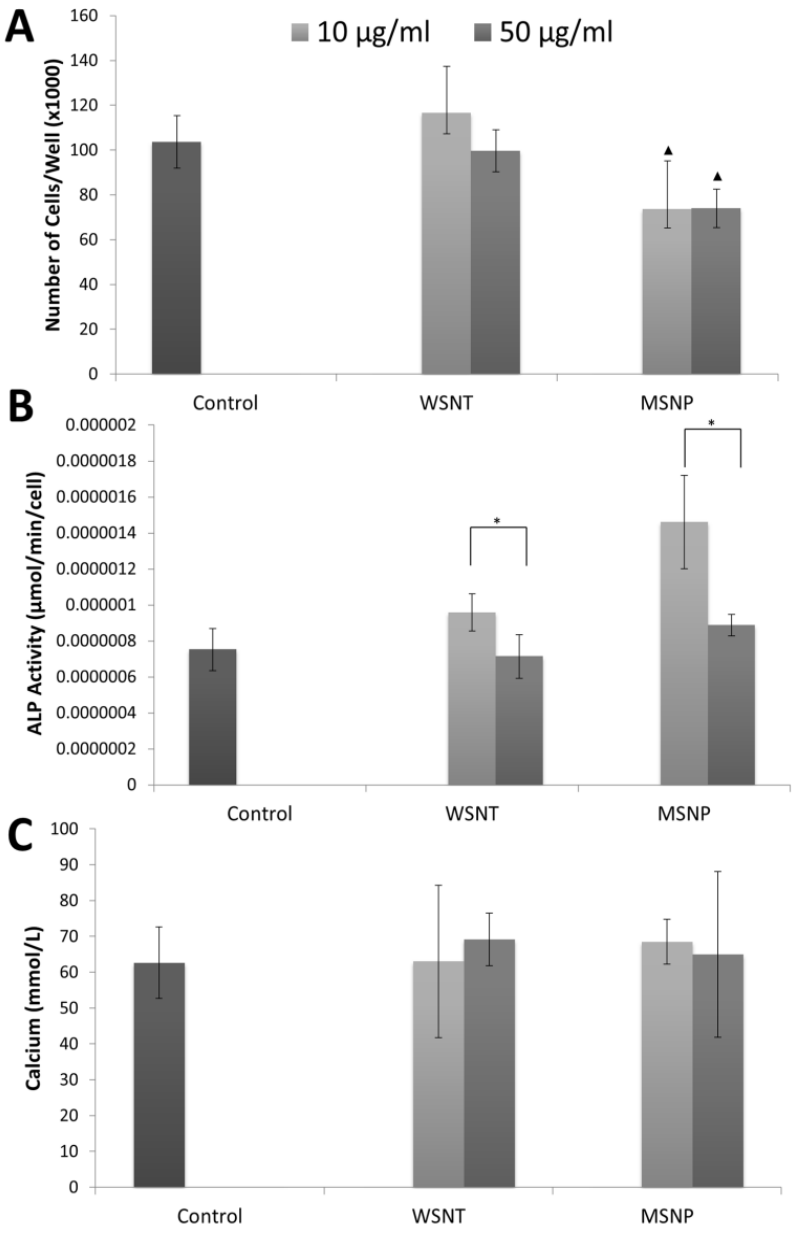

Figure 2.6. Osteogenesis results. (A) Cellularity for MSCs after treatment for 24 h with either 10 or 50 µg/ml of MSNPs or WSNTs respectively, followed by 14 days incubation with osteogenic differentiation media. (B) ALP activity for MSCs after treatment for 24 h with either 10 or 50 µg/ml of MSNPs or WSNTs respectively, followed by 14 days incubation with osteogenic differentiation media. (C) Calcium content after treatment for 24 h with either 10 or 50 µg/ml of MSNPs or WSNTs respectively, followed by 14 days incubation with osteogenic differentiation media. Data are presented as mean ± standard deviation (n = 3). Statistical significance ($p < 0.05$) was determined by the Kruskal-Wallis test with Dunn's post hoc as compared to the control (▲) or within groups (*).

Cell Uptake

TEM was performed to investigate cellular uptake of MSNPs and WSNTs. Figure 2.7 shows representative TEM images of MSCs treated with 50 µg/ml of MSNPs (A & B) and WSNTs (C & D). In Figure 2.7 A and B MSNPs were seen within the cytoplasm, enclosed in endocytic vesicles (red arrows) and against the cell membrane (orange arrows). WSNTs, shown in Figure 2.7 B and C, were seen in the cytoplasm within (red arrows) and outside (yellow arrow) endocytic vesicles. Vesicles containing MSNPs and WSNTs were seen in close proximity to the nuclear membrane. Neither of the nanoparticles was present within the nucleus.

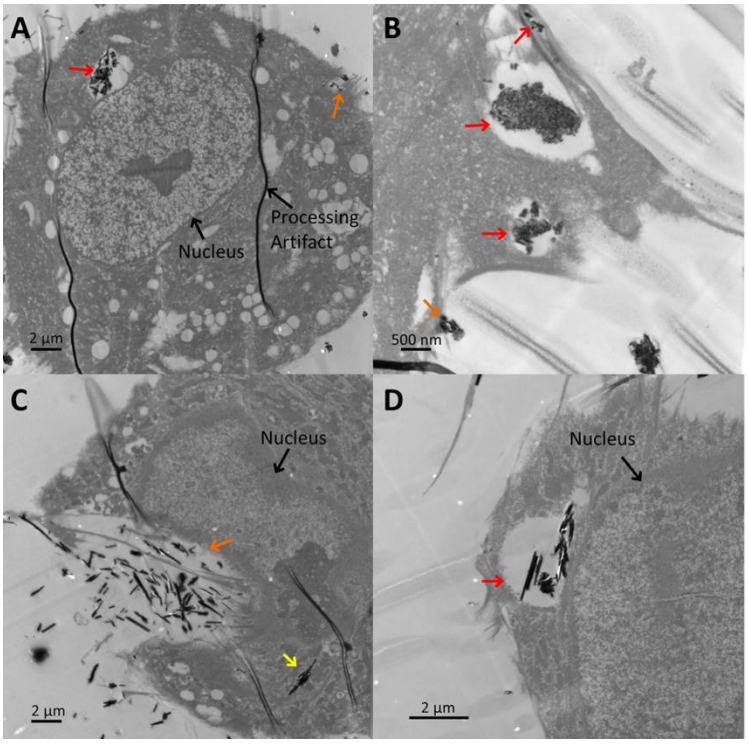

Figure 2.7. Representative TEM images of MSCs treated with MSNPs (A & B) and WSNTs (C & D). MSNPs are seen in endocytic vesicles (red arrows), and on the membrane of the cells (orange arrows). WSNTs are seen in the cytoplasm within (red arrows) and outside (yellow arrow) endocytic vesicles. Neither nanoparticle can be seen in the nucleus.

Discussion

The objective of this study was to investigate the response of WSNTs and MSNPs on NIH-3T3 fibroblasts and MSCs to identify potentially safe dosages for any eventual biomedical application. NIH-3T3 fibroblasts cells were chosen since they are widely used as model fibroblastic cells for cytotoxicity evaluation.[28] MSCs were chosen since they are routine used for tissue engineering and stem cell applications.[29-31] We performed cytotoxicity screening over a broad range of concentrations (0-300 µg/ml) and time points (6, 12, and 24 h) on fibroblasts (NIH3T3) and stem cells (MSCs) to identify a range of potentially safe doses. We then examined the effect of potentially safe low (10 µg/ml) and high (50 µg/ml) doses of nanoparticles on the adipo- and osteo-differentiation capabilities of MSCs. Through the cytotoxicity and differentiation studies, we identified a range of doses for the two nanoparticle formulations that do not significantly affect viability of fibroblasts and MSCs as well as differentiation capabilities of MSCs.

Characterization of nanoparticles was done by TEM and Raman spectroscopy. Raman spectroscopy revealed the common Raman active modes $E_{2g}{}^{1}$ and A_{1g} for transition metal dichalcogenides. The $E_{2g}{}^{1}$ peak indicates the in-plane phonon mode of the two sulfur atoms opposite vibration from the molybdenum or tungsten atom while the A_{1g} peak indicates the out-of-plane phonon mode of the sulfur atoms opposite vibration between layers.[32,33] A slight shift in wavenumbers is observed as compared to previous studies. This shift is due to the number of layers of nanoparticles stacked together during the measurements.[34]

The Presto Blue assay indicated a time and dose dependent cytotoxicity for NIH-3T3 cells treated with MSNPs. CD50 values of MSCs were 578 µg/ml, 250 µg/ml, and 140 µg/ml,

for 6, 12, and 24 hours respectively, calculated from concentration vs. viability graphs. This trend was not seen in viability assessed by LDH. There were no significant differences in any of the groups compared to untreated controls. Live cells reduce non-fluorescent resazurin to fluorescent resorufin that is detected by Presto Blue assay; whereas, LDH assay detects LDH enzyme that is released when cell membrane integrity is compromised in dying cells. The difference in trends observed from these two assays could be due to the nanoparticles affecting the cellular machinery without affecting their membrane integrity. Further investigations are required to identify to cause of these differences in outcomes of the two assays. Unlike MSNPs, NIH-3T3 cells treated with WSNTs showed no time or dose dependent cytotoxicity. Results of both Presto Blue and LDH were similar and indicate that concentrations up to 300 µg/ml of WSNTs have no significant effect on viability of NIH-3T3 cells. CD50 values at all time points for NIH-3T3 cells treated with MSNPs calculated from LDH assay results and for NIH-3T3 cells treated with WSNTs calculated from Presto Blue and LDH assay results were greater than 300 µg/ml.

MSCs treated with MSNPs or WSNTs show no time or dose dependent cytotoxicity in Presto Blue and LDH assays. Results from both the assays indicate that MSNPs or WSNTs at concentrations up to 300 µg/ml do not elicit a significant cytotoxic response. All CD50 values for MSCs treated with MSNPs or WSNTs at all time points were greater than 300 µg/ml. An increase in proliferation of MSCs was noted at all WSNT treatment concentrations with the highest increase of 45% compared to DSPE-PEG treated controls at the 24-hour time point. A previous report on carbon black and silica nanoparticles showed that these nanoparticles increase lung epithelial cell proliferation[35] via the activation of the protein kinase B pathway. However, this effect only occurred when the cells were treated with carbon black and silica nanoparticles

with a median diameter of 14 nm. Larger particles did not elicit the same results.[35] Even though the WSNTs and MSNPs used in this study, had sizes several times larger than the carbon black and silica nanoparticles, similar pathways maybe responsible for the increased cell proliferation. Further investigations are required to determine the mechanism.

Adipogenic differentiation was analyzed by Oil Red O staining and elution quantification. The results indicate that MSCs incubated for 24 hours with MSNPs or WSNTs at 10 µg/ml or 50 µg/ml concentrations that MSCs maintain their differentiation. Significantly higher Oil Red O staining in groups treated with 10 µg/ml concentrations compared to groups treated with the 50 µg/ml concentration for both MSNPs and WSNTs could be due to higher cell numbers. Viability analysis indicated that MSCs treated with MSNPs at 10 µg/ml had 52% higher viability compared to MSCs treated with 50 µg/ml. Since adipogenesis was induced using adipogenic induction media 24 hour after the treatment with the nanoparticles, groups treated with 50 µg/ml most likely had lower number of cells compared to groups treated with 10 µg/ml. Taking differences in cell numbers into consideration, the results imply that treatment with low and high concentrations of WSNTs and MSNPs should not hinder the adipogenesis.

Osteogenic differentiation was analyzed by ALP and calcium assays two weeks following treatment with nanoparticles. As a part of the ALP analysis, cell numbers were obtained for the treated and untreated groups. Cell number for groups treated with MSNPs was significantly lower than cell numbers for groups treated with WSNTs and untreated control. This result is in agreement with our viability assessment where we observed increased viability in groups treated with WSNTs and decreased viability in groups treated with MSNPs at 50 µg/ml concentration. For both MSNPs and WSNTs, ALP activity was significantly higher in groups treated with a lower concentration compared to groups treated with a higher concentration. This

difference in ALP activity at low and high doses may be due to variable propensity of the nanoparticles at these dosages to aggregate in cell media. We observed, at the high concentration, both MSNPs and WSNTs aggregate with time to form larger sized loosely held particles, and at the low concentrations, the particles remained well dispersed and did not aggregate during the incubation period. Thus, at higher concentration, the increased aggregation may prevent/ reduce the uptake of these nanoparticles into cells, and at the lower concentration, the nanoparticles could be internalized into cells at higher amounts.

We used calcium content in the matrix as another indicator of osteo-differentiation.[22] There were no significant differences in calcium concentration levels between the groups. The assays for osteogenic differentiation markers were performed following 14 days of incubation with osteogenic differentiation media. At this stage of differentiation MSCs produce increased amounts of organic extracellular matrix (ECM) proteins that is closely followed by deposition of inorganic components.[36] Additional studies are needed to examine if these nanoparticles affect the gene expression of osteo-differentiation markers and the mechanical properties of deposited matrix. The results of the osteo-differentiation studies taken together imply that treatment at 10 or 50 μg/ml of WSNTs or MSNPs concentrations should not adversely affect the osteogenic differentiation potential of MSCs.

TEM analysis of the histological specimens of the MSCs treated with the nanoparticles was performed to further investigate their uptake characteristics. Since no significant differences in viability or differentiation of MSCs were observed between groups treated with WSNTs and MSNPs compared to untreated controls, TEM analysis also allowed us to determine whether this lack of difference was due to poor uptake of these nanoparticles into these cells. TEM images of histological sections of MSCs treated with MSNPs and WSNTs qualitatively showed significant

uptake of both nanoparticles into cells. Additionally, the nanoparticles were present within and outside the cells. Inside the cell, MSNPs were seen only in vesicles within the cytoplasm whereas WSNTs were seen in vesicles as well as the cytoplasmic matrix. Outside the cell, MSNPs and WSNTs were observed on the cell membranes. However, cytoplasmic protrusions observed during micropinocytosis were seen only around the WSNT aggregates.[37] These observations suggest that WSNTs and MSNPs can enter the cells via different uptake mechanisms without affecting viability or differentiation potential of MSCs at concentrations up to 50 μg/ml.

Previous cytotoxicity studies on MSNPs and WSNTs mainly focused on their *in vitro* effect at low concentrations (0 to 3.52 mg/L and 0 to 100 μg/ml) on cells exposed during inhalation and oral ingestion.[6,17] The above results complement the results of those studies and provide guidelines on potentially safe dosages for biomedical applications. For instance, recently MSNPs and WSNTs have shown promise as reinforcing agents for polymeric bone tissue engineering nanocomposites.[9,10] Biodegradable polymer matrices incorporated with low concentrations (0.2 weight%; 0.2 grams of nanoparticles in 1 gram of polymer) of MSNPs or WSNTs showed up to 108% enhancement in mechanical (compressive and flexural modulus) properties compared to the polymer alone.[9,10] Thus, the total concentration of the nanoparticles released per cm^3 (or ml) of the 90% porous nanocomposite (nanocomposite volume = 10 cm^3) would be 20 μg/ml nanoparticles upon degradation of the polymer. As the scaffolds degrade, these nanoparticles will be released into the extracellular matrix and interact with surrounding tissue. Our results suggest that the released nanoparticles should not significantly affect the viability of fibroblasts and viability or differentiation of MSCs at concentrations higher than the estimated 20 μg/ml concentration. Additionally, these inorganic nanoparticles are better at

reinforcing biodegradable polymers employed for tissue engineering applications compared to carbon nanoparticles such as one dimensional carbon nanotubes or two dimensional graphene.[9,10] Furthermore, high concentrations of carbon nanotubes (>100 µg/ml) or graphene (300 µg/ml) affect MSC viability significantly (60-80% or 38-100% decrease, respectively) while treatment with similar high concentrations of MSNPs and WSNTs had minimal (~10%) to no decrease in MSC viability.[22,38] The results of our cytotoxicity study in conjugation with the previous efficacy studies identify optimal formulations of these inorganic nanoparticles to design and develop a new class of mechanically robust and biocompatible tissue engineering implants. Furthermore, the significant uptake of these nanoparticles in MSCs at potentially safe doses also open opportunities to introduce them as multifunctional agents for stem cell monitoring and therapeutics. These nanoparticles could, at potentially safe doses, serve as versatile platforms to attach drugs, genes, and/ or imaging agents and introduced *ex vivo* into MSCs. These labelled MSCs could then be employed for stem cell applications.

Conclusions

Treatment with MSNPs at concentrations up to 10 µg/ml does not significantly affect viability of NIH-3T3 cells. No dose or time dependent increase in cytotoxicity was observed for NIH-3T3 cells treated with WSNTs or MSCs treated with MSNPs or WSNTs. MSCs treated with low (10 µg/ml) and high (50 µg/ml) concentrations of MSNPs and WSNTs for 24 hours maintain their differentiation potential to adipocytes and osteoblasts. MSNPs are internalized in vesicles in the cells while WSNTs are internalized in vesicles as well as cytoplasmic matrix. The results taken together indicate that concentrations less than 50 µg/ml of MSNPs and WSNTs should be potentially safe for incubation with MSCs and fibroblasts up to 24 hours. The results provide preliminary safety guidelines to further explore these nanoparticles as reinforcing agents at the previously investigated 0.2 wt%.

Acknowledgements

This work was sponsored by National Institutes of Health (grant No. 1DP2OD007394-01). The authors would like to thank Susan Van Horn (Central Microscopy, Stony Brook University) for her help with transmission electron microscopy. Research was carried out in part at the Center for Functional Nanomaterials, Brookhaven National Laboratory, New York, which is supported by the U.S. Department of Energy, Office of Basic Energy Sciences, under Contract No. DE-AC02-98CH10886.

References

1 Mattheiss, L. Band structures of transition-metal-dichalcogenide layer compounds. *Physical Review B* **8**, 3719 (1973).

2 Wang, Q. H., Kalantar-Zadeh, K., Kis, A., Coleman, J. N. & Strano, M. S. Electronics and optoelectronics of two-dimensional transition metal dichalcogenides. *Nature Nanotechnology* **7**, 699-712 (2012).

3 Tenne, R. Inorganic nanotubes and fullerene-like nanoparticles. *Nature Nanotechnology* **1**, 103-111 (2006).

4 Demchenko, A. T. & Evseev, A. I. Molybdenum-disulfide lubricant. *Metallurgist* **8**, 42-43 (1964).

5 Prasad, S. V., McDevitt, N. T. & Zabinski, J. S. Tribology of tungsten disulfide–nanocrystalline zinc oxide adaptive lubricant films from ambient to 500 °C. *Wear* **237**, 186-196 (2000).

6 Wu, H. *et al.* Biocompatible inorganic fullerene-like molybdenum disulfide nanoparticles produced by pulsed laser ablation in water. *ACS Nano* **5**, 1276-1281 (2011).

7 Redlich, M. *et al.* Improved orthodontic stainless steel wires coated with inorganic fullerene-like nanoparticles of WS_2 impregnated in electroless nickel–phosphorous film. *Dental Materials* **24**, 1640-1646 (2008).

8 Katz, A., Redlich, M., Rapoport, L., Wagner, H. D. & Tenne, R. Self-lubricating coatings containing fullerene-like WS_2 nanoparticles for orthodontic wires and other possible medical applications. *Tribology Letters* **21**, 135-139 (2006).

9 Lalwani, G. *et al.* Two-dimensional nanostructure-reinforced biodegradable polymeric nanocomposites for bone tissue engineering. *Biomacromolecules* **14**, 900-909 (2013).

10 Lalwani, G. *et al.* Tungsten disulfide nanotubes reinforced biodegradable polymers for bone tissue engineering. *Acta Biomaterialia* **9**, 8365 (2013).

11 Hutmacher, D. W. Scaffolds in tissue engineering bone and cartilage. *Biomaterials* **21**, 2529-2543 (2000).

12 Lam, C.-W., James, J. T., McCluskey, R., Arepalli, S. & Hunter, R. L. A review of carbon nanotube toxicity and assessment of potential occupational and environmental health risks. *CRC Critical Reviews in Toxicology* **36**, 189-217 (2006).

13 Johnston, H. J. *et al.* A critical review of the biological mechanisms underlying *the in vivo* and *in vitro* toxicity of carbon nanotubes: The contribution of physico-chemical characteristics. *Nanotoxicology* **4**, 207-246 (2010).

14 Aschberger, K. *et al.* Review of carbon nanotubes toxicity and exposure-appraisal of human health risk assessment based on open literature. *Critical Reviews in Toxicology* **40**, 759-790 (2010).

15 Sanchez, V. C., Jachak, A., Hurt, R. H. & Kane, A. B. Biological interactions of graphene-family nanomaterials: An interdisciplinary review. *Chemical Research in Toxicology* **25**, 15-34 (2011).

16 Yang, K., Li, Y., Tan, X., Peng, R. & Liu, Z. Behavior and toxicity of graphene and its functionalized derivatives in biological systems. *Small* **9**, 1492-1503 (2013).

17 Pardo, M., Shuster-Meiseles, T., Levin-Zaidman, S., Rudich, A. & Rudich, Y. Low cytotoxicity of inorganic nanotubes and fullerene-like nanostructures in human bronchial

epithelial cells: Relation to inflammatory gene induction and antioxidant response. *Environmental Science & Technology* **48**, 3457-3466 (2014).

18 Caplan, A. I. Mesenchymal stem cells. *Journal of Orthopaedic Research* **9**, 641-650 (1991).

19 Caplan, A. I. & Dennis, J. E. Mesenchymal stem cells as trophic mediators. *Journal of Cellular Biochemistry* **98**, 1076-1084 (2006).

20 Kubinová, Š. & Syková, E. Nanotechnologies in regenerative medicine. *Minimally Invasive Therapy & Allied Technologies* **19**, 144-156 (2010).

21 Ferreira, L. Nanoparticles as tools to study and control stem cells. *Journal of Cellular Biochemistry* **108**, 746-752 (2009).

22 Talukdar, Y., Rashkow, J. T., Lalwani, G., Kanakia, S. & Sitharaman, B. The effects of graphene nanostructures on mesenchymal stem cells. *Biomaterials* **35**, 4863-4877 (2014).

23 Ferreira, L., Karp, J. M., Nobre, L. & Langer, R. New opportunities: The use of nanotechnologies to manipulate and track stem cells. *Cell Stem Cell* **3**, 136-146 (2008).

24 Castro-Guerrero, C. F. *et al.* Structure and catalytic properties of hexagonal molybdenum disulfide nanoplates. *Catalysis Science & Technology* **1**, 1024-1031 (2011).

25 Mullick Chowdhury, S. *et al.* Cell specific cytotoxicity and uptake of graphene nanoribbons. *Biomaterials* **34**, 283-293 (2013).

26 Ramirez-Zacarias, J., Castro-Munozledo, F. & Kuri-Harcuch, W. Quantitation of adipose conversion and triglycerides by staining intracytoplasmic lipids with oil red o. *Histochemistry* **97**, 493-497 (1992).

27 Sitharaman, B., Avti, P. K., Schaefer, K., Talukdar, Y. & Longtin, J. P. A novel nanoparticle-enhanced photoacoustic stimulus for bone tissue engineering. *Tissue Engineering Part A* **17**, 1851-1858 (2011).

28 Clothier, R., Beed, M., Samson, R. & Ward, R. An *in vitro* approach to the evaluation of repeat exposure in the prediction of toxicity. *Toxicology In Vitro* **11**, 679-682,(1997).

29 Marion, N. W. & Mao, J. J. Mesenchymal stem cells and tissue engineering. *Methods in Enzymology* **420**, 339-361 (2006).

30 Caplan, A. I. Adult mesenchymal stem cells for tissue engineering versus regenerative medicine. *Journal of Cellular Physiology* **213**, 341-347 (2007).

31 Bianco, P. & Robey, P. G. Stem cells in tissue engineering. *Nature* **414**, 118-121 (2001).

32 Berkdemir, A. *et al.* Identification of individual and few layers of WS_2 using Raman spectroscopy. *Scientific Reports* **3**, doi:10.1038/srep01755 (2013).

33 Li, H. *et al.* From bulk to monolayer MoS_2: Evolution of Raman scattering. *Advanced Functional Materials* **22**, 1385-1390 (2012).

34 Cunningham, G. *et al.* Solvent exfoliation of transition metal dichalcogenides: Dispersibility of exfoliated nanosheets varies only weakly between compounds. *ACS Nano* **6**, 3468-3480 (2012).

35 Unfried, K., Sydlik, U., Bierhals, K., Weissenberg, A. & Abel, J. Carbon nanoparticle-induced lung epithelial cell proliferation is mediated by receptor-dependent akt activation. *American Journal of Physiology-Lung Cellular and Molecular Physiology* **294**, L358-L367 (2008).

36 Birmingham, E., Niebur, G. & McHugh, P. Osteogenic differentiation of mesenchymal stem cells is regulated by osteocyte and osteoblast cells in a simplified bone niche. *European Cells & Materials* **12**, 13-27 (2012).

37 Mullick Chowdhury, S., Manepalli, P. & Sitharaman, B. Graphene nanoribbons elicit cell specific uptake and delivery via activation of epidermal growth factor receptor enhanced by human papillomavirus e5 protein. *Acta Biomaterialia* **10**, 4494-4504 (2014).

38 Mooney, E., Dockery, P., Greiser, U., Murphy, M. & Barron, V. Carbon nanotubes and mesenchymal stem cells: Biocompatibility, proliferation and differentiation. *Nano Letters* **8**, 2137-2143 (2008).

Chapter 3

In Vitro Bioactivity of One- and Two-Dimensional Nanoparticle Reinforced Bone Tissue Engineering Scaffolds

Contributions by: Jason T. Rashkow, Gaurav Lalwani, Balaji Sitharaman

Abstract

This study investigates the effect of nanoparticle composition and morphology on the bioactivity of poly(lactic-co-glycolic acid) (PLGA) nanocomposites reinforced with 0.2 wt% multiwalled carbon nanotubes (MWCNTs), multiwalled graphene nanoribbons (MWGONRs), graphene nanoplatelets (GONPs), molybdenum disulfide nanoplatelets (MSNPs), or tungsten disulfide nanotubes (WSNTs). Apatite collection on control and reinforced scaffolds was assessed after incubation in simulated body fluid (SBF) under physiological conditions for 1, 3, 7, or 14 days. All groups showed apatite precipitate on the surface after a one day in SBF. After soaking for 14 days, scaffolds reinforced with GONPs, MSNPs, or WSNTs showed significantly higher phosphate accumulation compared to PLGA scaffolds. Scaffolds reinforced with GONPs, MSNPs, or WSNTs may elicit a bioactive response when implanted *in vivo*.

Introduction

Limitations associated with current bone grafting techniques utilizing autologous or allogenous bone have led to an increase in research of synthetic bone grafting materials. An ideal synthetic bone graft would act as a scaffold with high porosity for ingrowth and nutrient and waste transport; have mechanical properties similar to the surrounding native tissue; have appropriate surface properties to allow cellular attachment, proliferation, and differentiation; and be biocompatible and bioresorbable.

Biodegradable polymers can fulfill many of the above listed requirements with the major limitation of poor integrity under load bearing conditions prompting investigation of nanoparticle-reinforced biodegradable polymer nanocomposites. Recently, the unique physiochemical properties of two-dimensional organic nanostructures (graphene nanoribbons (GONRs) and graphene nanoplatelets (GONPs)) and one- and two-dimensional inorganic nanostructures (molybdenum disulfide nanoplatelets (MSNPs) and tungsten disulfide nanotubes (WSNTs)) have been utilized to improve the mechanical properties of biodegradable polymer polypropylene fumarate. Incorporation of 0.2 wt% of two-dimensional organic and one- or two-dimensional inorganic nanoparticles led to significant enhancement in the compressive modulus, compressive yield strength, flexural modulus, and flexural yield strength of PPF nanocomposites with when compared to PPF alone or PPF reinforced with single- or multi-walled carbon nanotubes (SWCNTs or MWCNTs).[1,2]

In addition to improving mechanical properties, nanoparticle reinforcement may affect interaction between the tissue engineering construct and the *in vivo* environment. One way in which this may occur is through bioactivity or the propensity of the material to influence bone

growth through formation of a bone bonding layer of apatite on the surface.[3] Bioactivity is commonly investigated *in vitro* by soaking a tissue engineering construct in simulated body fluid (SBF) with ion concentrations nearly equal to those of human blood serum whereby apatite crystals selectively precipitate on the surface of a bioactive material. The addition of nanoparticles to the polymer matrix creates more surface area and nanotopography that act as nuclei for apatite crystals to form[4] as has been demonstrated with a variety of nanoparticles individually and in combination including hydroxyapatite,[5] bioactive glass,[6] titanium dioxide,[7] and magnetite[8]. Few studies however have investigated the influence of carbon nanotubes,[9] and graphene nanoparticles[10,11] without the concurrent addition of hydroxyapatite nanoparticles on bioactivity of biodegradable polymer nanocomposites. Zawadzak et al. employed polyurethane foams with MWCNTs electrophoretically deposited on the surface and investigated the apatite formation after soaking in 1.5x concentrated SBF for 14 or 28 days. Wan et al. examined the bioactivity of electrospun poly(caprolactone) or gelatin nanocomposites containing 0.3 wt% GONP (prepared using the modified Hummers method) after soaking in 10x concentrated SBF for 24 hours.[10,11]

MWCNTs, MWGONRs, GONPs, MSNPs, and WSNTs may possess different morphologies and physiochemical properties depending synthesis method. These properties could affect the bioactivity of the biodegradable polymer nanocomposite scaffolds. In this study, we have assessed the *in vitro* bioactivity of 90% porous poly(lactic-co-glycolic acid) (PLGA) scaffolds reinforced with 0.2 wt% of MWCNTs, MWGONRs, GONPs, MSNPs, or WSNTs soaked in SBF for 1, 3, 7, or 14 days. We report the influence of nanoparticle composition and morphology on formation of an apatite layer in order to determine what properties show the most promise toward application as bone tissue engineering scaffold reinforcing agents.

Materials and Methods

Nanoparticle Synthesis and Characterization

MWCNTs possessing outer diameters between 20 and 30 nm were purchased from Sigma Aldrich (Cat. No. 636487, St. Louis, MO). MWGONRs were synthesized from the MWCNTs using a modified longitudinal unzipping method.[12] GONPs were synthesized from graphite flakes using a modified Hummer's method.[13] MSNPs were synthesized through a high temperature reaction between MoO_3 and sulfur powder.[14] WSNTs were purchased from APNano (NY, USA).

All particles were characterized by high resolution transmission electron microscopy (HRTEM) and Raman spectroscopy. For HRTEM, nanoparticles were dispersed in a solution of equal parts water and ethanol by sonication. Dispersion was followed by ultracentrifugation and the supernatant was drop cast on a lacey carbon grid (300 mesh size, copper support, Ted Pella, USA). HRTEM imaging was performed using a JOEL 2100F high-resolution analytical transmission electron microscope with an accelerating voltage of 200 kV at the Center for Functional Nanomaterials, Brookhaven National Laboratory, New York. Raman spectra were recorded between 50 –3750 cm^{-1} at room temperature using WITec alpha300R Micro-Imaging Raman Spectrometer equipped with a 532 nm Nd-YAG excitation laser.

Scaffold Synthesis

PLGA (50:50 polylactic:glycolic acid; Polysciences, PA, USA) was dissolved in chloroform (Sigma-Aldrich). Nanoparticles (MWCNTs, MWGONRs, GNPs, MSNP, WSNTs) were dispersed in the solution by heating to 60 °C for one hour followed by sonication for 30

minutes to achieve loading of 0.2 wt%. PLGA with no added particles was used as control. Once well dispersed, scaffolds were prepared by adding polymer/nanoparticle solution to NaCl porogen (size range: 200 – 500 μm) at a ratio leading to 90% porosity in the final scaffolds and mixed thoroughly to create a paste. Scaffold porosity was calculated using the following equation:[15]

$$\varepsilon\ (\%) = \frac{V_{NaCl}}{V_{NaCl} + V_{NC}}$$

Where ε is the apparent porosity of the scaffold, V_{NaCl} is the volume of NaCl porogen, and V_{NC} is the volume of the nanocomposite. Volumes were calculated based on the theoretical density of NaCl = 2.16 g/cm^3 and PLGA nanocomposites = 1.34 g/cm^3.

The composite-porogen paste was pressed into cylindrical Teflon molds with diameter of 6.5 mm and depth of 14 mm and left for 72 hours to evaporate off residual chloroform. Once dry, samples were pressed out of the molds and cut into thirds, creating 3 scaffolds with dimensions of 6.5 x ~4.5 mm^3. The porogen was removed by submersion in agitated deionized water for 1 week followed by vacuum drying.

SBF Submersion

Six scaffolds from each group were sterilized by submersion in 70% ethanol for 30 minutes followed by 30 minutes exposure to UV light. Samples were placed in individual 20 ml scintillation vials and submerged in 20 ml SBF (composition found in Table 1). Samples in SBF were placed under vacuum for 10 minutes to force the SBF within the pores of the scaffold and incubated at 37 °C and 5% CO_2 for 1, 3, 7 or 14 days with the SBF changed every two days. Each time the SBF was changed, the vacuum process was repeated.

Table 3.1. Ionic Composition of Simulated Body Fluid.

Ion	**Ion concentrations [mM]**	
	Human Blood Plasma[16]	**SBF[4]**
Na^+	142	142
K^+	5	
Mg^{2+}	1.5	
Ca^{2+}	2.5	2.31
HCO^{3-}	27	34.88
HPO_4^{2-}	1	1.39
SO_4^{2-}	.5	
Cl^-	103	109.9

Scaffold Structural Analysis

Representative SBF soaked and non-soaked scaffolds from each group and time point were selected for scanning electron microscopy (SEM) analysis. Samples were imaged using a high resolution analytical SEM (JEOL 7600F) at the Center for Functional Nanomaterials Samples were imaged using at accelerating voltages between 5 and 10 kV and a secondary electron imaging detector.

Confocal Raman

For confocal Raman analysis, scaffolds were cut into 2 mm sections and pressed between two glass slides to flatten. Scaffolds were analyzed on a Renishaw inVia Confocal Raman Microscope (Wotton-under-Edge, UK) with a 20x objective and a 785 nm laser at 50% power with a pin hole inserted for 180 seconds. Analysis was carried out in three separate areas of each scaffold and the characteristic peak for apatite (960 nm) was observed.

Total Reflection X-ray Fluorescence (TXRF)

After each time point, three scaffolds from each group were dissolved in 66% acetic acid. For TXRF, 1% gallium standard (10 mg/L) was added to each sample and 10 µl of solution was drop cast onto freshly cleaned quartz glass sample carriers coated with silicone solution (SERVA Electrophoresis GmbH, Heidelberg, DE). TXRF was carried out using a S2 PICOFOX (Bruker, Berlin, DE) with an exposure time of 250 seconds. Molar concentrations of calcium and phosphorous were used to calculate Ca/P ratios.

Calcium and Phosphate Assays

For calcium and phosphate assays, four samples from each group and time point were dissolved in 66% acetic acid. Calcium assay was performed by adding 20 µl of sample or calcium chloride standard to a 96 well plate in triplicates and adding 280 µl of Arsenazo III assay reagent. Absorbance was measured at 650 nm on a SpectraMax M2E Microplate Reader (Molecular Devices, Sunnyvale, CA). For phosphate assay, 100 µl of sample or potassium phosphate standard in acetic acid were added to a 96 well plate in triplicates and 50 µl of ammonium molybdate were added. Plates were incubated for 10 minutes and the absorbance was measured at 400 nm.

Statistics

As data was not normally distributed, a Kruskal-Wallace test with Dunn's *post hoc* was performed to assess significant differences in levels of calcium, phosphorus and phosphate accumulation as measured by TXRF or calcium/phosphate assays with $p < 0.05$ being considered significant.

Results

Nanoparticle Characterization

Representative HRTEM images of the nanoparticles can be found in Figure 3.1 A-E. MWCNTs (Figure 3.1 A) were smooth cylindrical structures with diameters in the manufacturer specified range of 20-30 nm and lengths in the range of 500–1500 nm. MWGONRs (Figure 3.1 B) were multi-layered and have a ribbon-like appearance with widths of about 60-90 nm and similar lengths to the MWCNTs from which they were synthesized. GONPs (Figure 3.1 C) were disk shaped particles with diameters in the range of 10-40 nm. MSNPs (Figure 3.1 D) were platelet shaped particles with diameters ranging from 40 – 90 nm. WSNTs (Figure 3.1 E) were smooth tube shaped particles with diameters in the range of 50-100 nm and lengths ranging from 1-15 µm.

Raman spectra for the nanoparticles can be found in Figure 3.1 F. Peaks were observed at 1340 cm^{-1} (D band) and 1560 cm^{-1} (G band) for MWCNTs (Figure 3.1 F [i]). Peaks were observed at 1346 cm^{-1} and 1600 cm^{-1} for MWGONRs (Figure 3.1 F [ii]). Peaks were observed at 1350 cm^{-1} and 1606 cm^{-1} for GONPs (Figure 3.1 F [iii]. Peaks were observed at 376 cm^{-1}, 404 cm^{-1}, and 476 cm^{-1} for MSNPs (Figure 3.1 F [iv]). Peaks were observed at 344 cm^{-1} and 412 cm^{-1} for WSNTs (Figure 3.1 F [v]). The peak at 516 cm^{-1} is attributed to the silicon wafer.

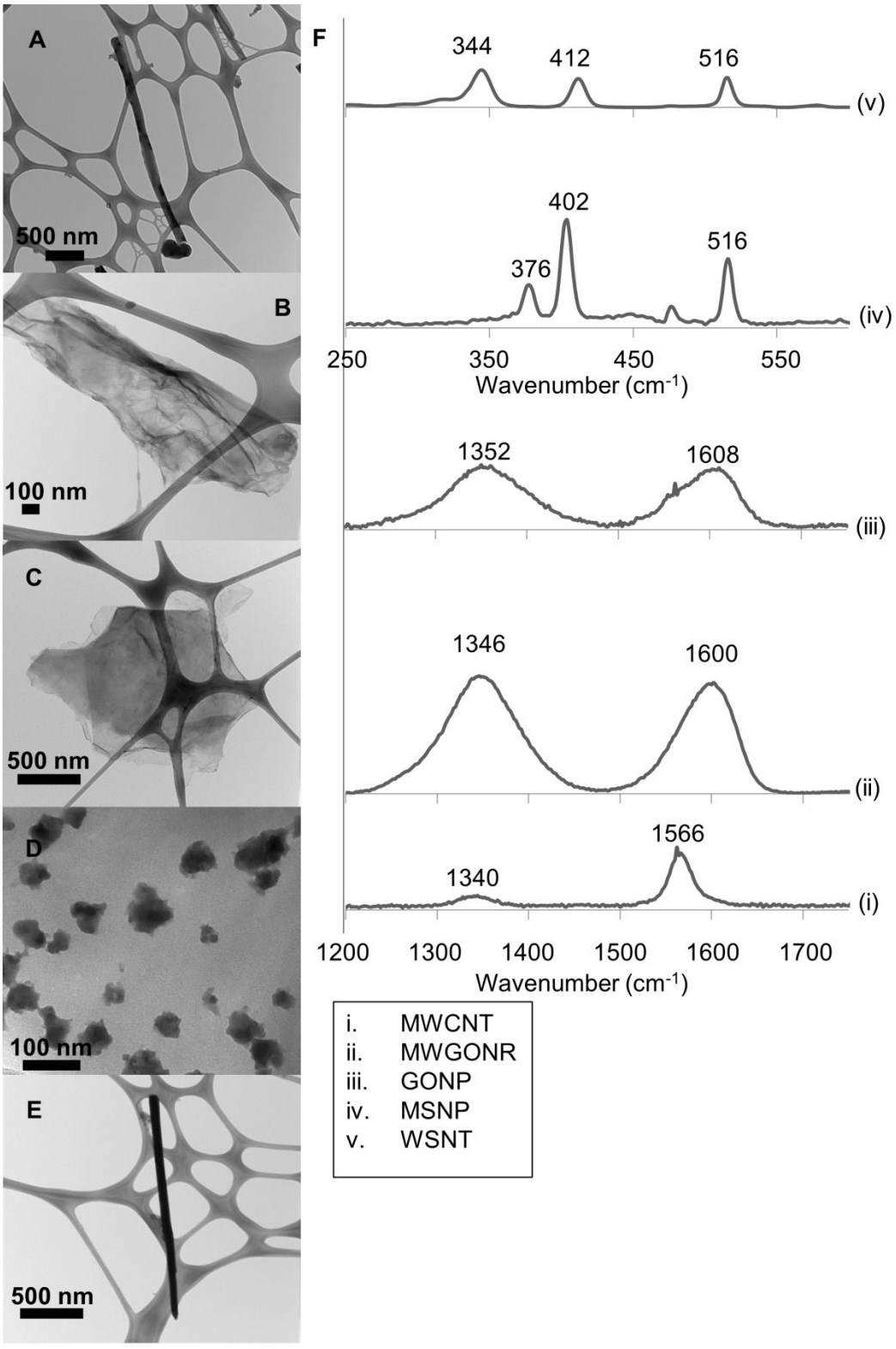

Figure 3.1. Representative HRTEM images of (A) MWCNTs, (B) MWGONRs, (C) GONPs, (D) MSNPs, and (E) WSNTs. (F) Raman spectra of MWCNTs (i), MWGONRs (ii), GONPs (iii), MSNPs (iv), and WSNTs (v).

Scaffold Structural Analysis

Figure 3.2 shows representative SEM images of control scaffolds or scaffolds reinforced with MWCNTs, MWGONRs, GONPs, MSNPs or WSNTs incubated in SBF for 1, 3, 7, or 14 days. Grossly, for all groups prior to incubation in SBF, scaffolds showed smooth surfaces with cubic spaces where NaCl porogen had been dissolved. After soaking in SBF, nodules of apatite were observed on the polymer surface with amount of apatite qualitatively increasing with increasing incubation time. There was no observable difference in the quantity of apatite between the groups. Nanoparticles could not be observed from SEM images.

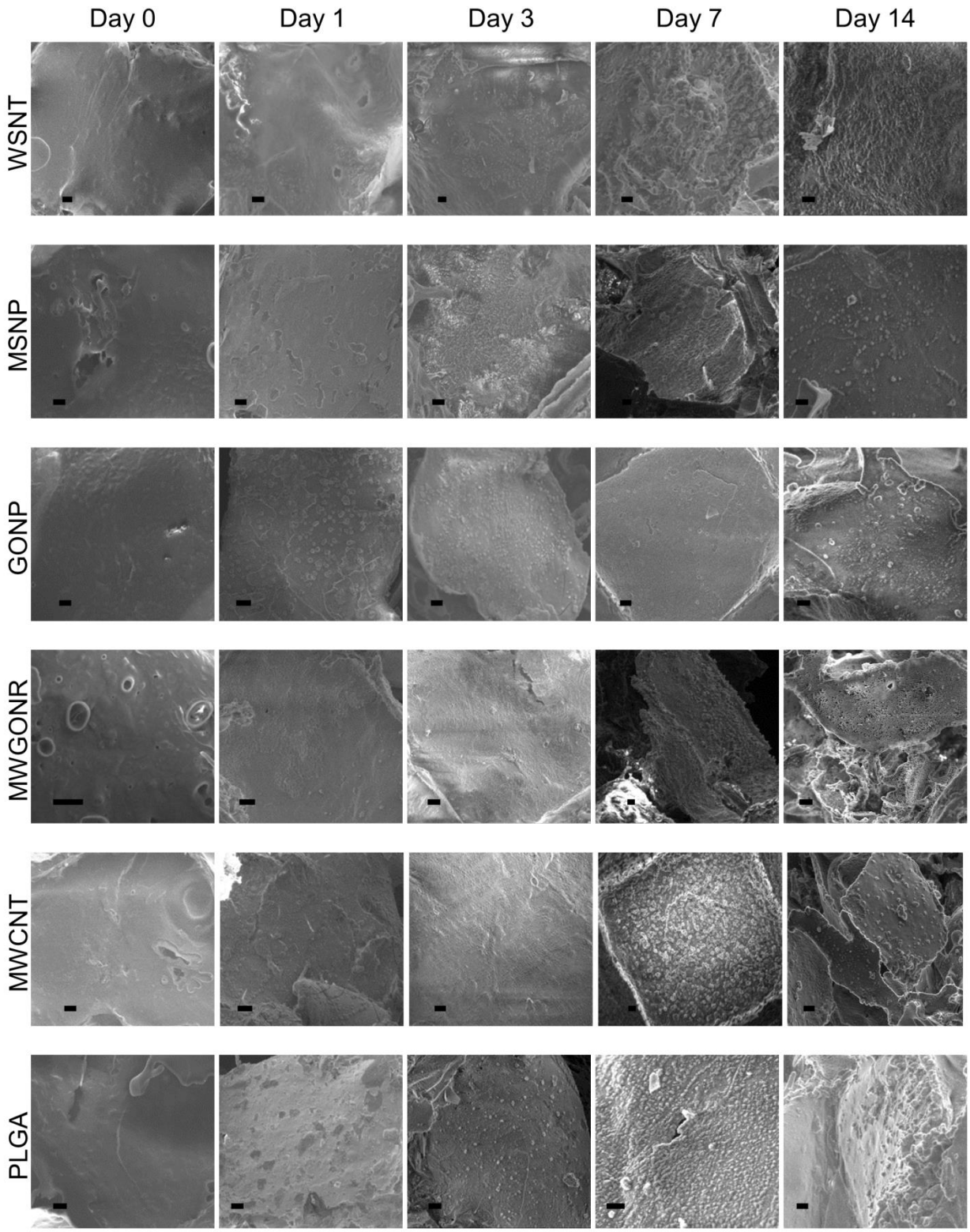

Figure 3.2. Representative SEM images of the surface morphology of control and nanoparticle reinforced scaffold groups prior to soaking in SBF and post soaking for 1, 3, 7, or 14 days. Scale bars = 10 μm.

Confocal Raman

Figure 3.3 shows the results of confocal Raman analysis of control and nanoparticle reinforced scaffolds soaked in SBF for 1, 3, 7 or 14 days. Prior to soaking, only peaks for PLGA polymer (~880 cm^{-1}) are observed for all groups. The characteristic apatite peak at 960 cm^{-1} appears after one day incubation in SBF for all groups and follows an increasing trend toward 14 days of incubation. MWGONRs gave rise to large G bands that spectrally overlapped with the apatite and polymer bands and therefore were not included.

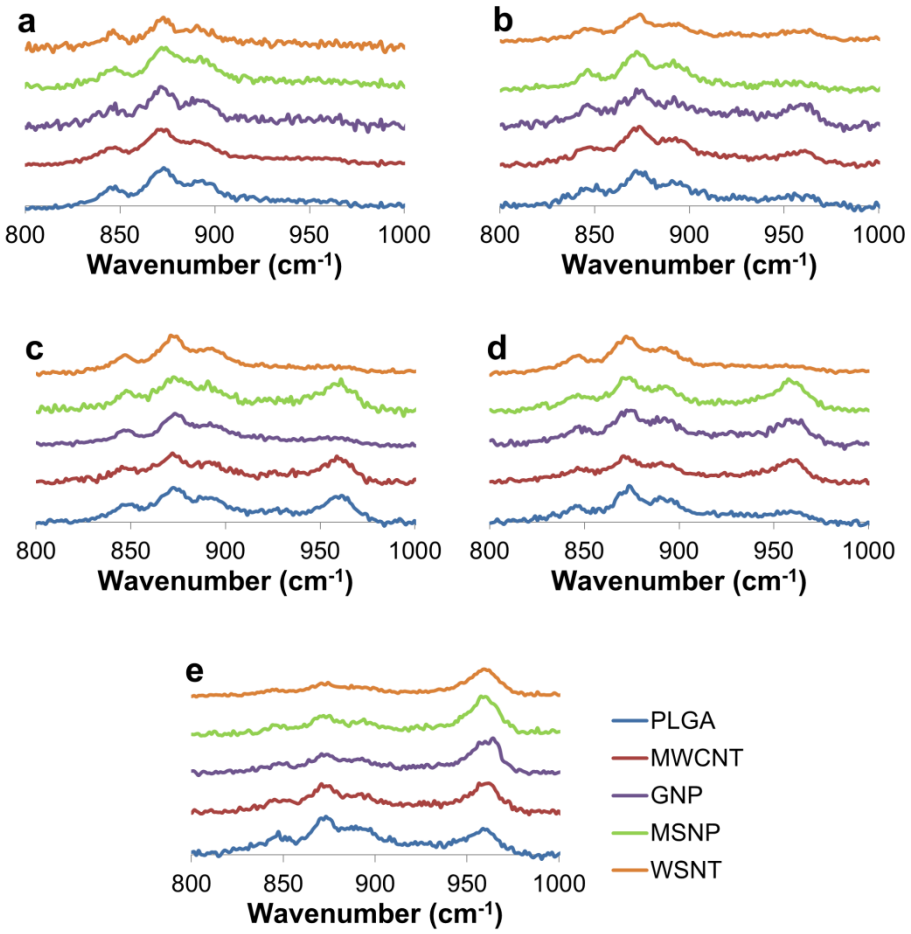

Figure 3.3. Confocal Raman spectra from surface of control and nanoparticle reinforced scaffolds prior to incubation in SBF (a), and after 1 (b), 3 (c), 7 (d), or 14 (e) days.

Total Reflection X-ray Fluorescence (TXRF)

Figure 3.4 shows the quantity of calcium (Figure 3.4 A) and phosphorus (Figure 3.4 B) collection on control and nanoparticle reinforced scaffolds over 1, 3, 7, or 14 days incubation in

SBF as found by TXRF analysis. Molar Ca/P ratio as calculated from the results is found in Figure 3.4 C. Quantity of calcium increased throughout the time points with highest amount occurring on day 14 of ~64 µg for PLGA. Quantity of phosphorus increased in earlier time points to a maximum of about 16 µg by day 3 and then decreased to as low as 4.8 µg for MWGONR by day 14. Ca/P ratio is below one prior to incubation in SBF and increases throughout the time points to as high as 9.79 for GONP reinforced scaffolds by day 14. No significant differences in calcium, phosphorus, or Ca/P ratio were observed between groups at any time point.

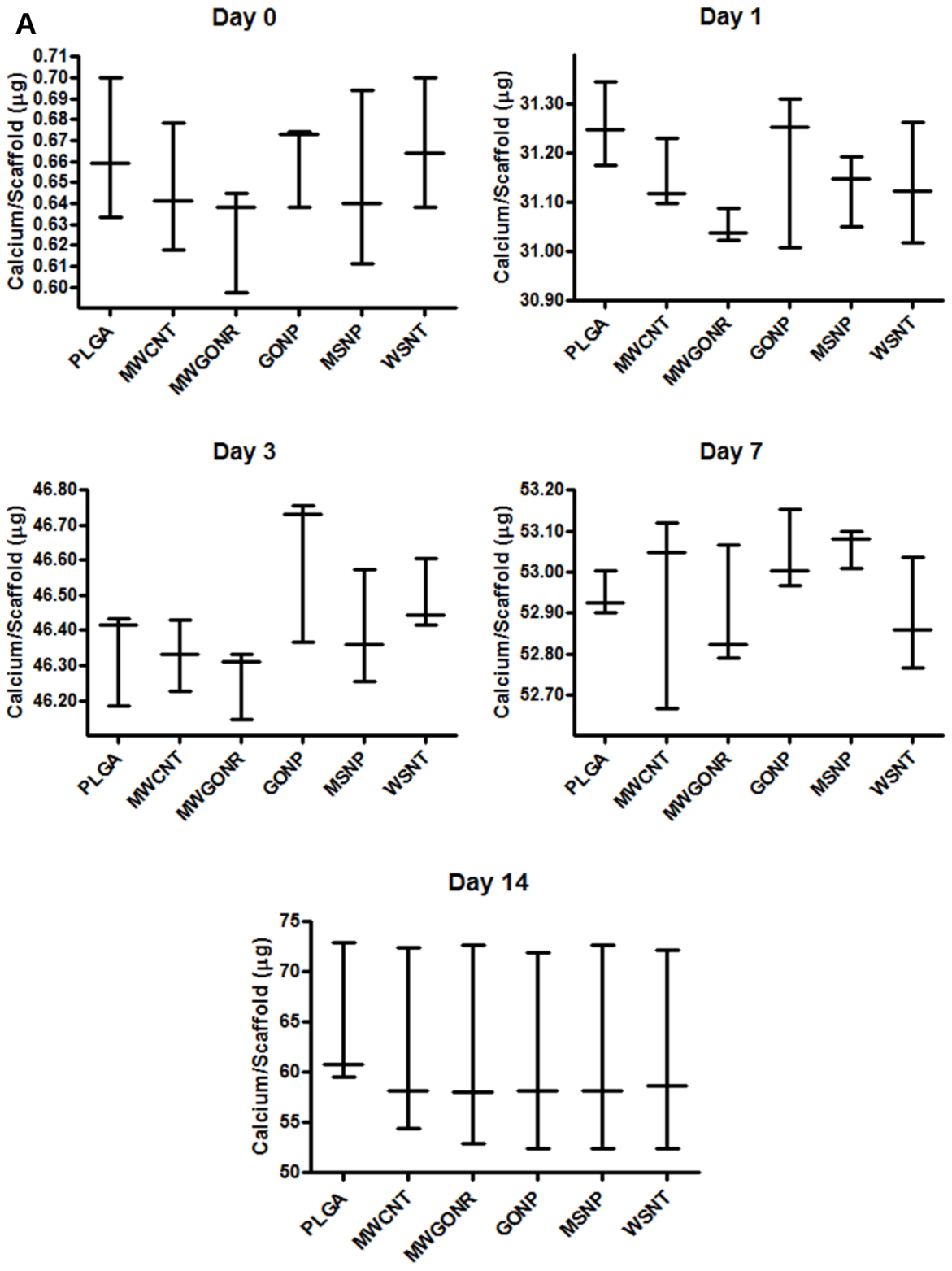
A
Day 0
Calcium/Scaffold (µg)
0.71
0.70
0.69
0.68
0.67
0.66
0.65
0.64
0.63
0.62
0.61
0.60
PLGA
MWCNT
MWGONR
GONP
MSNP
WSNT
Day 1
Calcium/Scaffold (µg)
31.30
31.20
31.10
31.00
30.90
PLGA
MWCNT
MWGONR
GONP
MSNP
WSNT
Day 3
Calcium/Scaffold (µg)
46.80
46.70
46.60
46.50
46.40
46.30
46.20
PLGA
MWCNT
MWGONR
GONP
MSNP
WSNT
Day 7
Calcium/Scaffold (µg)
53.20
53.10
53.00
52.90
52.80
52.70
PLGA
MWCNT
MWGONR
GONP
MSNP
WSNT
Day 14
Calcium/Scaffold (µg)
75
70
65
60
55
50
PLGA
MWCNT
MWGONR
GONP
MSNP
WSNT

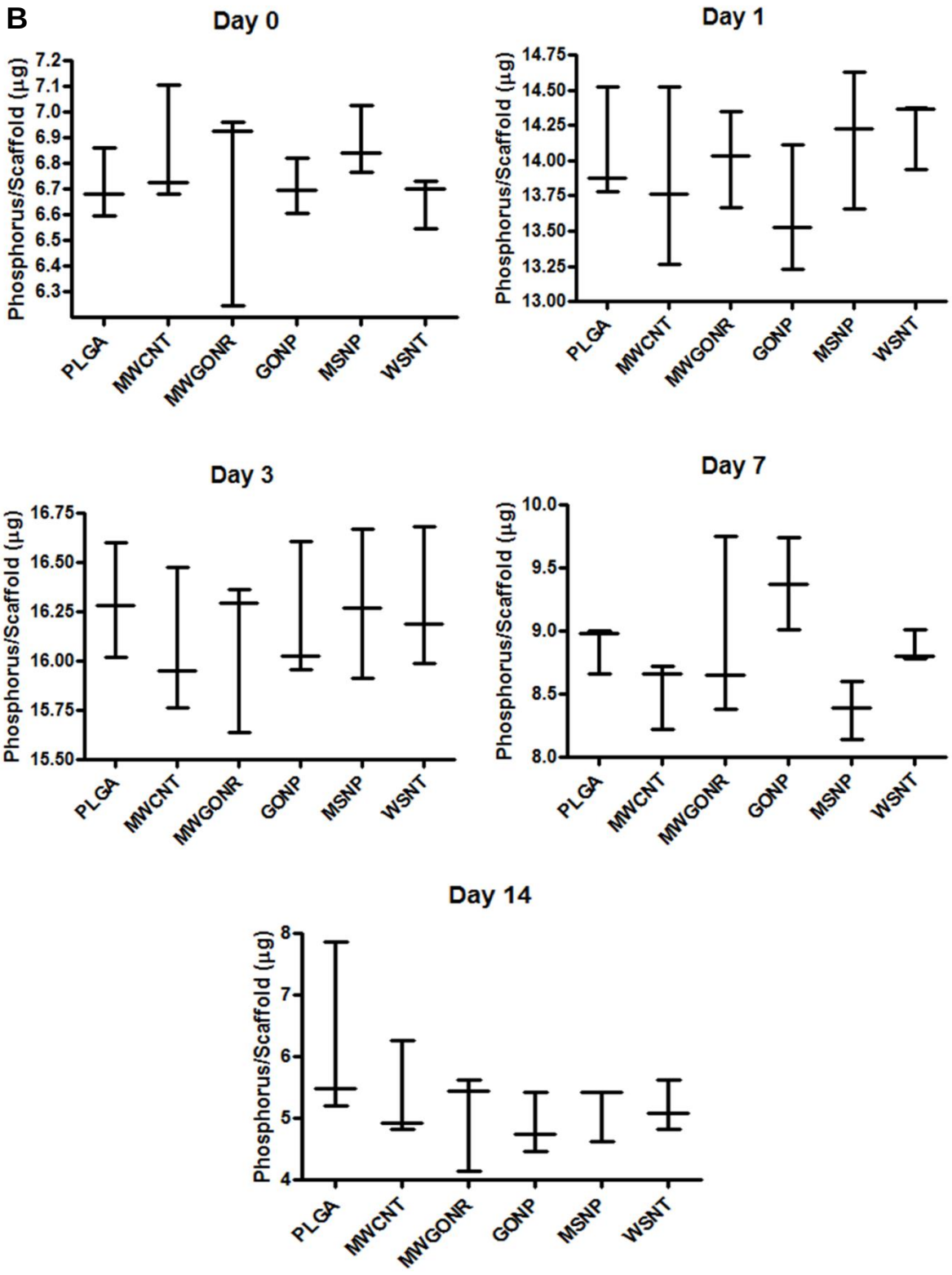
B
Day 0
Phosphorus/Scaffold (µg)
7.2
7.1
7.0
6.9
6.8
6.7
6.6
6.5
6.4
6.3
PLGA
MWCNT
MWGONR
GONP
MSNP
WSNT
Day 1
Phosphorus/Scaffold (µg)
14.75
14.50
14.25
14.00
13.75
13.50
13.25
13.00
PLGA
MWCNT
MWGONR
GONP
MSNP
WSNT
Day 3
Phosphorus/Scaffold (µg)
16.75
16.50
16.25
16.00
15.75
15.50
PLGA
MWCNT
MWGONR
GONP
MSNP
WSNT
Day 7
Phosphorus/Scaffold (µg)
10.0
9.5
9.0
8.5
8.0
PLGA
MWCNT
MWGONR
GONP
MSNP
WSNT
Day 14
Phosphorus/Scaffold (µg)
8
7
6
5
4
PLGA
MWCNT
MWGONR
GONP
MSNP
WSNT

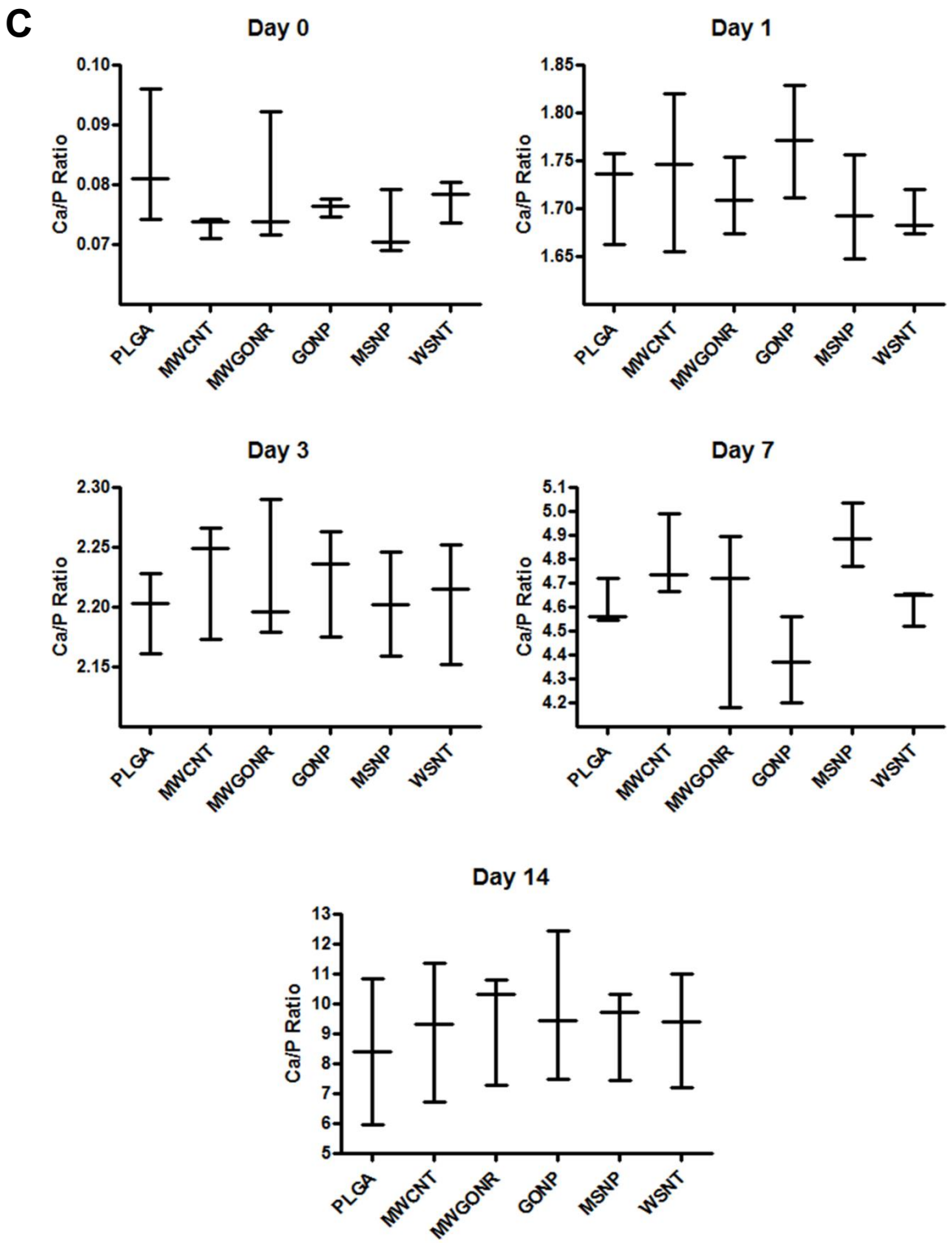

Figure 3.4. Box plots show TXRF results for (A) calcium and (B) phosphorus collection on control and nanoparticle reinforced scaffolds (n=3) soaked in SBF for 0, 1, 3, 7, or 14 days. Ca/P ratio, calculated from results is found in (C). Statistical significance was determined by Kruskal-Wallis test with Dunn's *post hoc* and $p<0.05$ being significant.

Calcium and Phosphate Assays

Figure 3.5 shows the calcium (Figure 3.5 A) and phosphate (Figure 3.5 B) collection on control or nanoparticle reinforced scaffolds after incubation in SBF for 1, 3, 7, or 14 days. Overall, calcium quantity remained at similar levels through seven days incubation and increased by about 100% after 14 days incubation. After one day of incubation, the quantity of calcium was significantly higher on PLGA and WSNT scaffolds as compared to MSNP reinforced scaffolds. No differences were observed after three days incubation in SBF. After seven days of incubation in SBF, GONP reinforced scaffolds showed significantly higher calcium compared to PLGA, MWGONR, and MSNP reinforced scaffolds, while MWCNT reinforced scaffolds had collected significantly more calcium than MWGONR reinforced scaffolds. After 14 days of incubation PLGA scaffolds showed significantly higher (as much as 20%) calcium collection compared to MWGONR scaffolds.

Phosphate collection also showed similar levels through the first 7 days of incubation followed by an increase in GONP, MSNP, and WSNT reinforced groups after 14 days of incubation. After one day of incubation, phosphate collection on PLGA was significantly greater than MWCNT and MSNP reinforced scaffolds. WSNT reinforced scaffolds had significantly greater phosphate collection compared to MWCNT or MSNP reinforced scaffolds. After three days of incubation PLGA scaffolds and scaffolds reinforced with MWCNTs had significantly greater phosphate accumulation than GONP, MSNP or WSNT scaffolds. No significant differences in phosphate collection were observed after seven days of incubation in SBF. After 14 days of incubation, PLGA had significantly less phosphate as compared to groups reinforced with GONP, MSNP or WSNT, accumulating just 46% of WSNT scaffold levels. MWCNT reinforced scaffolds accumulated significantly less phosphate compared to MSNP and WSNT

reinforced scaffolds and MWGONR reinforced scaffolds accumulated significantly less phosphate compared to WSNT reinforced scaffolds.

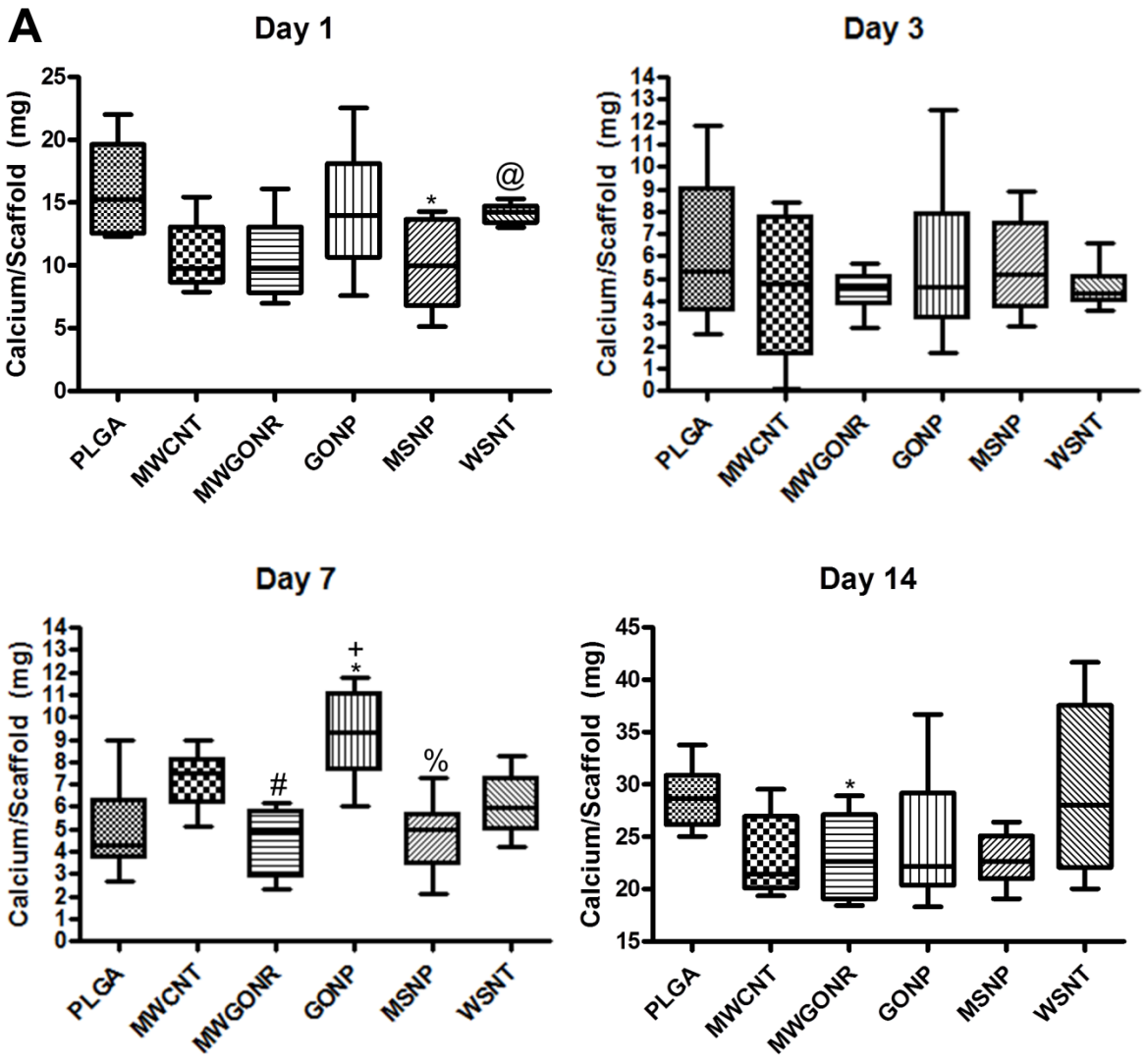

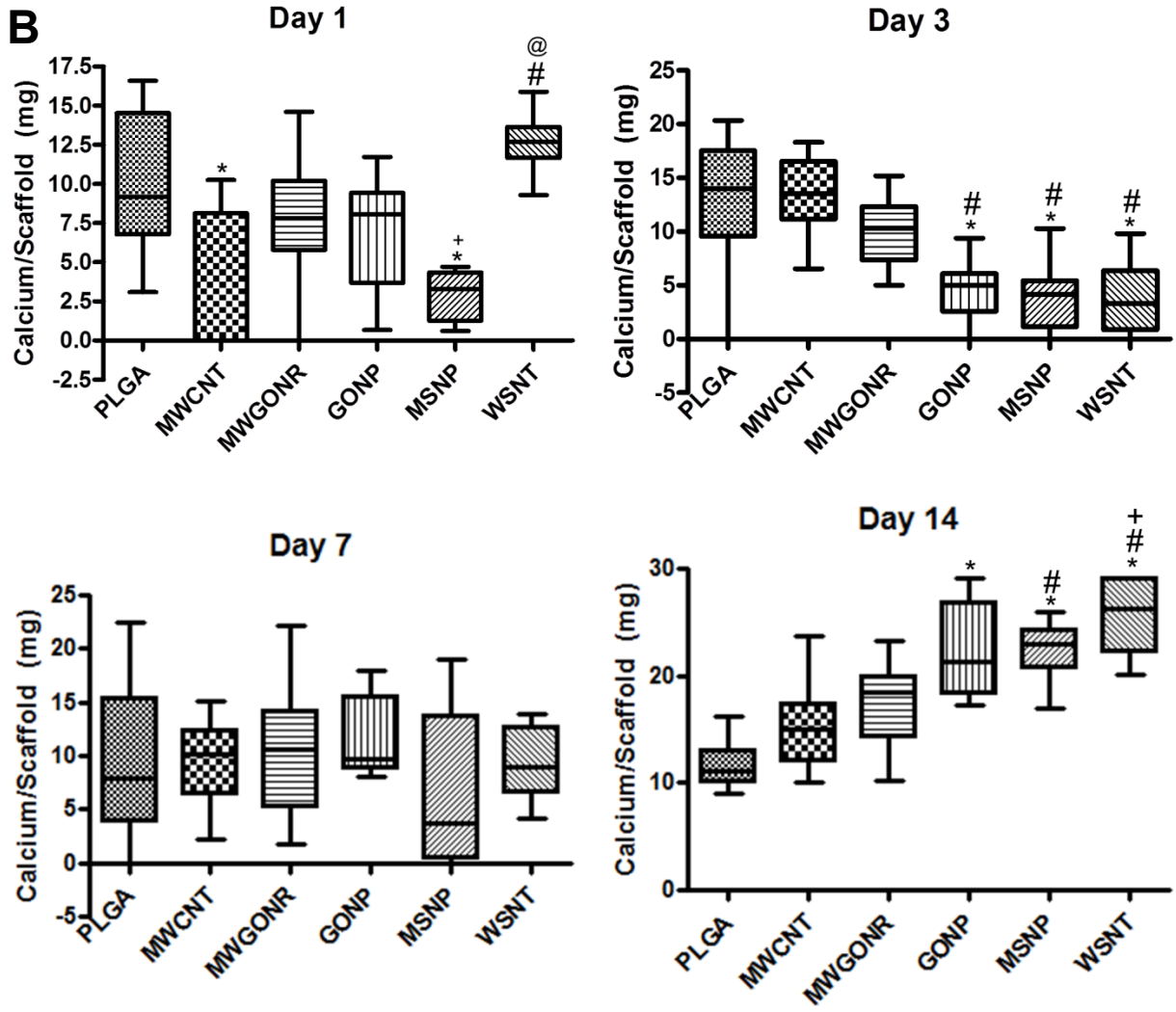

Figure 3.5. Box plots show results of (A) calcium assay and (B) phosphate assay as performed on control and nanoparticle reinforced scaffolds (n=4) soaked in SBF for 1, 3, 7, or 14 days. Statistical significance corresponds to Kruskal-Wallace with Dunn's *post hoc* and $p<0.05$ being significant. Statistical significance is denoted by (*) compared to PLGA, (#) compared to MWCNTs, (+) compared to MWGONR, (%) compared to GONP, and (@) compared to MSNP.

Discussion

The objective of this study was to investigate the effect of nanoparticle dimension and composition on the bioactivity of nanoparticle reinforced scaffolds soaked in SBF for up to 14 days. In the realm of bone tissue engineering, bioactivity is a material property; an ability to influence bone formation through formation of a bone bonding layer of apatite on the surface. The amount of influence a scaffold will have is strongly dependent on surface properties and chemistry.[3] Therefore, nanoparticles with distinct composition (organic or inorganic) and morphologies (nanotubes, nanoplatelets, or nanoribbons) were incorporated into PLGA-based scaffolds at a concentration of 0.2 wt% and bioactivity was tested through incubation in SBF for up to 14 days under physiological conditions. PLGA was selected for the biodegradable polymer matrix due to the large body of research around PGLA scaffolds[5,17-19], tunable degradation rate and well characterized degradation products, and Food and Drug Administration (FDA) approval.[20] 0.2 wt% nanoparticle reinforcement was chosen as this concentration has previously been shown to significantly improve the mechanical properties of polymer-based nanocomposites compared to polymer alone.[1,2] Additionally, previous studies have found that 0.2 wt% loading of these nanoparticles, which if released from a 90% porous scaffold with volume 10 cm^3 equals about 20 μg/ml, is potentially safe for stem cells.[14,21] 14 days of incubation in SBF was chosen as this was the longest time allowable to observe growth of an apatite layer in all groups without significant degradation of polymer, however it should be noted that that longer incubation times may lead to further growth of this layer.[22] This study of a broad range of nanoparticle reinforcing agents allowed identification of specific nanoparticle properties that may be most promising for eliciting a bioactive response when implanted in hard tissue.

Raman spectroscopy of the nanoparticles prior to scaffold incorporation is presented in Figure 3.1 E. MWCNTs, MWGONRs, and GONPS all exhibit the characteristic D- and G- bands for graphene at about 1350 cm^{-1} and 1580 cm^{-1}, respectively. The G-band is also first order and exists in all sp^2 carbon structures. This band represents the E_{2g} mode or C-C stretching that occurs within the plane of carbon atoms.[23] The D-band is a first order band representative of defects in the graphene structure.[23] The ratio of the intensities of the D- and G- bands is commonly used to infer the amount of defects in the graphene sheet.[24] Therefore, it follows that the I_D/I_G ratio is increased in MWGONRs and GONPs compared to pristine MWCNTs, indicating disruption of the sp^2-bonded carbon owing to oxidative unzipping of nanotubes during synthesis.[13] The Raman spectra of the inorganic nanoparticles, MSNPs and WSNTs, reveal the two major bands characteristic of dichalcogenides representing the $E_{2g}{}^1$ (in-plane) and A_{1g} (out-of-plane) Raman active modes.[14,25] The MSNP spectrum also contains a small peak around 474 cm^{-1} that is attributed to unreacted MoO_3 from the synthesis process.

SEM images found in Figure 3.2 of PLGA and nanoparticle reinforced scaffolds soaked in SBF over 14 days revealed that small seeds of apatite crystals began to appear after just one day of incubation. At early time points, apatite crystals were two-dimensional and with increasing time became more three-dimensional. This observation may indicate carbonate incorporation into the mineral structure, substituting for OH or PO_4^{3-}, as has been previously reported as causing apatite crystal morphology to become more spherulitic.[26] Nanoparticles were not observed in SEM images mostly likely due to their enfoldment in the polymer and the low magnification.

Confocal Raman analysis, found in Figure 3.3, showed the appearance of the peak for apatite at 960 cm^{-1}, representing the symmetric stretching of the PO_4^{3-} group, after one day

incubation in SBF. The variability in peak strength across the lower time points can be explained by the non-homogenous deposition of the apatite layer. As greater amounts of apatite form, the deposition becomes more ubiquitous and the 960 cm^{-1} peak becomes more prominent as was observed after 14 days of incubation.[27]

Calcium accumulation increased through the 14 days of incubation in SBF for all groups as detected by both TXRF (Figure 3.4 A) and calcium assay (Figure 3.5 A). Although the results of the two techniques show a similar trend, the values of the concentrations were not similar. This variability may be due to the potential of Arsenazo III to react with trace metals or other interferents that may have been present during the assay.[28] Taken together with the TXRF results, it can be concluded that the addition of 2 wt% of these organic and inorganic nanoparticles do not hinder calcium accumulation on the implant surface.

The amount of phosphorus detected by TXRF (Figure 3.4 B) and phosphate detected by phosphate assay (Figure 3.5 B) showed similar range of values but different trends with phosphorus increasing to a maximum by day three, followed by a decrease in concentration through day 14, while quantity of phosphate continued to increase throughout the time points. While TXRF detects phosphorus at an elemental level, the phosphate assay reagent reacts with PO_4^{3-}. Therefore, even though quantity of phosphorus atoms may decrease over time, as long as those that remain form PO_4^{3-}, it is possible to observe an increase in phosphate with a decrease in phosphorus.

Results from the phosphate assay showing the greatest increase in phosphate accumulation at the 14 day time point are in agreement with the results of the calcium assay, suggesting that the majority of mineralization occurred between days 7 and 14. In the current case, the significant increase in phosphate detected on nanoparticle reinforced scaffolds as

compared to the PLGA control after 14 days incubation in SBF may indicate that the nanoparticles act as nucleation sites for apatite formation.[29] This observation may relate to dispersion of nanoparticles in the polymer creating surface nanotopography and increased surface area.[29] The presence of nanoparticle defects or functional groups may also play a role, as negatively charged implant surfaces (i.e. carboxyl groups) have been shown to act as nucleation sites for apatite formation.[30] Additionally, the significant increase of phosphate on GONPs, MSNPs, and WSNTs reinforced scaffolds may indicate that nanoparticle composition and aspect ratio play a role in the mechanism of apatite layer formation. The organic particles follow the trend: nanoplatelets > nanoribbons > nanotubes; while conversely, the inorganic particles follow the trend: nanotubes > nanoplatelets. However, as the value for MSNPs shows equal phosphate concentration as the highest organic nanoparticle (GONPs), composition may play a greater role with inorganic being more favorable than organic nanoparticles and apatite formation on WSNT more favorable to MSNP regardless of morphology.

To the best of our knowledge, this is the first report investigating and comparing the bioactivity of one- and two-dimensional organic and inorganic nanomaterials as reinforcing agents for application as biomedical implants for bone tissue engineering. For polymeric nanocomposites, few reports have investigated the bioactivity in SBF of one or two-dimensional carbon nanostructures,[9-11,31-33] and no previous work relating to bioactivity of MSNP or WSNT containing scaffolds could be found. The work of Wan et al. incorporating low concentrations (0.3 wt%) of GONP into poly(caprolactone) or gelatin nanocomposites, qualitatively support the conclusion of this study that the addition of low concentrations of GONPs enhance the accumulation of apatite on scaffold surfaces compared to polymer alone.[10,11] Conversely to the results of this study, Zawadzak et al. found that the addition of MWCNTs to polyurethane foams

accelerated the precipitation of apatite compared to polyurethane alone.[9] This difference can most likely be explained by the differing synthesis methods with the mixture of polymer and MWCNT employed here leading to less nanoparticle exposure for apatite precipitation as compared to the electrophoretic deposition of MWCNTs on the surface of the polyurethane foams.

By providing comparisons of bioactivity for polymer nanocomposites reinforced with various one- or two-dimensional, organic or inorganic nanoparticles, this work significantly contributes to the existing body of work surrounding bioactive nanostructure-reinforced polymer nanocomposites. Additionally, the enhanced phosphate results of the two-dimensional GONP and MSNP and one-dimensional WSNT reinforced scaffolds gives additional support toward their application in bone tissue engineering and allows for further investigation *in vivo* to evaluate their biocompatibility and osteoinductivity.

Conclusions

Apatite nodules formed on the surface of PLGA and all nanoparticle reinforced scaffolds after incubation in SBF for up to 14 days. Apatite presence was confirmed by confocal Raman analysis. GONP, MSNP, and WSNT groups showed significantly greater phosphate accumulation compared to PLGA, MWCNT, or MWGONR groups. The results suggest that GONPs, MSNPs, and WSNTs at 0.2 wt% concentration in PLGA porous scaffolds may be able to elicit a bioactive response when implanted *in vivo*.

Acknowledgements

This work was supported by the National Institutes of Health (grants No. 1DP2OD007394-01). Research was carried out in part at the Center for Functional Nanomaterials, Brookhaven National Laboratory, New York, which is supported by the U.S. Department of Energy, Office of Basic Energy Sciences, under Contract No. DE-AC02-98CH10886. Confocal Raman data were acquired in SoMAS' NAno-Raman Molecular Imaging Laboratory (NARMIL), a community facility dedicated to environmental sciences' applications and founded with NSF-MRI grant OCE-1336724. The authors would like to thank Susan Van Horn (Central Microscopy, Stony Brook University) for her help with Transmission Electron Microscopy.

References

1 Lalwani, G. *et al.* Two-dimensional nanostructure- reinforced biodegradable polymeric nanocomposites for bone tissue engineering. *Biomacromolecules* **14**, 900-909, (2013).

2 Lalwani, G. *et al.* Tungsten disulfide nanotubes reinforced biodegradable polymers for bone tissue engineering. *Acta Biomaterialia* **9**, 8365-8373, (2013).

3 Blokhuis, T. & Arts, J. C. Bioactive and osteoinductive bone graft substitutes: definitions, facts and myths. *Injury* **42**, S26-S29 (2011).

4 Bohner, M. & Lemaitre, J. Can bioactivity be tested *in vitro* with SBF solution? *Biomaterials* **30**, 2175-2179 (2009).

5 Kim, S.-S., Park, M. S., Gwak, S.-J., Choi, C. Y. & Kim, B.-S. Accelerated bonelike apatite growth on porous polymer/ceramic composite scaffolds *in vitro*. *Tissue Engineering* **12**, 2997-3006 (2006).

6 Hong, Z., Reis, R. L. & Mano, J. F. Preparation and in vitro characterization of scaffolds of poly(l-lactic acid) containing bioactive glass ceramic nanoparticles. *Acta Biomaterialia* **4**, 1297-1306 (2008).

7 Gerhardt, L.-C., Jell, G. & Boccaccini, A. Titanium dioxide (TiO_2) nanoparticles filled poly(D, L lactid acid) (PDLLA) matrix composites for bone tissue engineering. *Journal of Materials Science: Materials in Medicine* **18**, 1287-1298 (2007).

8 Kim, J.-J. *et al.* Magnetic scaffolds of polycaprolactone with functionalized magnetite nanoparticles: physicochemical, mechanical, and biological properties effective for bone regeneration. *RSC Advances* **4**, 17325-17336 (2014).

9 Zawadzak, E. *et al.* Polyurethane foams electrophoretically coated with carbon nanotubes for tissue engineering scaffolds. *Biomedical Materials* **4**, 015008 (2009).

10 Wan, C. & Chen, B. Poly(ε-caprolactone)/graphene oxide biocomposites: mechanical properties and bioactivity. *Biomedical Materials* **6**, 055010 (2011).

11 Wan, C., Frydrych, M. & Chen, B. Strong and bioactive gelatin–graphene oxide nanocomposites. *Soft Matter* **7**, 6159-6166 (2011).

12 Chowdhury, S. M. *et al.* Cell specific cytotoxicity and uptake of graphene nanoribbons. *Biomaterials* **34**, 283-293 (2013).

13 Paratala, B. S., Jacobson, B. D., Kanakia, S., Francis, L. D. & Sitharaman, B. Physicochemical characterization, and relaxometry studies of micro-graphite oxide, graphene nanoplatelets, and nanoribbons. *PLoS One* **7**, e38185 (2012).

14 Rashkow, J. T., Talukdar, Y., Lalwani, G. & Sitharaman, B. Interactions of 1D- and 2D-layered inorganic nanoparticles with fibroblasts and human mesenchymal stem cells. *Nanomedicine* **10**, 1693-1706, (2015).

15 Kim, J., Yaszemski, M. J. & Lu, L. Three-dimensional porous biodegradable polymeric scaffolds fabricated with biodegradable hydrogel porogens. *Tissue Engineering Part C: Methods* **15**, 583-594 (2009).

16 Kokubo, T. & Takadama, H. How useful is SBF in predicting in vivo bone bioactivity? *Biomaterials* **27**, 2907-2915 (2006).

17 Ngiam, M. *et al.* The fabrication of nano-hydroxyapatite on PLGA and PLGA/collagen nanofibrous composite scaffolds and their effects in osteoblastic behavior for bone tissue engineering. *Bone* **45**, 4-16 (2009).

18 Zhang, R. & Ma, P. X. Biomimetic polymer/apatite composite scaffolds for mineralized tissue engineering. *Macromolecular Bioscience* **4**, 100-111 (2004).

19 Murphy, W. L., Kohn, D. H. & Mooney, D. J. Growth of continuous bonelike mineral within porous poly(lactide-co-glycolide) scaffolds *in vitro*. *Journal of Biomedical Materials Research* **50**, 80-58 (2000).

20 Makadia, H. K. & Siegel, S. J. Poly (lactic-co-glycolic acid) (PLGA) as biodegradable controlled drug delivery carrier. *Polymers* **3**, 1377-1397 (2011).

21 Talukdar, Y., Rashkow, J. T., Lalwani, G., Kanakia, S. & Sitharaman, B. The effects of graphene nanostructures on mesenchymal stem cells. *Biomaterials* **35**, 4863-4877 (2014).

22 Chen, Q. Z., Thompson, I. D. & Boccaccini, A. R. 45S5 Bioglass®-derived glass–ceramic scaffolds for bone tissue engineering. *Biomaterials* **27**, 2414-2425 (2006).

23 Ferrari, A. *et al.* Raman spectrum of graphene and graphene layers. *Physical Review Letters* **97**, 187401 (2006).

24 Salzmann, C. G. *et al.* The role of carboxylated carbonaceous fragments in the functionalization and spectroscopy of a single-walled carbon-nanotube material. *Advanced Materials* **19**, 883-887 (2007).

25 Molina-Sanchez, A. & Wirtz, L. Phonons in single-layer and few-layer MoS_2 and WS_2. *Physical Review B* **84**, 155413 (2011).

26 Choi, S., Yu, X., Jongpaiboonkit, L., Hollister, S. J. & Murphy, W. L. Inorganic coatings for optimized non-viral transfection of stem cells. *Scientific Reports* **3**, doi:10.1038/srep01567 (2013).

27 Bonadio, T. G. M. *et al.* Bioactivity and structural properties of nanostructured bulk composites containing Nb_2O_5 and natural hydroxyapatite. *Journal of Applied Physics* **113**, 223505 (2013).

28 Morgan, B. R., Artiss, J. D. & Zak, B. Calcium determination in serum with stable alkaline Arsenazo III and triglyceride clearing. *Clinical Chemistry* **39**, 1608-1612 (1993).

29 Tran, P. A., Sarin, L., Hurt, R. H. & Webster, T. J. Opportunities for nanotechnology-enabled bioactive bone implants. *Journal of Materials Chemistry* **19**, 2653-2659 (2009).

30 Aryal, S. *et al.* Carbon nanotubes assisted biomimetic synthesis of hydroxyapatite from simulated body fluid. *Materials Science and Engineering: A* **426**, 202-207, (2006).

31 Cai, Q., Mao, J., Li, X. & Yang, X. Macroporous and nanofibrous PLLA scaffolds reinforced with calcium phosphate-coated multiwalled carbon nanotubes. *Materials Letters* **128**, 238-241 (2014).

32 Dorj, B. *et al.* Robocasting nanocomposite scaffolds of poly(caprolactone)/hydroxyapatite incorporating modified carbon nanotubes for hard tissue reconstruction. *Journal of Biomedical Materials Research, Part A* **101**, 1670-1681 (2013).

33 Siqueira, I. A. *et al. In vitro* and *in vivo* studies of novel poly(d,l-lactic acid), superhydrophilic carbon nanotubes, and nanohydroxyapatite scaffolds for bone regeneration. *ACS Applied Materials & Interfaces* **7**, 9385-9398 (2015).

Chapter 4

In Vivo Biocompatibility of Two-Dimensional Nanoparticle Reinforced PLGA Bone Tissue Engineering Scaffolds

Contributions by: Jason T. Rashkow, Yahfi Talukdar, Gaurav Lalwani, Balaji Sitharaman

Abstract

This study investigates the hard and soft tissue *in vivo* biocompatibility of 90% porous poly(lactic-co-glycolic acid) (PLGA) nanocomposite scaffolds reinforced with 0.2 wt% graphene oxide nanoplatelets (GONPs) or molybdenum disulfide nanoplatelets (MSNPs). Scaffolds were implanted in a non-critical sized monocortical defect in the tibia or subcutaneously on the dorsum of a rat. Comparable *in vivo* biocompatibility was observed between the nanoparticle reinforced scaffolds and PLGA alone. In addition, 2 weeks after implantation, significantly less bone growth was observed for the PLGA group compared to the empty defect group that was not observed for the experimental groups. This may indicate that the addition of the nanoparticles induces bioactivity of the scaffolds. Scaffolds reinforced with GONPs or MSNPs show promise for bone tissue engineering applications.

Introduction

Biodegradable polymers show promise as bone replacement materials for bone tissue engineering due to inherent biocompatibility and degradability, and osteoconductivity.[1,2] These polymers are also easily manipulated, allowing for porous structures with custom morphology.[2,3] However, the main limitation for application of biodegradable polymers as bone replacement materials is inferior mechanical properties.[3] The mechanical strength of a bone tissue engineering scaffold is an especially important consideration during the design process as a weak scaffold could lead to an unstable defect area while a material much stronger than bone can cause resorption of the surrounding tissue.[4] This limitation has led to the emergence of biodegradable polymer nanocomposites reinforced with various nanoparticles.

Zero- and one-dimensional carbon-based nanomaterials such as fullerenes and carbon nanotubes have been extensively explored for their ability to reinforce biodegradable polymers for bone tissue engineering;[5-12] and a few studies have investigated the biocompatibility of these nanocomposites.[13-16]

Recently, we have examined the suitability of some two-dimensional organic (graphene nanoribbons (GONR) and graphene nanoplatelets (GONP)) and inorganic (molybdenum disulfide nanoplatelets (MSNP)) two-dimensional nanoparticles to reinforce biodegradable polymer nanocomposites. We demonstrated that the addition of 0.2 wt% of two-dimensional nanoparticles significantly enhances the compressive and flexural moduli of the nanocomposites compared to polymer alone or polymer reinforced with one-dimensional single- or multi-walled carbon nanotubes.[17] This increase in mechanical strength Additionally, we investigated the cytocompatibility of these nanocomposites to NIH-3T3 fibroblasts and MC3T3-E1

preosteoblasts and observed high viability (78-100%) and cellular attachment to the nanocomposites.[18] However, few studies have investigated the *in vivo* biocompatibility of GONP reinforced nanocomposites and to the best of our knowledge; no studies have examined MSNP reinforced scaffolds.[19-22] Kanayama et al. examined the soft tissue biocompatibility of GONP and reduced-GONP coated collagen scaffolds in a rat model after being implanted for 10 days.[20] Zhou et al. reported the inflammatory response by microglia and astrocytes after implanting electrospun poly(ε-caprolactone) microfiber scaffolds coated with colloidal graphene into the striatum or into the subventricular zone of adult rats for 7 weeks.[22] Wang et al. investigated the addition of graphene to polyethylene-terephthalate for use in an extra-articular graft-to-bone healing procedure in New Zealand rabbits for 4, 8, and 12 weeks.[21] Finally, Duan et al. examined the biocompatibility of mesenchymal stem cell (MSC) seeded graphene reinforced poly(L-lactic acid) scaffolds implanted intramuscularly in nude mice for 2, 4, and 8 weeks.[19]

The effects that a nanoparticle will have on cells and tissues will vary depending on particle composition, morphology, and even synthesis method. Therefore, it is necessary to investigate the effects that all nanoparticles will have on nanocomposite biocompatibility. Beyond bone biocompatibility, it is common to implant bone tissue engineering constructs ectopically, either subcutaneously or intramuscularly, in order to more easily observe the cellular encapsulation and foreign body response to the material. Therefore, in this study we have examined the *in vivo* hard and soft tissue biocompatibility of 90% porous poly(lactic-co-glycolic acid) (PLGA) scaffolds reinforced with 0.2 wt% of two-dimensional nanoparticles GONP and MSNP. We report the tissue response of these scaffolds in a rat model after being implanted for 2 and 6 weeks.

Materials and Methods

Nanoparticle Synthesis and Characterization

GONPs were synthesized from graphite flakes using a modified Hummer's method.[23] MSNPs were synthesized through a high temperature reaction between MoO_3 and sulfur powder (Sigma-Aldrich, St. Louis, MO, USA).[24] Particles were characterized by high resolution transmission electron microscopy (HRTEM) and Raman spectroscopy. For HRTEM, nanoparticles were dispersed in water and ethanol (1:1 solution) by sonication. Dispersion was followed by ultracentrifugation and the supernatant was drop cast on a lacey carbon grid (300 mesh size, copper support, Ted Pella, Redding, CA, USA). HRTEM imaging was performed using a JOEL 2100F high-resolution analytical transmission electron microscope (Peabody, MA, USA) with an accelerating voltage of 200 kV at the Center for Functional Nanomaterials, Brookhaven National Laboratory, New York. Raman spectra were recorded on a silicon substrate (Type P: (Boron), Orientation <100>, Ted Pella) between 50–3750 cm^{-1} using WITec alpha300R Micro-Imaging Raman Spectrometer (Ulm, DE) equipped with a 532 nm Nd-YAG excitation laser at room temperature.

Scaffold Synthesis

PLGA (50:50 polylactic:glycolic acid; Polysciences, Warrington, PA, USA) was dissolved in chloroform (Sigma-Aldrich). To achieve loading of 0.2 wt% GONPs or MSNPs, particles were dispersed in the polymer solution by heating to 60 °C for one hour followed by sonication for 30 minutes. PLGA with no added particles was used as control. 90% porous scaffolds were prepared by adding polymer/nanoparticle solution to NaCl porogen (size range:

200–500 μm) at a ratio leading to desired porosity in the final scaffolds and mixed thoroughly to create a paste. Scaffold porosity was calculated using the following equation:[25]

$$\varepsilon\ (\%) = \frac{V_{NaCl}}{V_{NaCl} + V_{NC}}$$

Where ε is the apparent porosity of the scaffold, V_{NaCl} is the volume of NaCl porogen, and V_{NC} is the volume of the nanocomposite. Volumes were calculated based on the theoretical density of NaCl = 2.16 g/cm^3 and PLGA nanocomposites = 1.34 g/cm^3.

The composite-porogen paste was pressed into cylindrical Teflon molds with diameter of 4 mm and depth of 4 mm and left for 48 hours to evaporate off residual chloroform. Once dry, samples were pressed out of the molds and the porogen was removed through submersion in agitated deionized water for 3 days followed by vacuum drying. Prior to implantation, all scaffolds were be submerged in 70% ethanol for 30 minutes and exposed to UV light for another 30 minutes. For BMP-2 scaffolds, immediately before implantation, 20 PLGA scaffolds were saturated with a solution containing 30 μg/ml BMP-2 (Novoprotein, Summit, NJ, USA).

Animals

All animal procedures were approved by Stony Brook University's Institutional Animal Care and Use Committee (IACUC). 100 Male Wistar rats (12 weeks old, weight = 350-400 g, Charles River, Wilmington, MA, USA) were used to investigate nanoparticle reinforced scaffold hard and soft tissue biocompatibility. Throughout the study, all rats were allowed to roam freely and were provided with standard chow diet and water ad libitum. All rats were kept on a 12 hour light / dark cycle, where the lights were turned on during the day and off at night. When time points were reached, the animals were euthanized using carbon dioxide inhalation.

Implantations

For hard tissue biocompatibility the animals were divided into 5 groups and two time points; 2 and 6 weeks (10 rats per group), found in Table 1. For soft tissue biocompatibility, 60 of the 100 animals also had scaffolds implanted under the skin. Table 1 lists group and number of animals per group for the hard and soft tissue biocompatibility studies. Animals were anesthetized for surgery with Isoflurane (1-2.5%, IsoThesia, Henry Shein, Melville, NY, USA) in O_2 by inhalation. After the surgery, animals were administered analgesics to reduce pain (Buprenorphine 0.015mg/ml, dose 0.01 mg/kg).

Table 4.1. Groups for soft and hard tissue analysis.

	Animals per group Hard Tissue		Animals per group Soft Tissue	
Groups	2 Weeks	6 Weeks	2 Weeks	6 Weeks
Empty defect	10	10		
PLGA scaffold with BMP-2	10	10		
PLGA scaffold	10	10	10	10
PLGA scaffold reinforced with GONP	10	10	10	10
PLGA scaffold reinforced with MSNP	10	10	10	10

Hard Tissue Implantation

Non-critical sized monocortical plug defects were created unilaterally at the anteromedial surface of the tibia. An incision was made in the skin exposing the proximal tibia, the location of the hole was marked on the bone based on the distance from the joint. The hole (4 mm in diameter and depth) was made using a hand drill with a trephine burr and the scaffold was pressed into the hole. Finally, the surrounding area was washed with saline and the muscle and skin layers were sutured back into place.

Soft Tissue Implantation and Blood Collection

Control and nanocomposite scaffolds were implanted within subcutaneous pockets in the dorsum of the rats. The dorsum of the rat was shaved, washed and disinfected with povidone-iodine. Two longitudinal incisions of 1 cm were made through the full thickness of the skin, one on each side of the spinal column. The subcutaneous pockets were created laterally to the incision by blunt dissection and the scaffolds were placed in the pockets. Once implanted, the area was irrigated with saline and the skin was sutured.

In addition to scaffold implantation, levels of proinflammatory cytokine TNF-α in animal plasma were determined using an enzyme-linked immunoassay (ELISA) kit from R&D Systems (Minneapolis, USA). Prior to surgery and at the 2 week end point, 1 ml of blood was collected from the rats through an intravenous catheter that was inserted into the tail vein. Blood was centrafuged at 1000 rpm for 20 minutes and stored at -80 °C until analysis.

Microcomputed Tomography (Micro-CT) Evaluation

At the end of each time point, the animals were euthanized by 100% CO_2 inhalation. Bones with defects were collected and fixed in 10% formalin for 24 hours, then washed with PBS and stored in 70% ethanol until analysis. Bone volume fraction (BV/TV) and bone density were obtained with a micro-CT system (μCT-40, Scanco, PA, USA). The boundary of the drilled hole was contoured as region of interest for 150 slices of each scaffold. The CT system was operated at a voltage of 55 kVp, current of 145 A, giving a resolution of 20 μm^3. Evaluations were done using the Scanco evaluation software with a threshold of 220, Gaussian noise filter of 1.2, and support of 2.

Histological Analysis

After Micro-CT, five samples from each group were decalcified and embedded in paraffin. The tissues were cross-sectioned at 5 μm thickness in the longitudinal parallel direction. Mineralized bone matrix and osteoid were evaluated by Masson's trichrome staining. Histological analysis was used as a second method to quantitatively measure bone ingrowth at 2 and 6 weeks and multinucleated giant cell response at 2 weeks. Using Osteomeasure software (OsteoMetrics, GA, USA), bone ingrowth was calculated by selecting the area of the scaffold as the region of interest (ROI) and outlining bone growth within the ROI as the bone ingrowth area (BIA) in a histological section of each sample. Using these values, percentage bone ingrowth area was calculated: (BIA/ROI x 100%). For further quantification of foreign body response, multinucleated giant cells were counted within four regions selected in the defect area.

Histological Scoring Analysis

Analysis of the hard tissue response was graded using an adapted scale found in Table 4.2.[13,26] After the animals were euthanized at 2 and 6 weeks, scaffolds and surrounding skin were collected for histological analysis. Samples were immediately placed in 10% formalin for 24 hours followed by PBS rinse and kept in 70% ethanol until histological processing. Three samples from each group were embedded in paraffin and sectioned at a thickness of 5 μm. Staining of the sections was completed using hematoxylin and eosin (H & E) and alizarin red S. H & E stained sections were used for histological grading of capsule thickness and interstitium tissue quality. Analyses of tissue architecture were completed though a previously used scoring system which can be found in Tables 4.3 and 4.4.[13,26] Capsule thickness was analyzed by measuring the distance from the scaffold surface to the adjacent muscle tissue in four locations

around the scaffold. Alizarin red S stained sections were used to determine if ectopic bone formation had occurred within the tissue.

Table 4.2. Histological grading scale for hard tissue response.

Description	Score
Tissue in pores is mostly bone	5
Tissue is mostly bone with some fibrous tissue and/or a few inflammatory response elements	4
Tissue in pores consists of some bone with fibrous tissue and/or a few inflammatory response elements	3
Tissue in pores is mostly fibrous tissue (with or without bone) and young fibroblasts invading the space with giant cells present	2
Tissue in pores consists mostly of inflammatory cells and connective tissue components in between (with or without bone) OR the majority of the pores are empty or filled with fluid	1
Tissue in pores is dense and exclusively of inflammatory type (no bone present)	0

Table 4.3. Capsule thickness score.

Description	Score
1–4 cell layers	4
5–9 cell layers	3
10–30 cell layers	2
> 30 cell layers	1
Not applicable	0

Table 4.4. Histological grading scale for capsule interstitium quality.

Description	Score
Tissue in interstitium is fibrous, mature, not dense, resembling connective or fat tissue in the non-injured regions	4
Tissue in interstitium shows blood vessels and young fibroblasts invading the spaces, few giant cells may be present	3
Tissue in interstitium show giant cells and other inflammatory cells in abundance but connective tissue components in between	2
Tissue in interstitium is dense and exclusively of inflammatory type	1
Implant cannot be evaluated because of problems that may not only be related to the materials to be tested	0

Statistics

MicroCT and histological analysis graphs are presented as average ± standard deviation. These data were analyzed for significance by analysis of variance (ANOVA) with Tukey *post hoc*. For ordinal histological scoring data, nonparametric Kruskal-Wallace test with Dunn's *post hoc* were used to determine significant differences. Differences with $p < 0.05$ were considered significant.

Results

Nanoparticle Characterization

Representative HRTEM images of GONPs and MSNPs can be found in Figure 4.1 A and B. GONPs, in Figure 4.1 A, are observed to be flat disk-like sheets of with diameters of 100-200 nm. Figure 4.1 B shows MSNPs with similar characteristics to GONPs with a disk-shape and diameters in the range of 40-90 nm. Raman spectra of the two nanoparticles can be found in Figure 4.1 C. Peaks for GONP (Figure 4.1 C [i]) were observed at 1352 cm^{-1} and 1602 cm^{-1}. Peaks for MSNPs, found in Figure 4.1 C [ii], were observed at 370 cm^{-1}, 398 cm^{-1} and 476 cm^{-1}.

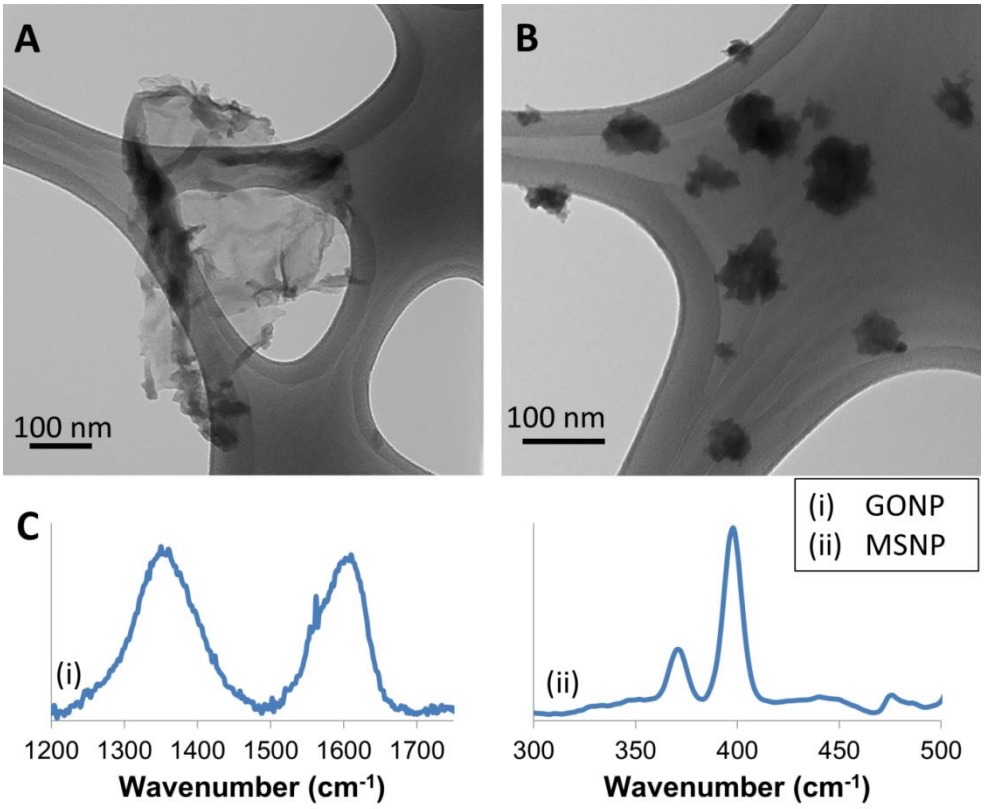

Figure 4.1. Representative HRTEM images of (A) GONPs and (B) MSNPs. (C) Raman spectra of GONPs (i) and MSNPS (ii).

General Health of Experimental Animals

All 100 animals recovered without issue after the surgical procedures and remained in good health for the remainder of the study. No signs of wound complications or abnormal behavior were observed in any of the animals. Additionally, proinflammatory cytokine TNF-α plasma levels were below the detection threshold (5 pg/ml) of the ELISA assay for blood collected at baseline as well as 2 weeks after surgery (data not shown).

Micro-CT Evaluation

Figure 4.2 shows the results of micro-CT analysis at 2 and 6 weeks. Representative three-dimensional reconstructions, shown in Figure 4.2 a-j, qualitatively show a smaller defect in the empty defect group at 2 weeks (Figure 4.2 a-e) compared the groups that received scaffolds and similar healing across all groups by 6 weeks (Figure 4.2 f-j). Evaluations of the microCT data, found in Figure 4.2 A-D, show that after two weeks (Figure 4.2 A), animals with PLGA scaffolds showed significantly less healing (~35%) than those animals with empty defects. Animals implanted with BMP-2, GONP, or MSNP scaffolds showed similar healing to the empty defect group. After 6 weeks, Figure 4.2 B, significant healing had occurred in all groups with no significant differences in bone volume fraction. No significant differences in bone density were observed after 2 weeks (Figure 4.2 C), however after 6 weeks, microCT revealed that bone in the empty defect was significantly denser compared to all groups that received scaffolds (Figure 4.2 D).

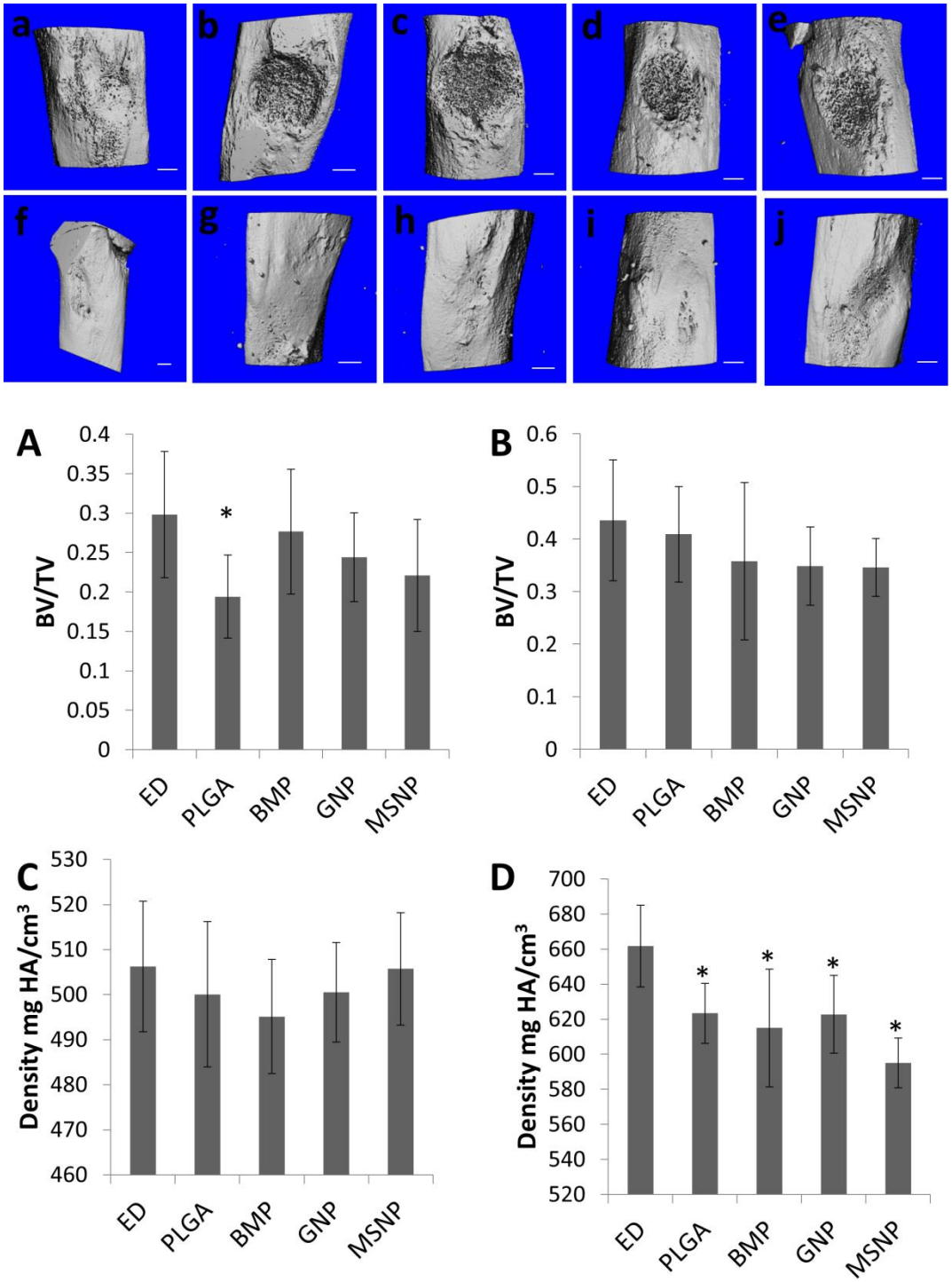

Figure 4.2. MicroCT results. Representative three-dimensional reconstructions of monocortical defects 2 weeks (a-e) or 6 weeks (f-j) after surgery, treated with: (a, f) empty defect, (b, g) PLGA, (c, h) BMP-2, (d, i) GONP, or (e, j) MSNP. Scale bars are 1 mm. Quantitative microCT evaluations for bone volume fraction (BV/TV) 2 weeks (A) or 6 weeks (B) after surgery. Measurement of bone density within the defect site 2 weeks (C) or 6 weeks (D) after surgery. Data is presented as mean +/- standard deviation (n=10). Statistical significance was determined by ANOVA with Tukey *post hoc* and $p<0.05$ considered significant.

Histological Analysis

Figure 4.3 shows percent bone ingrowth for empty defects and defects filled with control and experimental scaffolds as quantified by histological analysis after 2 (Figure 4.3 A) or 6 weeks (Figure 4.3 B). No significant differences were found between the groups at either time point however the trend observed corroborates the microCT data.

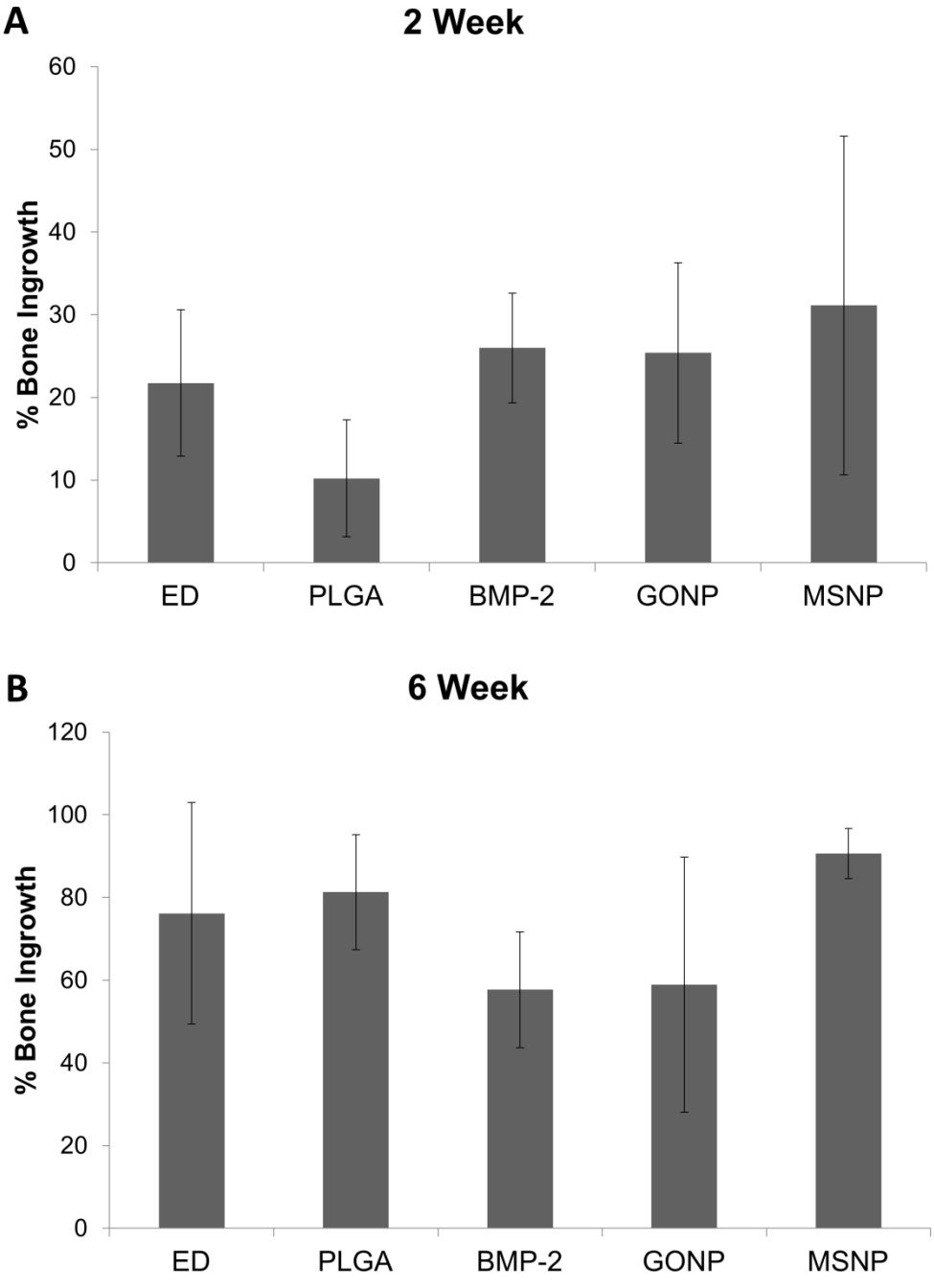

Figure 4.3. Histological results of percent bone ingrowth after (A) 2 weeks or (B) 6 weeks. Data is presented as mean +/- standard deviation (n=5). Statistical significance was determined by ANOVA with Tukey *post hoc* and $p<0.05$ considered significant.

Figure 4.4 shows the results for number of multinucleated giant cells in 2 week hard tissue samples. The empty defect group was not included as multinucleated giant cells are associated with a foreign body response and therefore few of these cells were observed within the defects that did not receive scaffolds. No significant differences were observed though the GONP reinforced group had slightly more cells compared to the other groups. Counting was not completed on the 6 week samples due to the extensive healing that had occurred.

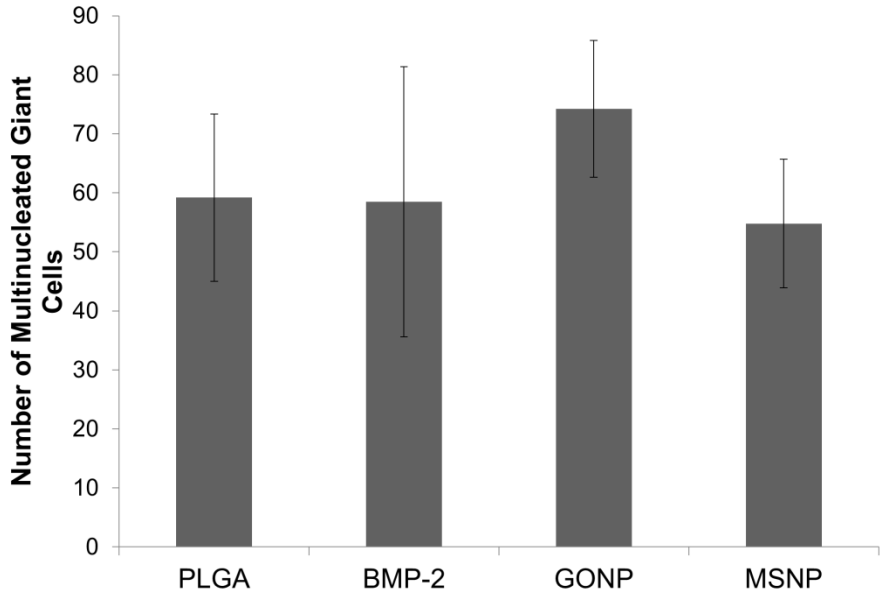

Figure 4.4. Number of multinucleated giant cells counted in hard tissue sections 2 weeks after scaffold implantation. Data are presented as mean +/- standard deviation (n=5). Statistical significance was determined by ANOVA with Tukey *post hoc* and $p<0.05$ considered significant.

Descriptive Light Microscopic Evaluation

Hard tissue implants at 2 and 6 weeks are shown in Figure 4.5 A-J. Empty defects showed new bone formation with primarily fibrous tissue, some new bone marrow and blood vessels in the surrounding area. Empty defect groups were observed to have formed a cartilaginous layer over the defect that was not observed in the implant groups (Figure 4.5 A). For implant receiving groups, polymer degradation was complete for nearly every sample and few nanoparticles were observed in the GONP or MSNP sections. Areas of bone ingrowth were highest and most mature closer to the endosteum and decreased in maturity moving toward the

periosteum. Between areas of bone was mostly granulation tissue with multinucleated giant cells (Figure 4.5 G and I). Areas of granulation tissue and giant cells appeared darker purple color in the GONP and MSNP sections compared to the control groups. New blood vessels and bone marrow were both observed in the defect areas. At 6 weeks, healing of the bone was nearly complete and it was difficult to determine where the defect was made for some samples. The new cortical shell was thicker and less organized compared to the healthy surrounding cortical bone indicating that remodeling had not yet completed.

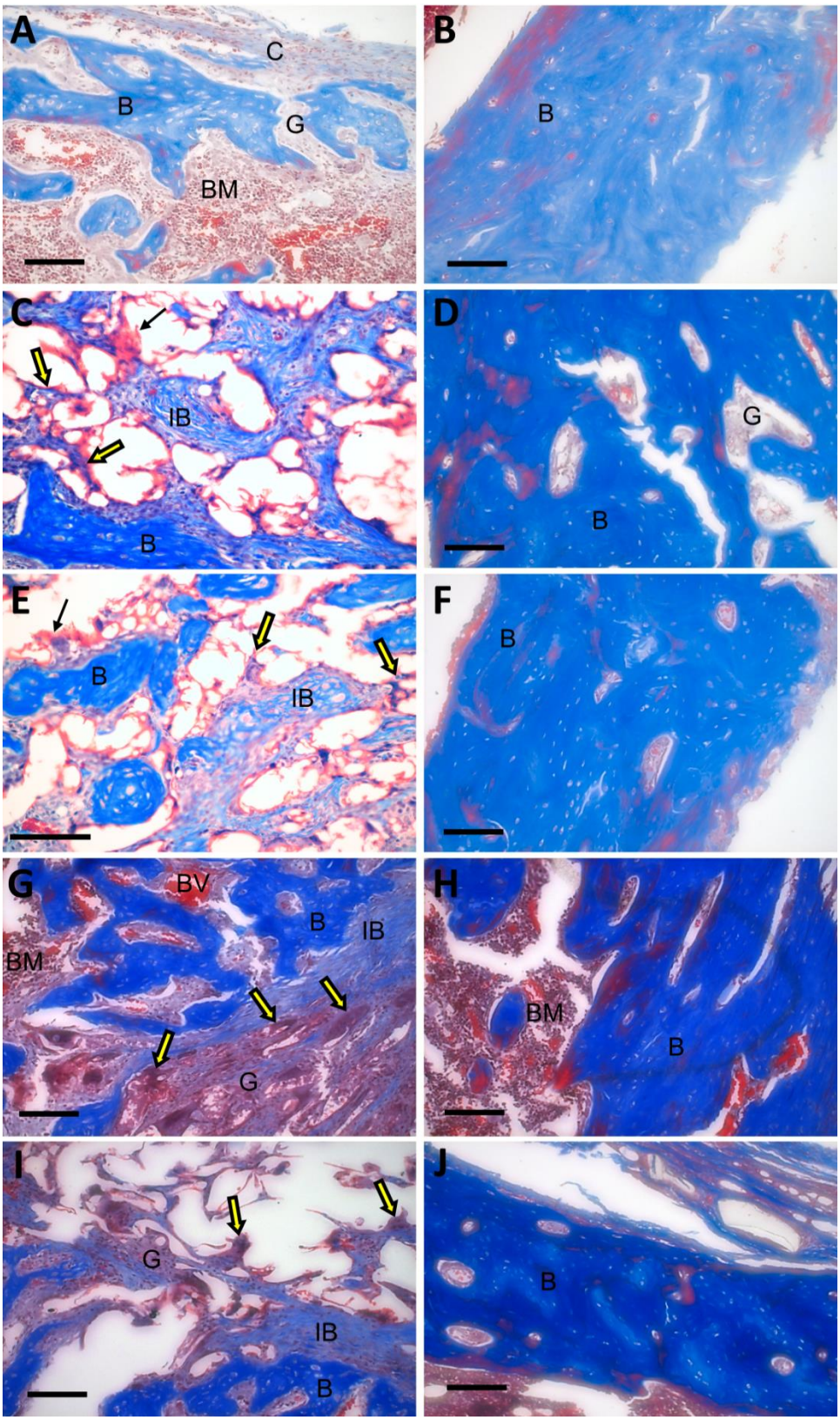

Figure 4.5. Representative hard tissue histological sections of defect areas (A-I) 2 weeks or (B-J) 6 weeks. (A,B) Empty defect, (C, D) PLGA, (E, F) BMP-2, (G,H) GONP, and (I, J) MSNP. The images are presented at 20x magnification. Scale bars are 100 µm. The scaffold material (solid black arrows) appears orange fragments in images. Bone tissue (B) appears blue while immature bone (IB) appears light blue. Granulation tissue (G) appears between bone areas. Cartilage (C) was observed over the empty defect. Multinucleated giant cells (black outlined arrows), bone marrow (BM), and blood vessels (BV) are also seen in the images.

Figure 4.6 A-F shows soft tissue histology of PLGA and experimental group scaffolds implanted for 2 or 6 weeks. Near complete scaffold degradation was observed with only small fragments of polymer observed, although some polymer may have been lost during histological processing. Additionally, few nanoparticles were observed in the sections. At 2 weeks, lesions consisted mainly of fibrous tissue and varying amounts of foreign body response with multinucleated giant cells surrounding scaffold fragments and some leukocyte invasion. Some nuclear fragmentation of multinucleated giant cells was observed, indicating cell apoptosis. Small blood vessels were also observed within the interstitium. At 6 weeks, response was generally similar but with greater fibrosis and widening spaces and fewer multinucleated giant cells. Fibrous capsule formation was minimal at both time points but was not easily discerned from native fibrous tissue in some samples. No ectopic bone formation was observed by alizarin red S staining in the PLGA or two experimental groups.

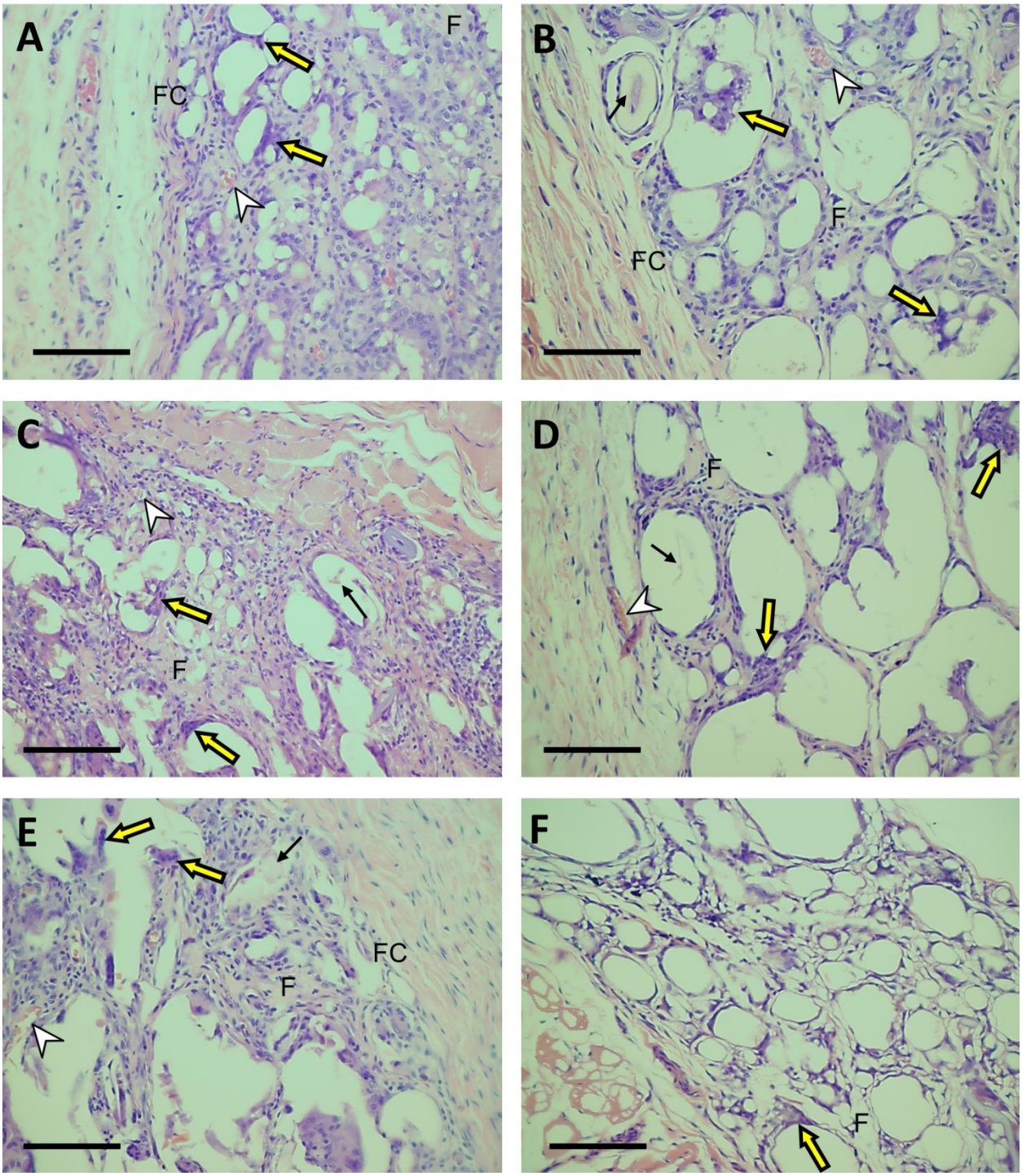

Figure 4.6. Representative histological sections of soft tissue implant areas (A-E) 2 weeks or (B-F) 6 weeks after implantation, treated with (A, B) PLGA, (C, D) GONP, (E, J) MSNP. The images are presented at 20x magnification. Scale bars are 100 µm. The scaffold material appears white or light pink (solid black arrows) in the images. Fibrous tissue (F) appears pink within the cellular interstitium. Multinucleated giant cells (black outlined arrows) and blood vessels (white arrowheads) also appear in the images. Fibrous capsule (FC) is visible in some images and appears as pink fibrous connective tissue.

Histological Scoring

Figure 4.7 shows the results of scoring hard and soft histological sections in 2 and 6 week samples. The bone sections were scored for tissue response, while soft tissue sections were scored for capsule thickness and interstitium tissue quality. For bone sections (Figure 4.7 A-B), no significant differences in hard tissue response were observed at either time point. An overall increase in hard tissue response was observed for all groups between 2 weeks and 6 weeks. For soft tissue response, MSNP reinforced scaffolds were found to induce significantly thinner capsule compared to PLGA at 2 weeks (Figure 4.7 C). No significant differences were observed for capsule thickness at 6 weeks (Figure 4.7 D) or capsule interstitium quality (Figure 4.7 E-F) at either time point.

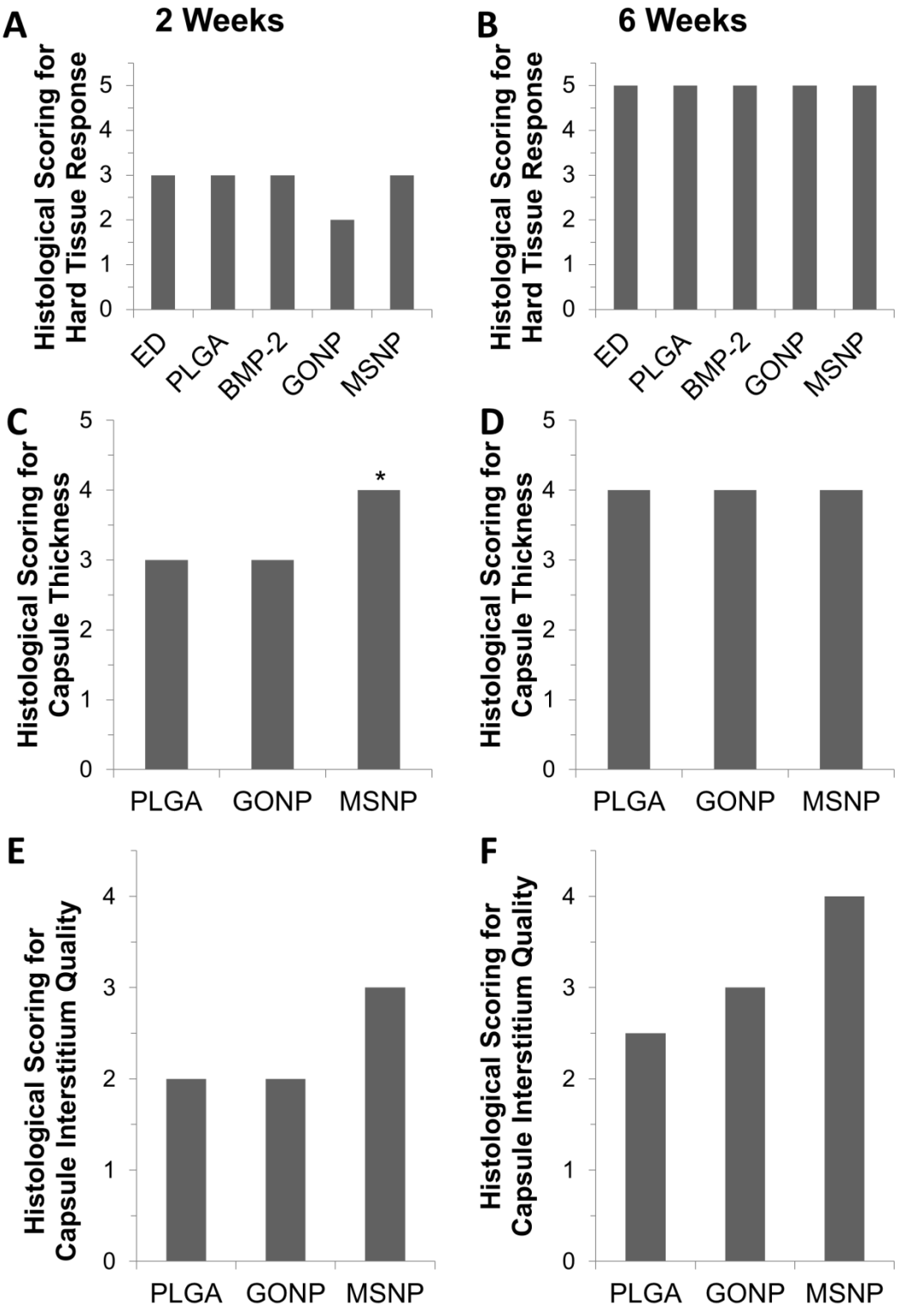

Figure 4.7. Results of histological scoring of (A, B) hard tissue response, (C, D) soft tissue capsule thickness, and (E, F) soft tissue capsule interstitium quality after 2 or 6 weeks implantation. Scoring data are presented as median for n=5. Statistical significance was determined by Kruskal-Wallace test with Dunn's *post hoc* and $p<0.05$ considered significant.

Discussion

The objective of this study was to investigate the biocompatibility of two-dimensional nanoparticle reinforced scaffolds after implantation in hard or soft tissue for 2 or 6 weeks. The composition and dimension of nanoparticle will affect scaffold properties and may influence the interaction between the surrounding tissue and the construct. Therefore, we selected two-dimensional nanoparticles with organic (GONP) and inorganic (MSNP) composition that have previously shown good reinforcement of nanocomposites[17] and cytocompatibility[24,27] for incorporation into PLGA scaffolds at a concentration of 0.2 wt% and to be implanted into a 4 x 4 mm^3 defect in a rat tibia or subcutaneously on the rat dorsum. 0.2 wt% nanoparticle loading was selected as this has been shown to be the maximum concentration possible without significant nanoparticle aggregation, causing the material to behave like a viscoelastic solid.[28] In order to make comparisons of bone ingrowth, PLGA scaffolds soaked with BMP-2 were used as positive control due to BMP-2's proven promotion of bone formation and current clinical use.[29,30] The concentration of 30 µg/ml was used as this concentration has been shown to fuse a segmental defect in rats without causing adverse effects observed at higher doses.[31]

Characterization of GONPs and MSNPs by Raman spectroscopy is shown in Figure 4.1 C. The two bands observed at 1354 cm^{-1} and 1604 cm^{-1} in the GONP spectra signify the D- and G- bands, respectively. Both bands are first order with the G-band indicating the stretching of carbon-carbon bonds and the D-band representing structural defects in the graphene sheet.[32] The ratio of the intensity of D- to G-bands is used to represent the amount of defects in the structure.[33] The I_D/I_G for GONP was 1.03, much higher compared to pristine carbon structures[23] which indicates disruption of sp^2 domains during the synthesis process. The bands observed in

the MSNP Raman spectra are the two central bands for dichalcogenide materials. The band observed at 370 cm^{-1} represents the $E_{2g}{}^{1}$ Raman active mode indicating in-plane vibration. The second band at 398 cm^{-1} represents the A_{1g} Raman active mode for the out-of-plane vibrations between the molybdenum and sulfur atoms.[34,35] The small peak at 476 cm^{-1} represents small amounts of unreacted MoO_3.

A porosity of 90% with porogen in the range of 200-500 μm was employed as previous work has shown that a minimum pore size of 100 μm is necessary for cellular infiltration and transport of nutrients and waste however scaffolds with pores of 300 μm show greater vascularization and osteogenesis.[36] Though porosity is critical for proper cellular infiltration and bone ingrowth, this addition will decrease the mechanical properties of the construct; necessitating a compromise between these properties.[37] In this study, the use of a noncritical-sized monocortical plug defect allowed us to employ 90% porous scaffolds for easier study of biocompatibility without compromising the stability of the animal. Moreover, this defect minimizes variation between animals as compared to segmental defect which requires a more invasive surgery.[38]

Hard tissue response, found in Figure 4.7 A and B, found no significant differences in tissue response across the groups at either time point. Empty defect groups appeared healthy and many animals formed a cartilaginous layer over the defect that was not observed in the scaffold groups. This is most likely a result of the natural bone healing process in which the body creates a fibrocartilaginous callus around a defect or fracture to protect and stabilize the area.[39] This observation may indicate that the use of a scaffold in this non-critical defect assumes some of that role, leading to less callous outside the defect. Tissue sections for GONP and MSNP groups did appear darker purple in color within the granulation tissue compared to control groups,

associated with foreign body response by multinucleated giant cells; however the count of giant cells (Figure 4.4) was similar among all the groups, indicating that the dark color may be due to nanoparticles within the granulation tissue. Polymer degradation was nearly complete for all groups after 2 weeks of implantation and no polymer could be observed in any of the 6 week implants. PLGA 50:50 was selected for this study due to reported short degradation time to match the fast healing time of rats. For future long-term studies in larger animals, a PLGA with higher molar ratio of polylactic to glycolic acid should be used to slow degradation time.[40]

Results for soft tissue response to subcutaneously implanted PLGA control or experimental scaffolds for 2 or 6 weeks are found in Figure 4.7 C-F. While little fibrous capsule formation and minimal inflammatory response was observed across the groups, the capsule thickness for MSNP treated groups was found to be significantly thinner compared to PLGA at 2 weeks. It is of note, that although not always statistically significant, the results for 2 week hard and soft tissue response for MSNPs did appear superior to that of plain PLGA or GONPs for all histological scoring criteria and multinucleated giant cell count. Previous studies of these nanoparticles interactions with MSCs found that both GONPs and MSNPs were internalized by cells but that only GONPs entered the nucleus. While both of these particles were found to be potentially safe for MSCs at similar concentrations to that within the scaffolds of this study, it may be that MSNPs are particularly suited for interactions with cells.[24,27]

Bone growth into the pores of the scaffolds in all groups was observed after 2 weeks of implantation as shown by microCT (Figure 4.2 A) and histological analysis (Figure 4.3 A). The quantity of bone measured by microCT however, was significantly decreased in the PLGA group compared to that of the empty defect group. Although not significant, this trend was corroborated by histological analysis. As this was not a critical-sized defect, the empty defect healed and may

therefore be considered a positive control with expected results similar to the BMP-2 group. Comparatively, GONP and MSNP groups showed 80% and 73% of the empty defect levels and 20% and 15% greater bone volume fraction compared to the PLGA group, respectively. In order to best mimic bone morphology and function, and to integrate with the surrounding tissue, a bone tissue engineering scaffold would be osteoconductive, bioactive and osteoinductive. Porous biodegradable polymer scaffolds are inherently osteoconductive but not bioactive or osteoinductive. Besides strategies utilizing peptides[41] or other bioactive supplements,[42,43] the addition of nanoparticles may help to impart these properties through increasing scaffold surface area and topography, and negatively charged functional groups.[44] In a study of bioactivity, PLGA scaffolds reinforced with GONP and MSNP have induced spontaneous generation of an apatite layer on the surface with up to 47% greater phosphate accumulation compared to PLGA alone when soaked in simulated body fluid for up to 14 days.[45] In this study, our subcutaneous histological sections stained with alizarin red S showed no ectopic bone formation associated with osteoinductivity however this was not surprising as ectopic bone formation by agents other than decalicified bone matrix, BMPs, and MSCs has not been observed in small animals.[46] Therefore, although we cannot comment about the bioactivity of these scaffolds as we did not have a critical sized defect to ensure that healing was due to the nanocomposite and not natural processes, the significant decrease in healing observed in the PLGA scaffold group compared to the empty defect group that was not observed in the experimental groups may indicate that these nanoparticles do play a role in assisting bone augmentation.

Density measurements by microCT (Figure 4.3 C and D) show no significant differences after 2 weeks implanted but significantly higher density in the empty defect group compared to all groups that received scaffolds after 6 weeks. The addition of a scaffold, while meant to assist

in bone formation across a defect, will slow this process as oxygen, nutrients, and cells must travel through the pores of a scaffold as well as degrade the polymer.[47] Since the defect used in this study was noncritical-sized, it follows that bone healing continued normally without the hindrance of a degrading scaffold, creating more naturally dense bone.

The good *in vivo* biocompatibility results reported here are in agreement with previous studies of graphene containing scaffolds. Kanayama et al. found significantly increased soft tissue ingrowth rates in rats that received collagen implants containing graphene oxide (~50% higher) or reduced graphene oxide (~60% higher) compared to collagen alone.[20] Zhou et al. reported suppressed inflammatory microglia an astrocyte activation after implanting electrospun poly(ε-caprolactone) microfiber scaffolds coated with colloidal graphene into the striatum or into the subventricular zone of adult rats for 7 weeks compared to electrospun scaffolds without graphene.[22] Wang et al. found that addition of graphene to polyethylene-terephthalate resulted in significantly improved mineral apposition rate and biomechanical properties (each >25%) when used in an extra-articular graft-to-bone healing procedure in New Zealand rabbits for 4, 8, and 12 weeks.[21] Finally, Duan et al. observed similar biocompatibility of mesenchymal stem cell (MSC) seeded graphene reinforced poly(L-lactic acid) scaffolds implanted intramuscularly in nude mice for 2, 4, and 8 weeks to pure poly(L-lactic acid) scaffolds.[19]

The nanoparticle reinforced scaffolds examined in this study show much promise for bone tissue engineering applications. In addition to mechanical strength and potential bioactivity elicited by the nanoparticles alone, incorporation of other bioactive or osteoinductive factors such as BMPs, platelet rich plasma, or MSCs would only further improve the integration of these scaffolds. Future studies should also take advantage of the interesting physicochemical properties

of these nanoparticles to create scaffolds that that can release drugs, be imaged to observe healing longitudinally, or stimulated to enhance bone growth.

Conclusions

PLGA scaffolds reinforced with 0.2 wt% GONPs or MSNPs showed comparable *in vivo* biocompatibility to PLGA alone. For scaffolds reinforced with both nanoparticles, soft tissue response showed minimal fibrous capsule formation and similar capsule interstitium quality to PLGA. Hard tissue response was similar among all groups. A significant decrease in the quantity of bone ingrowth was observed for the PLGA group after 2 weeks compared to the empty defect group that was not observed in the experimental groups. This may indicate that the addition of nanoparticles to the PLGA induces bioactivity of the scaffolds.

Acknowledgements

This work was supported by the National Institutes of Health (grants No. 1DP2OD007394-01). Research was carried out in part at the Center for Functional Nanomaterials, Brookhaven National Laboratory, New York, which is supported by the U.S. Department of Energy, Office of Basic Energy Sciences, under Contract No. DE-AC02-98CH10886. The authors would like to thank Dr. Kenneth Shroyer, MD (Professor and Chair of the Department of Pathology at Stony Brook Medicine) for his assistance with the descriptive light microscopy evaluation. The authors would additionally like to thank Susan Van Horn (Central Microscopy, Stony Brook University) for her help with transmission electron microscopy.

References

1 Liu, X. & Ma, P. X. Polymeric scaffolds for bone tissue engineering. *Annals of Biomedical Engineering* **32**, 477-486 (2004).

2 Rezwan, K., Chen, Q., Blaker, J. & Boccaccini, A. R. Biodegradable and bioactive porous polymer/inorganic composite scaffolds for bone tissue engineering. *Biomaterials* **27**, 3413-3431 (2006).

3 Agrawal, C. M. & Ray, R. B. Biodegradable polymeric scaffolds for musculoskeletal tissue engineering. *Journal of Biomedical Materials Research* **55**, 141-150, (2001).

4 Kokubo, T., Kim, H.-M. & Kawashita, M. Novel bioactive materials with different mechanical properties. *Biomaterials* **24**, 2161-2175 (2003).

5 Sitharaman, B. *et al.* Injectable in situ cross-linkable nanocomposites of biodegradable polymers and carbon nanostructures for bone tissue engineering. *Journal of Biomaterials Science, Polymer Edition* **18**, 655-671 (2007).

6 Jell, G. *et al.* Carbon nanotube-enhanced polyurethane scaffolds fabricated by thermally induced phase separation. *Journal of Materials Chemistry* **18**, 1865-1872 (2008).

7 Lau, C., Cooney, M. J. & Atanassov, P. Conductive macroporous composite chitosan−carbon nanotube scaffolds. *Langmuir* **24**, 7004-7010 (2008).

8 Ma, P.-C., Siddiqui, N. A., Marom, G. & Kim, J.-K. Dispersion and functionalization of carbon nanotubes for polymer-based nanocomposites: a review. *Composites Part A: Applied Science and Manufacturing* **41**, 1345-1367 (2010).

9 MacDonald, R. A., Laurenzi, B. F., Viswanathan, G., Ajayan, P. M. & Stegemann, J. P. Collagen–carbon nanotube composite materials as scaffolds in tissue engineering. *Journal of Biomedical Materials Research, Part A* **74**, 489-496 (2005).

10 Sahithi, K., Swetha, M., Ramasamy, K., Srinivasan, N. & Selvamurugan, N. Polymeric composites containing carbon nanotubes for bone tissue engineering. *International Journal of Biological Macromolecules* **46**, 281-283 (2010).

11 Shi, X. *et al.* Injectable nanocomposites of single-walled carbon nanotubes and biodegradable polymers for bone tissue engineering. *Biomacromolecules* **7**, 2237-2242 (2006).

12 Venkatesan, J., Ryu, B., Sudha, P. & Kim, S.-K. Preparation and characterization of chitosan–carbon nanotube scaffolds for bone tissue engineering. *International Journal of Biological Macromolecules* **50**, 393-402 (2012).

13 Sitharaman, B. *et al. In vivo* biocompatibility of ultra-short single-walled carbon nanotube/biodegradable polymer nanocomposites for bone tissue engineering. *Bone* **43**, 362-370 (2008).

14 Paiyz, E. M. *et al.* Functionalized carbon nanotube reinforced scaffolds for bone regenerative engineering: fabrication, *in vitro* and *in vivo* evaluation. *Biomedical Materials* **9**, 035001 (2014).

15 Dorj, B. *et al.* Robocasting nanocomposite scaffolds of poly(caprolactone)/hydroxyapatite incorporating modified carbon nanotubes for hard tissue reconstruction. *Journal of Biomedical Materials Research, Part A* **101A**, 1670-1681 (2013).

16 Gupta, A. *et al.* Biocompatibility of single-walled carbon nanotube composites for bone regeneration. *Bone and Joint Research* **4**, 70-77 (2015).

17 Lalwani, G. *et al.* Two-dimensional nanostructure- reinforced biodegradable polymeric nanocomposites for bone tissue engineering. *Biomacromolecules* **14**, 900-909 (2013).

18 Farshid, B., Lalwani, G. & Sitharaman, B. *In vitro* cytocompatibility of one-dimensional and two-dimensional nanostructure-reinforced biodegradable polymeric nanocomposites. *Journal of Biomedical Materials Research, Part A* **103**, 2309-2321 (2015).

19 Duan, S. *et al.* Enhanced osteogenic differentiation of mesenchymal stem cells on poly(L-lactide) nanofibrous scaffolds containing carbon nanomaterials. *Journal of Biomedical Materials Research, Part A* **103**, 1424-1435 (2015).

20 Kanayama, I. *et al.* Comparative study of bioactivity of collagen scaffolds coated with graphene oxide and reduced graphene oxide. *International Journal of Nanomedicine* **9**, 3363 (2014).

21 Wang, C. H. *et al.* Effects of graphene modification on the bioactivation of polyethylene-terephthalate-based artificial ligaments. *ACS Applied Materials & Interfaces* **7**, 15263-15276 (2015).

22 Zhou, K. *et al.* Graphene functionalized scaffolds reduce the inflammatory response and supports endogenous neuroblast migration when implanted in the adult brain. *PLoS One* **11**, e0151589 (2016).

23 Paratala, B. S., Jacobson, B. D., Kanakia, S., Francis, L. D. & Sitharaman, B. Physicochemical characterization, and relaxometry studies of micro-graphite oxide, graphene nanoplatelets, and nanoribbons. *PLoS One* **7**, e38185 (2012).

24 Rashkow, J. T., Talukdar, Y., Lalwani, G. & Sitharaman, B. Interactions of 1D- and 2D-layered inorganic nanoparticles with fibroblasts and human mesenchymal stem cells. *Nanomedicine* **10**, 1693-1706 (2015).

25 Kim, J., Yaszemski, M. J. & Lu, L. Three-dimensional porous biodegradable polymeric scaffolds fabricated with biodegradable hydrogel porogens. *Tissue Engineering Part C: Methods* **15**, 583-594 (2009).

26 Jansen, J. A., Dhert, W. J., van der Waerden, J. P. & von Recum, A. F. Semi-quantitative and qualitative histologic analysis method for the evaluation of implant biocompatibility. *Journal of Investigative Surgery: The Official Journal of the Academy of Surgical Research* **7**, 123-134 (1994).

27 Talukdar, Y., Rashkow, J. T., Lalwani, G., Kanakia, S. & Sitharaman, B. The effects of graphene nanostructures on mesenchymal stem cells. *Biomaterials* **35**, 4863-4877 (2014).

28 Shi, X. *et al.* Rheological behaviour and mechanical characterization of injectable poly (propylene fumarate)/single-walled carbon nanotube composites for bone tissue engineering. *Nanotechnology* **16**, S531 (2005).

29 Burg, K. J. L., Porter, S. & Kellam, J. F. Biomaterial developments for bone tissue engineering. *Biomaterials* **21**, 2347-2359 (2000).

30 Chan, D. S., Garland, J., Infante, A., Sanders, R. W. & Sagi, H. C. Wound complications associated with bone morphogenetic protein-2 in orthopaedic trauma surgery. *Journal of Orthopaedic Trauma* **28**, 599-604 (2014).

31 Zara, J. N. *et al.* High doses of bone morphogenetic protein 2 induce structurally abnormal bone and inflammation *in vivo*. *Tissue Engineering Part A* **17**, 1389-1399 (2011).

32 Ferrari, A. *et al.* Raman spectrum of graphene and graphene layers. *Physical Review Letters* **97**, 187401 (2006).

33 Salzmann, C. G. *et al.* The role of carboxylated carbonaceous fragments in the functionalization and spectroscopy of a single-walled carbon-nanotube material. *Advanced Materials* **19**, 883-887 (2007).

34 Molina-Sanchez, A. & Wirtz, L. Phonons in single-layer and few-layer MoS_2 and WS_2. *Physical Review B* **84**, 155413 (2011).

35 Li, H. *et al.* From bulk to monolayer MoS_2: evolution of Raman scattering. *Advanced Functional Materials* **22**, 1385-1390 (2012).

36 Hutmacher, D. W., Schantz, J. T., Lam, C. X. F., Tan, K. C. & Lim, T. C. State of the art and future directions of scaffold-based bone engineering from a biomaterials perspective. *Journal of Tissue Engineering and Regenerative Medicine* **1**, 245-260 (2007).

37 Karageorgiou, V. & Kaplan, D. Porosity of 3D biomaterial scaffolds and osteogenesis. *Biomaterials* **26**, 5474-5491 (2005).

38 Bernabé, P. F. E. *et al.* Bone healing in critical-size defects treated with either bone graft, membrane, or a combination of both materials: a histological and histometric study in rat tibiae. *Clinical Oral Implants Research* **23**, 384-388 (2012).

39 Fazzalari, N. L. Bone fracture and bone fracture repair. *Osteoporosis international: A journal established as result of cooperation between the European Foundation for Osteoporosis and the National Osteoporosis Foundation of the USA* **22**, 2003-2006 (2011).

40 Makadia, H. K. & Siegel, S. J. Poly(lactic-co-glycolic acid) (PLGA) as biodegradable controlled drug delivery carrier. *Polymers* **3**, 1377 (2011).

41 Dee, K. C., Rueger, D. C., Andersen, T. T. & Bizios, R. Conditions which promote mineralization at the bone-implant interface: a model *in vitro* study. *Biomaterials* **17**, 209-215 (1996).

42 Li, B. *et al.* The effects of rhBMP-2 released from biodegradable polyurethane/microsphere composite scaffolds on new bone formation in rat femora. *Biomaterials* **30**, 6768-6779 (2009).

43 Yasko, A. W. *et al.* The healing of segmental bone defects, induced by recombinant human bone morphogenetic protein (rhBMP-2). A radiographic, histological, and biomechanical study in rats. *The Journal of Bone & Joint Surgery* **74**, 659-670 (1992).

44 Aryal, S. *et al.* Carbon nanotubes assisted biomimetic synthesis of hydroxyapatite from simulated body fluid. *Materials Science and Engineering: A* **426**, 202-207 (2006).

45 Rashkow, J. T., Talukdar, Y., Lalwani, G. & Sitharaman, B. *In vitro* bioactivity of one- and two-dimensional nanoparticle reinforced bone tissue engineering scaffolds. *In Preparation* (2016).

46 Le Nihouannen, D. *et al.* Ectopic bone formation by microporous calcium phosphate ceramic particles in sheep muscles. *Bone* **36**, 1086-1093 (2005).

47 Amini, A. R., Laurencin, C. T. & Nukavarapu, S. P. Bone Tissue Engineering: Recent Advances and Challenges. *Critical Reviews in Biomedical Engineering* **40**, 363-408 (2012).

Chapter 5

Conclusions and Future Work

Conclusions and Discussion

The large number of bone defects and consequential bone graft procedures in the US, as well as the limitations of current autografting and allografting techniques, has created a need for a synthetic bone graft that can fulfill the complex requirements of bone repair. In Chapter 1, we have reviewed the advantages and limitations of current natural and synthetic bone grafts and the promise of using nanocomposite solutions toward finding the ideal scaffold. Of these nanocomposites, those reinforced with two-dimensional organic and one- or two-dimensional inorganic dichalcogenide nanoparticles have unique physicochemical properties which make them promising as reinforcing agents for bone tissue engineering scaffolds. However, to utilize these materials in bone tissue engineering applications, investigation of these nanoparticles and nanocomposites to fulfill the requirements of the ideal synthetic bone graft is required. Specifically, the implants should have sufficient porosity to allow for the flow of nutrients and waste, mechanical properties similar to that of the surrounding native tissue, surface properties that are conducive to cellular attachment and proliferation, and biocompatibility and biodegradability to allow for regeneration of healthy native tissue. These nanoparticles have been shown to provide some of these advantages for bone tissue engineering applications as scaffolds reinforced with 0.2 wt% of these nanomaterials have shown significant enhancement of compressive and flexural moduli compared to non-reinforced polymer and can also support cell growth with little cytotoxicity. However, the effect that these nanoparticles and nanocomposites have on cells and tissues is known to be dependent on nanoparticle composition, morphology, and synthesis method and therefore it is necessary to investigate the cytocompatibility and biocompatibility of all nanoparticles and their nanocomposites. It is the goal of this work to

determine what nanoparticle chemistry and dimensionality show the most promise as a reinforcing agent.

In Chapter 2, we reported the cytocompatibility of molybdenum disulfide nanoplatelets (MSNPs) and tungsten disulfide nanoplatelets (WSNTs) to fibroblasts and mesenchymal stem cells (MSCs). We selected these cell types as both are important in bone repair processes and are likely to be exposed to nanoparticles upon degradation of the construct. Additionally, MSCs are commonly used in tissue engineering applications as deliverable agents to augment healing. We first performed a cytotoxicity screening over a broad range of concentrations (0-300 μg/ml) after 6, 12, and 24 hours of treatment. We then examined the effect of potentially safe low (10 μg/ml) and high (50 ug/ml) doses of nanoparticles on the differentiation capabilities of MSCs. Moreover, these doses straddle the ~20 μg of particles per cm^3 used to reinforce the PLGA scaffolds in the future studies. We found that only NIH-3T3 cells treated with MSNPs showed dose or time dependent increase in cytotoxicity. Differentiation markers of MSCs in treated groups were unaffected compared with untreated controls. We concluded that MSNPs and WSNTs at concentrations less than 50 μg/ml are potentially safe for treatment of fibroblasts or MSCs for up to 24 h.

In Chapter 3, we describe investigation of the *in vitro* bioactivity of nanocomposites soaked in simulated body fluid (SBF) for up to 14 days. We performed evaluation of apatite collection on 90% porous PLGA nanocomposite scaffolds reinforced with 0.2 wt% of the two-dimensional organic (multiwalled graphene nanoribbons (MWGONR) and GONP) and inorganic (MSNP) nanoparticles that led to the greatest enhancement of mechanical properties (compressive and flexural modulus) when incorporated into non-porous poly(propylene fumarate) (PPF). Additionally, to investigate the effect of nanoparticle dimensionality, we

included the one-dimensional organic (multiwalled carbon nanotubes (MWCNT)) and inorganic (WSNT) nanoparticles that showed the highest mechanical properties. We found that apatite nodules formed on the surface of control and all nanoparticle reinforced scaffolds after 14 days incubation in SBF. GONP, MSNP, and WSNT reinforced scaffolds showed significantly greater phosphate accumulation compared to PLGA, MWCNT, or MWGONR groups. We concluded that the addition of 0.2 wt% of GONPs, MSNPs, or WSNTs to PLGA scaffolds may elicit a bioactive response when implanted *in vivo.*

In Chapter 4, we present the *in vivo* biocompatibility of 90% porous nanocomposite scaffolds reinforced with 0.2 wt% GONPs or MSNPs. These two nanoparticles were selected based the results of the previous chapters as well as earlier studies. Earlier studies reported that reinforcement with two-dimensional nanoparticles GONPs and MSNPs led to the greatest enhancement of compressive and flexural properties of the non-porous nanocomposites. GONRs and GONPs, MSNPs, and WSNTs showed similar cytocompatibility when exposed to cells directly and when incorporated into nanocomposites. Finally, GONP, MSNP, and WSNT reinforced scaffolds were found to prompt the greatest apatite collection when soaked in SBF. From these results we selected GONPs and MSNPs to implant in a non-critical sized monocortical defect in the tibia or subcutaneously on the dorsum of a rat. Comparable *in vivo* biocompatibility was observed between the nanoparticle reinforced scaffolds and PLGA alone. In addition, 2 weeks after implantation, significantly less bone growth was observed for the PLGA group compared to the empty defect group that was not observed for the experimental groups. This result may indicate that the addition of the nanoparticles induces bioactivity of the scaffolds. We conclude that scaffolds reinforced with GONPs or MSNPs show promise for bone tissue engineering applications.

We set out in this work with the objective of finding the most promising nanoparticle composition and dimensionality in order to improve upon current bone tissue engineering scaffolds. More specifically, we wanted to answer three questions: 1) Are these nanoparticles safe for exposure to cells? 2) Does the addition of these nanoparticles change the bioactivity of the constructs? 3) Does the addition of these nanoparticles change the biocompatibility of the constructs? Looking at the first of these questions, we found that the inorganic nanoparticles investigated were indeed safe for exposure to cells at the concentration required for mechanical reinforcement. However, the results indicate that these particles are safe for cells at higher concentrations, leading to increasing possibilities beyond scaffold reinforcement, including drug delivery and bioimaging where higher concentrations of nanoparticles might be needed. Examining the second question, we found that there was indeed an effect of nanoparticle incorporation on the bioactivity of the constructs and that inorganic nanoparticles led to greater bioactivity than organic nanoparticles regardless of dimensionality. This is valuable as it indicates better integration of these scaffolds with the surrounding environment and faster bone growth. Finally, looking at the third question, we found that incorporation of two-dimensional organic and inorganic nanoparticles did not negatively affect the biocompatibility of the constructs and also found further evidence of the bioactivity of these nanocomposite scaffolds and should be safe to use *in vivo*. Overall, the use of the two-dimensional organic and one- and two-dimensional inorganic nanoparticles investigated here improve upon previously studied nanoparticle reinforced scaffolds through decreased cytotoxicity and improved bioactivity.

The first bone replacement materials had the main objective of being bioinert. Next, researchers began to take advantage of the natural bioactivity of some materials in order to create better bone bonding and integration of materials. Now, the objective of bone biomaterials is to

integrate and allow for regeneration of native tissue. The materials investigated here fall into the second two categories and the results observed here are promising for the use of two-dimensional GONP and MSNP reinforced scaffolds for bone tissue engineering applications. Based on results of previous mechanical testing studies, two-dimensional nanoparticles lead to the enhancement of mechanical properties in the range of trabecular bone. The bioactivity study in Chapter 3 showed that inorganic nanoparticles lead to the greatest bioactivity. Taken together with the thinner capsule thickness and fewer multinucleated giant cells observed in the biocompatibility study in Chapter 4, we suggest that MSNPs show the most promise for future investigation toward clinical use as a scaffold reinforcing agent.

Future Work

This work has opened many avenues for future studies. While in the work in this study, we have described nanocomposites that fulfill many of the requirements of the ideal tissue engineering scaffold, many improvements could still be made. Moreover, before these scaffolds could be used clinically, more studies need to be completed. Below we summarize some of the studies that would be necessary as preclinical studies and some which aim to improve scaffold interactions with the *in vivo* environment.

1) While we provide some evidence of the bioactivity of these scaffolds through *in vitro* study with SBF and *in vivo* study, further study of the bioactivity of these scaffolds is required. This would include an *in vivo* study with a critical-sized defect to act as a negative control. In this way, all healing that occurs throughout the study is only due to the placement of a scaffold and not natural healing processes. This would allow for a better comparison of healing through nanoparticle reinforced scaffolds compared to a negative and positive control. In addition, to examine the osteoinductivity of these scaffolds, a study should be carried out in which nanocomposite scaffolds are implanted subcutaneously or intramuscularly in a large animal. It is known that most materials cannot elicit formation of bone subcutaneously in small animals, but can in large animal models. Therefore, this would be an indication of the nanoparticles osteoinductivity.
2) We selected the nanoparticles used in these studies based on the results of mechanical property studies of non-porous PPF nanocomposites. However, the addition of

porosity to a scaffold can lead to extreme loss of mechanical strength. Porous PPF based nanocomposites have compressive strength similar to that of porous trabecular bone; meaning these materials still cannot be used for load-bearing applications. 0.2 wt% nanoparticle reinforcement is based on previous work which has shown that this is the maximum concentration at which the nanoparticles do not aggregate and the nanocomposites do not act as viscoelastic solids. Future work should focus on a method to better disperse these particles within the polymer matrix without aggregation so that greater loading and thereby greater mechanical reinforcement can be achieved. This may be attained through use of high shear mixing, functionalization of the nanomaterials, or through acid purification.

3) While we have shown potential bioactivity of these nanocomposite scaffolds there are methods by which osteoinductivity could be increased. As observed in the Chapter 4, BMP-2, a member of a natural group of proteins expressed during bone development and repair, is a strong osteoinductive factor that has been used to augment the osteoinductivity of scaffolds. The addition of BMP-2 to the scaffolds reinforced with nanoparticles may show enhanced bone growth compared even to positive control scaffolds of PLGA soaked with BMP-2. BMP-2 however, is not the only osteoinductive factor that could be included in scaffolds. Other factors that have increased bone growth include mesenchymal stem cells, endothelial growth factor, fibroblast growth factor, SAOS-2 human osteosarcoma cells, or platelet rich plasma.
4) Some of the nanoparticles used in this study are known bioimaging agents for magnetic resonance, computed tomography, ultrasound, and photoacoustic. The incorporation of these nanoparticles into scaffolds could allow for enhanced

longitudinal monitoring of the healing within a defect. Additionally, this would allow for tracking of the particles as the scaffolds degrade so as to learn more about excretion pathways. Besides imaging, some of the above techniques (ultrasound and photoacoustic) and some other methods including applied electrical field have been used to stimulate bone growth. The addition of these nanoparticles to scaffolds could lead to stimulated bone regeneration within the defect.